



Universität Hamburg
DER FORSCHUNG | DER LEHRE | DER BILDUNG

Fabrication of Stimuli-responsive, Chemically Tunable Nanostructures by Template-assisted Replication Method

Doctoral Thesis

To be awarded the degree of Doctor of Natural Sciences

Dr. rer. nat.

by the Department of Chemistry

of the Faculty of Mathematics, Computer Science and Natural Sciences of the
University of Hamburg

Hanju Jo

from Gimpo, Republic of Korea

Hamburg, 2017

The present work was conducted under the supervision of Prof. Patrick Theato from December 2012 to July 2017 at the Institute for Technical and Macromolecular Chemistry of the University of Hamburg.

1. First Evaluator: Prof. Dr. Patrick Theato
2. Second Evaluator: Prof. Dr. Martin Trebbin
3. Date of the Oral Defense: 15.09.2017

Contents

Abbreviations	iii
Zusammenfassung.....	1
Abstract.....	4
1 Introduction.....	6
1.1 Soft Materials Nanofabrication	6
1.2 Porous Anodic Aluminum Oxide (AAO).....	7
1.2.1 Electrochemical Formation of AAO	9
1.2.1.1 Elementary Interfacial Reactions	9
1.2.1.2 Pore Formation.....	11
1.2.1.3 Mild Anodization	12
1.2.2 Structure of AAO	14
1.2.3 Experimental Set-up.....	15
1.3 AAO Template-Assisted Fabrication of Nanostructures by Template Wetting	17
1.4 Stimuli-responsive Polymers.....	24
1.4.1 Thermo-responsive Polymers.....	25
1.4.2 Light-responsive Polymers.....	28
1.5 Post-Polymerization Modification of Nanostructures.....	30
1.5.1 Post-Polymerization Modification via Activated Esters	32
1.5.2 The Use of Post-Polymerization Modification on Nano-objects	33
1.5.2.1 Reactive Polymeric Nanorods	33
1.5.2.2 Functionalized Nanoparticles.....	35
1.5.2.3 Functionalized Electrospun Polymer Fibers	36
2 Scope and Objectives	38
3 Results and Discussion.....	39

3.1 Fabrication of Chemically Tunable, Hierarchically Branched Polymeric Nanostructures by Multi-branched AAO templates	39
3.2 Fabrication of Drug Releasable Nanostructured Poly(N-vinylcaprolactam) Thin Films	53
3.3 Fabrication of Temperature Responsive Block-like Nanorods	61
3.4 Fabrication of Multi-functionalized Nanowires via Post-polymerization Modification	74
4 Conclusion and outlook	84
5 Experimental Section	86
5.1 Characterization Methods	86
5.2 Fabrication of AAO Templates	87
5.3 Fabrication of Hierarchically Branched AAO Templates	87
5.4 Synthesis of PFPA	88
5.5 Synthesis of Spiropyran-amine	88
5.6 Preparation of Self-assembly Monolayer (SAM)	90
5.7 Fabrication of PPFPA Nanopillars	91
5.8 Surface Modification of PPFPA Nanopillars	91
5.9 Fabrication of PNVCL Nanostructured Thin Films	91
5.10 Adsorption and Release of Dye and Drug	92
5.11 Fabrication of TPT Molds	92
5.12 Fabrication of Physically Bonded Block-like Nanorods	92
5.13 Fabrication of Chemically Bonded Block-like Nanorods	92
5.14 Fabrication of PPFPA Nanowires	94
5.15 Removal of Barrier Layer via RIE	94
5.16 Removal of Barrier Layer via Wet-etching	94
5.17 Tip modification of PPFPA Nanowires	94
5.18 List of Chemicals	95
6 References	100

7 Appendix.....	112
7.1 Appendix A	112
7.2 Appendix B	113
7.3 Appendix C	114
7.4 Appendix D	114
8 Acknowledgement.....	115
Declaration on oath.....	117

Abbreviations

AAO	anodic aluminum oxide
AIBN	azobisisobutyronitrile
APTES	aminopropyltriethoxysilane
ATRP	atom transfer radical polymerization
AuNPs	gold nanoparticles
CuAAC	copper-catalyzed azide/alkyne cycloaddition
CW	continuous wave
CYPAM	<i>N</i> -cyclopropylacrylamide
D_{int}	interpore distance
DLS	dynamic light scattering
D_p	pore diameter
E	electric field
EDA	ethylenediamine
F_c	capillary force
g	gravitational acceleration
j	current
LCST	lower critical solution temperature
LP	long pass
ML	mode locking
MMA	methyl methacrylate
MW	molecular weight
Nd:YVO ₄	neodymium-doped yttrium orthovanadate
NHSA	<i>N</i> -hydroxy succinimide acrylate
NIPAM	<i>N</i> -isopropylacrylamide
NMP	nitroxide-mediated polymerization

Abbreviations

NorbNHSA	endo- <i>N</i> -hydroxy-5-norbornene-2,3-dicarboxyimidacrylate
PDEAM	poly(<i>N,N</i> -diethylacrylamide)
PDMS	polydimethylsiloxane
PEO	poly(ethylene oxide)
PFFPA	pentafluorophenyl acrylate
PFFPMA	pentafluorophenyl methacrylate
PFFPVB	pentafluorophenyl 4-vinyl benzoate
PIOZ	poly(2-isopropyl-2-oxazoline)
PL	photoluminescence
PNHSA	poly(<i>N</i> -hydroxy succinimide acrylate)
PNIPAM- <i>co</i> -MBAA	poly(<i>N</i> -isopropylacrylamide)- <i>co</i> -(<i>N,N'</i> -methylenebisacrylamide)
PNIPAM	poly(<i>N</i> -isopropylacrylamide)
PNVCL	poly(<i>N</i> -vinyl caprolactam)
PPFPA	poly(pentafluorophenyl acrylate)
PPFPMA	poly(pentafluorophenyl methacrylate)
PS	polystyrene
R	radius of nanopillars
RAFT	reversible addition-fragmentation chain transfer polymerization
RIE	reactive ion etching
r.t.	room temperature
SAM	self-assembled monolayer
SEM	scanning electron microscopy
t_b	barrier layer thickness
TCP	2,4,5-trichlorophenyl acrylate
T_g	glass transition temperature
THF	tetrahydrofuran

Abbreviations

Ti:Sa	titanium-doped sapphire
TPO	diphenyl (2,4,6-trimethylbenzoyl) phosphine oxide
TPT	trimethylolpropane propoxylate triacrylate
t_w	pore wall thickness
U	applied potential
UCST	upper critical solution temperature
W_c	capillary interaction energy
γ	surface energy
θ	contact angle
ρ	density

Zusammenfassung

In dieser Arbeit wurde ein Template-unterstütztes Replikationsverfahren unter Verwendung von anodischen Aluminiumoxid (AAO)-Templates, die hexagonal gepackte und hochgeordnete Poren mit einstellbaren Längen und Durchmessern haben, für die Herstellung von stimuli-responsiven oder chemisch einstellbaren Nanoobjekten (z.B. Nanostäbchen und Nanodrähte) sowie dünnen nanostrukturierten Filmen veranschaulicht und angewendet. Polymere Nanoobjekte und dünne nanostrukturierte Filme, die den Abmessungen der Templateporen entsprachen, wurden durch Infiltrieren der Templates mit verschiedenen Ausgangsstoffen, gefolgt von einer UV-initiierten Vernetzung und einer selektiven Entfernung der Templates hergestellt. Die vorbereiteten polymeren Nanoobjekte und dünnen nanostrukturierten Filme wurden hinsichtlich ihrer Reaktionsfähigkeit auf externe Stimuli und im Hinblick auf ihre durch Post-Polymerisationsmodifikation erzielte chemische Variabilität untersucht.

Chemisch einstellbare und hierarchisch verzweigte Poly(pentafluorphenylacrylat) (PPFPA) - Nanostrukturen wurden durch mehrfach verzweigte AAO-Templates erzeugt, die durch ein asymmetrisches zweistufiges Anodisierungsverfahren hergestellt wurden. Der modifizierte zweistufige Anodisierungsprozess führte zu einer Komplexität in den Strukturen der Templates und ermöglichte die Herstellung der hochentwickelten komplexen Nanostrukturen, die für die Einstellung der Benetzbarkeit und der Klebeeigenschaft nützlich sein können. Durch die Modifizierung und die Steuerung des Anodisierungsprozesses wurden verschiedene Formen von AAO-Templates (z. B. Himbeer-, Blüten- und verzweigte Formen) hergestellt, und es wurden ihre entsprechenden PPFPA-Nanostrukturen gebildet. Mittels einer Post-Polymerisationsmodifikation wurden die hierarchisch verzweigten PPFPA-Nanostrukturen mit Spiropyranamin modifiziert, was zu licht-responsiven Nanostrukturen führte. Die Änderungen der Benetzbarkeitseigenschaften bei UV-Bestrahlung wurden mittels einer dynamischen Kontaktwinkelmessung untersucht, wobei signifikante Änderungen des Kontaktwinkels in Abhängigkeit von den Formen der Nanostrukturen und dem Vorhandensein eines externen Stimulus festgestellt wurden.

Biokompatible und wärmeempfindliche dünne nanostrukturierte Poly(*N*-vinylcaprolactam)-Filme (PNVCL-Filme), die durch das Template-unterstützte Replikationsverfahren hergestellt wurden, wurden als Arzneimittelabgabesystem (engl.: Drug Carrier System) verwendet. Die

Adsorption und Freisetzung von Arzneimitteln wurde dabei mit einem Fluoreszenzfarbstoff, Rhodamin B, und einem potenten hydrophilen Medikament, Aspirin, getestet. Es konnte beobachtet werden, dass die dünnen nanostrukturierten PNVCL-Filme einen Farbstoff oder ein Arzneimittel durch kräftiges Rühren unter Standardbedingungen aufnahmen und bei Erwärmung aufgrund der niedrigeren kritischen Lösungstemperatur (LCST) von PNVCL erfolgreich freisetzen. Der Messbereich der LCST von PNVCL reichte von 35 bis 65 °C und umfasste somit die durchschnittliche menschliche Körpertemperatur (36 °C), welche die erforderliche Temperatur für Arzneimittelabgabesysteme ist. Die Fähigkeit der dünnen nanostrukturierten PNVCL-Filme zur Aufnahme und Freisetzung von Farbstoffen oder Arzneimitteln wurde mit einem dünnen nicht-strukturierten PNVCL-Film und einem hochvernetzten dünnen PNVCL-Film verglichen. Dabei wurde festgestellt, dass der dünne nanostrukturierte PNVCL-Film, der mit 15 Gew.-% eines Vernetzers hergestellt wurde, aufgrund seiner großen Fläche und seines Eignungsgrades zur Vernetzung eine wesentlich höhere Adsorption und Freisetzung von Farbstoff aufwies. Außerdem wurden die Wiederverwendbarkeit von dünnen nanostrukturierten PNVCL-Filmen und die strukturellen Veränderungen von Nanostrukturen auf der Oberfläche vor und nach der Freisetzung von Farbstoff untersucht, wobei die Ergebnisse zeigten, dass die dünnen nanostrukturierten PNVCL-Filme ohne strukturelle Schäden wiederverwendbar sind.

Block-ähnliche stimuli-responsive Nanostäbchen, die sowohl responsive als auch nicht-responsive Blöcke enthielten, wurden in dem Hohlraum von AAO-Templates unter Verwendung verschiedener Ansätze hergestellt. Temperatur-responsives Poly(*N*-isopropylacrylamid) (PNIPAM) wurde als stimuli-responsiver Block verwendet und Polystyrol (PS) und PPFPA wurden als nicht-responsiver Block verwendet. Zwei Blöcke wurden entweder physikalisch oder chemisch gebunden, und die Topographie der Nanostäbchen mit zwei Blöcken wurde mittels Rasterelektronenmikroskopie (SEM) beobachtet.

Es wurden hochentwickelte Nanodrähte gezeigt, die mit mehreren Fluoreszenzfarbstoffen an unterschiedlichen Stellen ihrer Oberflächen chemisch einstellbar sind und die die Herstellung von multifunktionalisierten intelligenten Nanoobjekten ermöglichen. Um auf beide Enden der in den AAO-Templates gebildeten Nanodrähte zugreifen zu können, wurde die Sperrschicht der Templates entweder durch reaktives Ionenätzen (RIE) oder durch Naßätzverfahren entfernt und die Enden der Nanodrähte wurden mittels Post-Polymerisationsmodifikation mit zwei

verschiedenen Fluoreszenzfarbstoffen chemisch modifiziert: NBD-Amin und Cresylviolett. Mittels Fluoreszenzmikroskopie wurde gezeigt, dass die Enden der Nanodrähte selektiv mit zwei verschiedenen Farbstoffen modifiziert werden können.

Zusammenfassend lässt sich sagen, dass durch das Template-unterstützte Replikationsverfahren mit verschiedenen funktionalen Vorstufen stimuli-responsive oder chemisch einstellbare Nanoobjekte und dünne nanostrukturierte Filme hergestellt werden konnten, die ein großes Potenzial haben, in Bioanwendungen eingesetzt zu werden. Es wird erwartet, dass die in dieser Arbeit vorgestellten Konzepte als ein flexibles und effektives Herstellungsverfahren zur Entwicklung einer wirkungsvollen Biomimetik und eines Arzneimittelabgabesystems beitragen.

Abstract

In this thesis, a template-assisted replication method using anodic aluminum oxide (AAO) templates, which provide hexagonally packed and highly ordered pores having adjustable lengths and diameters, is demonstrated and utilized for the fabrication of stimuli-responsive or chemically tunable nano-objects (e.g. nanorods and nanowires) and nanostructured thin films. Polymeric nano-objects and nanostructured thin films corresponding to the dimensions of the template pores are fabricated by infiltrating the templates with various precursors, followed by an UV-initiated cross-linking and a selective removal of the template. The prepared polymeric nano-objects and nanostructured thin films are investigated with regard to their responsiveness to external stimuli and their chemical variability via post-polymerization modification. Four different systems are studied and discussed in this thesis.

First, chemically tunable and hierarchically branched poly(pentafluorophenyl acrylate) (PPFPA) nanostructures are prepared by multi-branched AAO templates, fabricated via an asymmetric two-step anodization process. The modified two-step anodization process introduces a complexity into the structures of templates and allows to produce the advanced complex nanostructures which can be useful to control the wettability and adhesive property. By modifying and controlling the anodization process, various shapes of AAO templates (e.g. raspberry, flower, and branched shape) are produced and their corresponding PPFPA nanostructures are formed. Via post-polymerization modification, the hierarchically branched PPFPA nanostructures are modified with spiropyran-amine, resulting in light-responsive nanostructures. The changes of wettability properties upon UV light irradiation are studied by a dynamic contact angle measurement, and significant changes of contact angle are detected, depending on the shapes of the nanostructures and the presence of an external stimulus.

Next, biocompatible and thermosensitive nanostructured poly(*N*-vinyl caprolactam) (PNVCL) thin films, fabricated by the template-assisted replication method, are used as a drug delivery system and the adsorption and release of drugs are tested with a fluorescent dye, rhodamine B, and a potent hydrophilic drug, aspirin. It is observed that the nanostructured PNVCL thin films adsorb dye or drug by vigorous stirring under ambient conditions and successfully release them upon heating due to the lower critical solution temperature (LCST) of PNVCL. The measured range of LCST of PNVCL is from 35 to 65°C and it encompasses the average human body temperature (36°C) which is a target temperature for drug delivery systems. The capability of

nanostructured PNVCL thin films to adsorb and release dye or drug is compared with a non-structured PNVCL thin film and a highly cross-linked PNVCL thin film, and the nanostructured PNVCL thin film fabricated with 15 wt% of a cross-linker shows superior adsorption and release of dye due to its large area and the degree to which it is suitable for cross-linking. In addition, the reusability of nanostructured PNVCL thin films and the structural changes of nanostructures on the surface before and after the release of dye are investigated, and the results show that the nanostructured PNVCL thin films are reusable without structural damages.

In a third system, block-like stimuli-responsive nanorods containing both responsive and non-responsive blocks are fabricated in the cavity of AAO templates using various approaches. Temperature-responsive poly(N-isopropylacrylamide) (PNIPAM) is applied as a stimuli-responsive block, and polystyrene (PS) and PPFPA are used as a non-responsive block. Two blocks are bonded either physically or chemically, and the topography of nanorods having two blocks is observed by scanning electron microscopy (SEM).

Last but not least, advanced nanowires which are chemically tunable with multiple fluorescent dyes on the different sites of their surfaces are demonstrated which allow the fabrication of multi-functionalized smart nano-objects. To access both ends of nanowires formed in AAO templates, the barrier layer of templates is etched by either reactive ion etching (RIE) or wet etching methods, and the ends of nanowires are chemically modified via post-polymerization modification with two different fluorescent dyes: NBD-amine and cresyl violet. By means of fluorescence microscopy it could be shown that the ends of nanowires are selectively modified with two different dyes.

In conclusion, the template-assisted replication method with various functional precursors fabricates stimuli-responsive or chemically tunable nano-objects and nanostructured thin films which have a great potential to be used in bio-applications. The concepts presented in this thesis are expected to contribute to the development of an effective bio-mimetic and drug delivery system as a facile and effective fabrication method.

1. Introduction

1.1 Soft materials nanofabrication

Novel and intriguing properties of one-dimensional polymeric nanostructures attract great attention. The increasing number of publications based on one-dimensional polymeric nanostructures shows the high demand and interest in nanomaterial science. In addition, numerous nanofabrication methods have been developed and varied to prepare the advanced nanostructures and to meet the demands on time and cost. In general, nanofabrication methods can be divided into two main categories: “bottom-up” and “top-down”.¹ Literally, the bottom-up means the nanostructures are built up from the smallest level such as atoms or molecules, and top-down implies the nanostructures are obtained by removing the undesired parts of base material.

Self-assembly processes, which spontaneously organize the molecules into stable and well-defined structures, are generally referred to as the most used methods for the bottom-up fabrication.² By using self-assembly, the functionality of surface and the arrangement of molecules on the surface can be precisely controlled. The conventional top-down fabrication technique can be nanolithography such as electron-beam, focused-ion-beam, and X-ray or UV lithography. However, these nanolithography methods only can be used to directly pattern resist materials that are placed on planar and rigid substrates.³ As an alternative to the conventional lithography, soft lithography is introduced and used to fabricate micro-sized polymeric arrays for various applications. An elastomeric polymer, polydimethylsiloxane (PDMS), is generally used for the fabrication of soft lithographic molds, and ultra-small features can be replicated easily.⁴⁻⁶ However, the size of features that can be fabricated by soft lithography is limited due to the processing limitation, and the patterned structures of soft lithographic molds having high-aspect-ratio can irreversibly collapse due to the softness of PDMS.

Template-assisted fabrication technique is a facile and cost effective method, which allows the fabrication of high-aspect-ratio nano-objects. Furthermore, this method is widely accessible and able to use the top-bottom fabrication techniques with nanoscale precision.^{7,8} Template-assisted fabrication can be conducted by nano-molding or in-situ polymerization of polymers into the pores of templates, and either soft templates such as selectively etched di-block

copolymer⁹ and supramolecular gels¹⁰ or a hard template such as AAO^{11,12} can be used. Especially, porous AAO templates have been mostly used for the fabrication of nanostructures due to their large versatility and well-ordered homogeneous pores. AAO templates are also thermally stable in the range of temperature where the polymerization process occurs. In addition, by a simple wetting process with polymer melts or solutions, various nano-objects such as nanorods, nanotubes, and nanowires with range from a few tens of nanometers to micrometers can be prepared. The resulting polymeric nano-structural arrays can have uniform structures over a large area. The highly ordered nano-structural arrays were used for optoelectronics, sensors, high-density data storage materials, and photovoltaic cells.¹³ The details of porous AAO will be discussed in following chapters.

1.2 Porous Anodic Aluminum Oxide (AAO)

Aluminum is a material that is naturally and rapidly oxidized in ambient atmospheres. Due to the thin native oxide layer on the aluminum surface, further oxidation and corrosion can be prevented; however, the local corrosion can still occur in harsh environments or with corrosive chemicals. In 1857, Buff first found the phenomenon called “anodization”, which aluminum formed a thick oxide layer by an electrochemical oxidation reaction in an electrolytic cell, and the study was applied to the industrial applications in the early 1920s for the protection of metals from corrosion and abrasion.¹⁴ Since then, the anodization of metals including aluminum has been widely used in various industries, and now anodized products can be found almost everywhere in daily life.

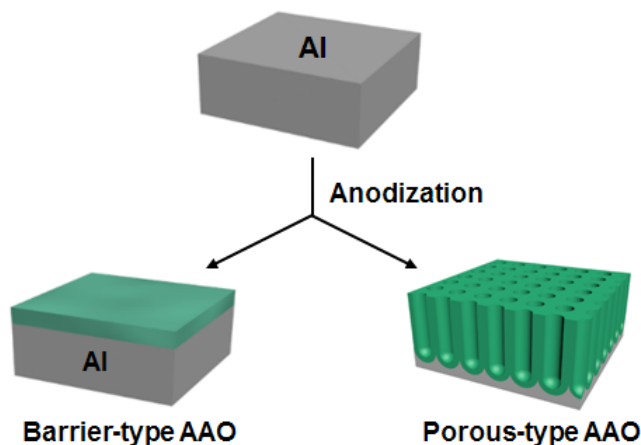


Figure 1. Two different types of AAO formed by barrier-type and porous-type anodization.

Two different types of AAO (i.e., nonporous barrier-type AAO and porous-type AAO) can be formed depending on the condition of anodization. The type of electrolytes plays an important role determining the morphology of AAOs.¹⁵⁻¹⁷ A nonporous barrier-type AAO can be produced in neutral electrolytes (pH 5-7) such as borate, oxalate, citrate, while, a porous-type AAO can be produced in acidic electrolytes such as sulfuric acid, oxalic acid, phosphoric acid.^{18,19} Particularly, the porous-type AAO has received great attention because of its excellent corrosion resistance and good adhesion base for paints and dyes.¹¹ In the 1970s, porous AAO was also used for magnetic memories and recording devices; however, the storage density of devices was low because of imperfect ordering of pores.^{19,20} A breakthrough was made by Masuda and co-workers in the 1990s by reporting on self-ordered porous AAO fabricated by a two-step anodization process (see Figure 2).^{11,16,21}

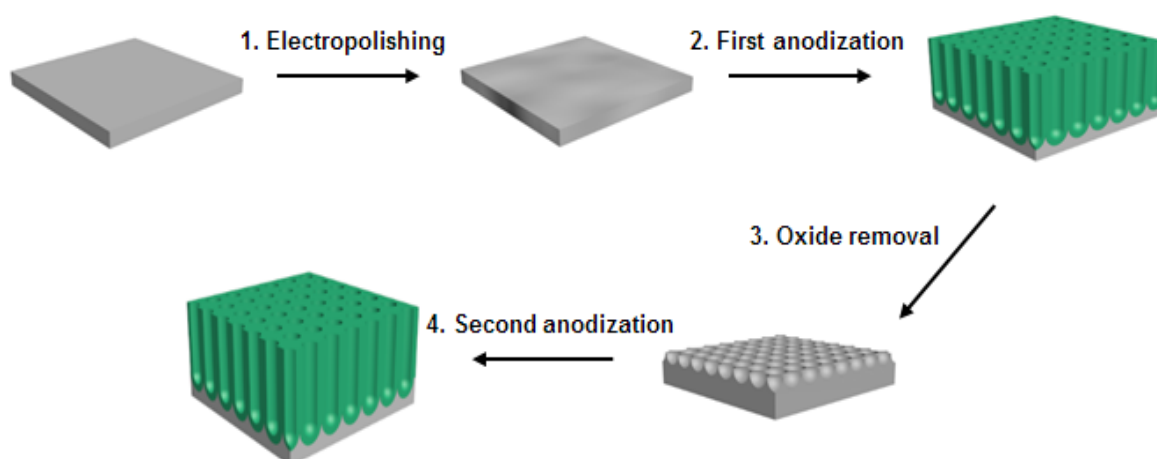


Figure 2. Schematic formation of AAO membranes following a two-step anodization route.

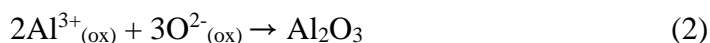
Briefly described, a first anodization is conducted in an acidic electrolyte under constant voltage on a finely polished aluminum and results in disordered pores at the top surface, but hexagonally well-ordered pores near to the oxide-aluminum interface. These hexagonally ordered pores grown during first anodization sculpt hemispherical concaves on the aluminum substrate which act as nucleation points for the further new pore growth. Subsequently, the oxide layer containing both disordered pores and ordered pores from the first anodization is dissolved by wet-chemical etching to make the hexagonally ordered indentations appear on the aluminum surface. In the following second anodization, hexagonally well-ordered nanopores are grown uniformly from the ordered indentation of the aluminum surface.

In this thesis, several significant advantages of nanoporous self-ordered AAOs are presented: (i) the dimensions of AAO such as pore diameter, pore length, and interpore distances can be easily tailored; (ii) the patterning of polymer nanostructures is achievable in a well-ordered fashion; (iii) identical dimensions of AAO lead to the production of polymer nanostructures that are highly monodisperse in size and shape; (iv) numerous polymers in solution or molten state can be infiltrated in AAOs for the fabrication of nanostructures; (v) sacrificial AAO templates can be readily removed by acidic or alkaline solution without damage of embedded nanostructured polymers. These novel features of AAOs have been intensively exploited for the fabrication of diverse nanostructured materials with complex architectures in size and structure and the development of function nanodevices.

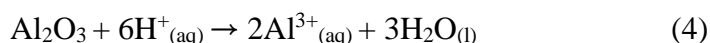
1.2.1 Electrochemical Reactions of AAO Formation

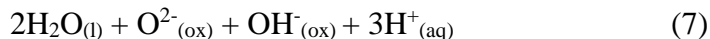
1.2.1.1 Elementary Interfacial Reactions

The anodic growth of aluminum oxide can be explained by the mobility of cations and anions within the anodic oxide at the aluminum/ aluminum oxide interfaces or the aluminum oxide/ electrolyte interfaces. It is generally accepted that Al^{3+} cations and O^{2-} or OH^- anions migrate toward the aluminum oxide/ electrolyte interfaces and the aluminum/ aluminum oxide interfaces, respectively, under high electric field (E). At both interfaces, the anodic oxide is formed by the following elementary reactions. The possibly occurring reactions at the aluminum/ aluminum oxide interfaces:

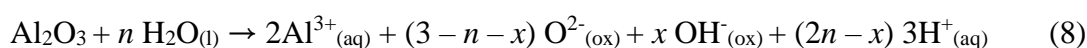


and at the aluminum oxide/ electrolyte interfaces:





The formation of anodic oxide at the both interfaces is described by the corresponding reactions 2 and 3, and it is assumed that all oxide anions generated from the dissolution of Al_2O_3 at the oxide/ electrolyte interfaces reform Al_2O_3 at the aluminum/ aluminum oxide interfaces. The overall reaction at the aluminum oxide/ electrolyte interfaces can be described as:



where, x indicates the ratio of O^{2-} and OH^- which has not been exactly determined yet, and n denotes the ratio of the amount of dissociated water and Al_2O_3 dissolution.

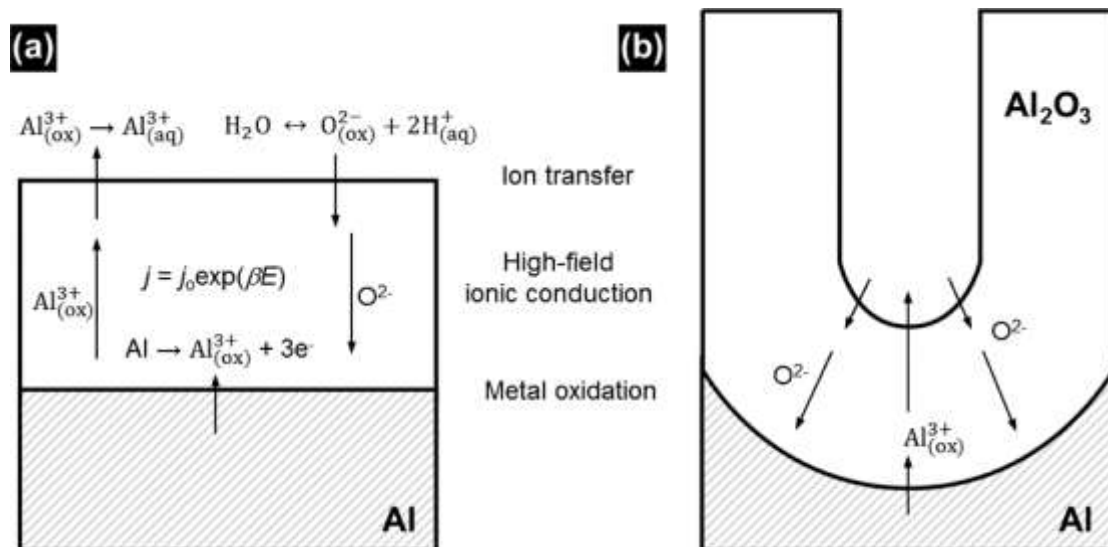


Figure 3. Schematic diagrams showing elementary interfacial reactions for (a) barrier-type and (b) porous-type anodic oxide. Reprinted with permission from Ref. ²² Copyright 2014 American Chemical Society.

As shown in Figure 3, aluminum cations and oxygen-containing anions migrate through the interfaces and form the anodic oxide by two chemical processes: (i) the oxidation of aluminum at the aluminum/ aluminum oxide interfaces and (ii) the dissolution of Al_2O_3 at the oxide/ electrolyte interface.

1.2.1.2 Pore Formation

Porous AAO can be fabricated under either potentiostatic (with a constant potential) or galvanostatic (with a constant current) condition. The potentiostatic anodization method is commonly employed for the fabrication of AAO due to the linear relation between the structural parameters of the fabricated AAO and the applied potential (U).²² The schematic diagram in Figure 4 shows the kinetics of pore formation under (a) potentiostatic and (b) galvanostatic conditions.

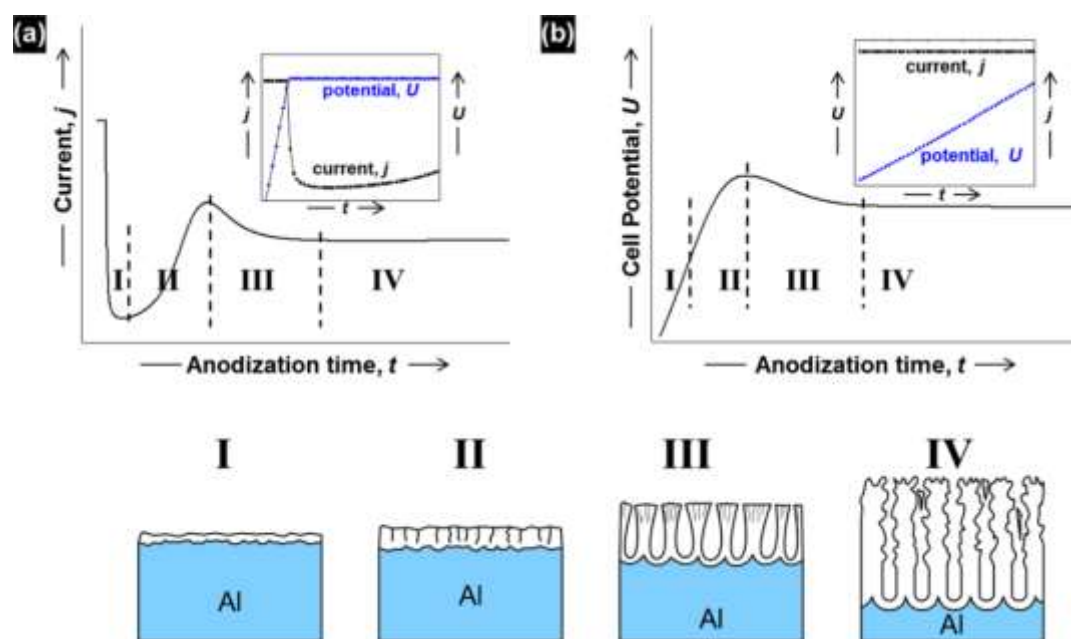


Figure 4. Schematic diagram of the kinetics of porous AAO growth in (a) potentiostatic and (b) galvanostatic conditions. Reprinted with permission from Ref. ²² Copyright 2014 American Chemical Society.

At the initial stage under potentiostatic condition, a thin compact oxide layer is formed over the entire surface of the aluminum by applying a constant applied potential (U). Due to the growth of an oxide layer over time (t), the resistance of the anodization circuit increases and, as a result, the current (j) of power supply decreases rapidly and reaches the minimum value (stage I). At this stage, the initiative points where the pores can be developed is generated on the oxide layer due to either the local imperfections (e.g., impurity, defects, pits, etc.) existing on the initial oxide layer or the local cracking of the initial oxide layer generated by tensile stress. The pores start to be formed on the initiative points and the current (j) gradually increases to a maximum due to the diffusion of electrolyte (stage II). The pores keep growing

and the current (j) becomes stable (stage III). Subsequently, the current (j) reaches a steady value and the pores are developed in a well-ordered array by the internal stresses (stage IV).

Galvanostatic anodization undergoes a similar progression from stage I to stage IV, while a constant current is applied. Under galvanostatic conditions, the oxide growth rate is proportional to the applied current density (j); therefore, a constant electric field should be applied to maintain the constant current (j). As shown in Figure 4 (b), the potential (U) increases with time and with a growth of the thickness of the barrier oxide (t_b). At the end of stage II, a drop in potential (U) is observed due to a transition from the growth of barrier oxide to the growth of porous oxide. Various mechanisms were pointed out to explain the growth of pores, and a morphological instability has been considered as the major cause of the initiation of the growth.

1.2.1.3 Mild Anodization

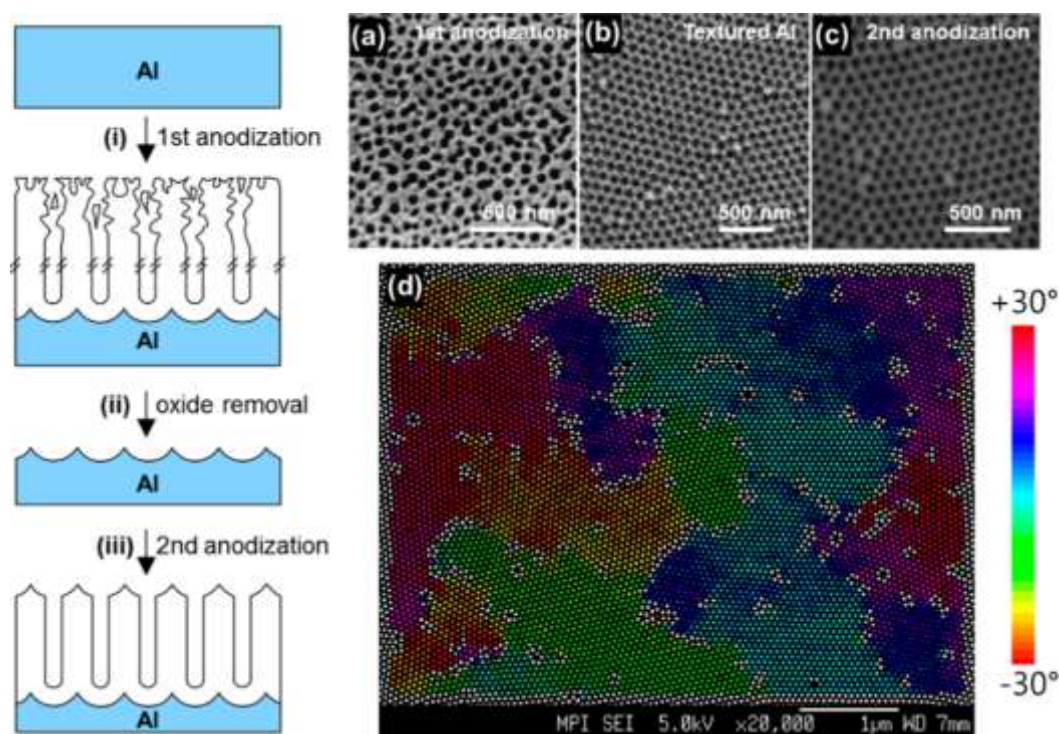


Figure 5. (Left) Schematic diagram of a conventional two-step mild anodization process for self-ordered porous AAO. (Right) Representative surface SEM images of the respective samples are shown in panels (a), (b), and (c), respectively. (d) A colored SEM image of AAO formed by two-step anodization using oxalic acid, showing a poly-domain structure. Reprinted with permission from Ref. ²² Copyright 2014 American Chemical Society.

Since Masuda and Fukuda demonstrated the fabrication of self-ordered pore structure by anodizing an aluminum in oxalic acid, the anodization methods have been developed and optimized with various electrolytes and conditions to produce highly ordered and uniform nanoporous AAO.¹¹ Today, porous AAO is conventionally fabricated by the “two-step anodization” process developed by Masuda and Satoh.²¹

The first anodization is typically carried out for more than 24 h to provide sufficient time for the pores to self-order, resulting in a textured surface of aluminum. The resulting porous AAO consists of the disordered pores produced during the initial anodization process and the ordered pores attained by following process, as shown in Figure 5. The whole aluminum oxide layer containing the disordered pores is removed by chemical etching with an aqueous mixture of 6wt% phosphoric acid and 1.8wt% chromic acid at 45°C. By etching, the textured hemispherical concaves work as the seeds of growth for further processes on the surface of aluminum, and the second anodization is conducted on this textured aluminum. The pores grow in an ordered arrangement with a polydomain structure, however, most of the area features well-ordered cylindrical pores. Particularly, the two-step anodization with sulfuric, oxalic, or phosphoric acid has been actively explored to find optimum conditions and understand the mechanism. Studies have shown the anodization conditions for the optimum ordering of pores: (i) sulfuric acid (0.3M H₂SO₄) at the anodizing potential (U) = 25V, 1 ~ 8°C; (ii) oxalic acid (0.3M H₂C₂O₄) at U = 40V, 1 ~ 8°C; and (iii) phosphoric acid (1.0wt% H₂PO₄) at U = 195V, < 1.4°C.

1.2.2 Structure of AAO

Porous AAO has close-packed arrays of hexagonally ordered cylindrical pores surrounded by a thin oxide barrier layer with a hemispherical morphology at one end. The structure of porous AAO can be defined with several parameters such as pore diameter (D_p), interpore distance (D_{int}), pore wall thickness (t_w), and barrier layer thickness (t_b). As shown in Figure 6, the porous AAO has the hexagonally ordered pores and a closed barrier layer.

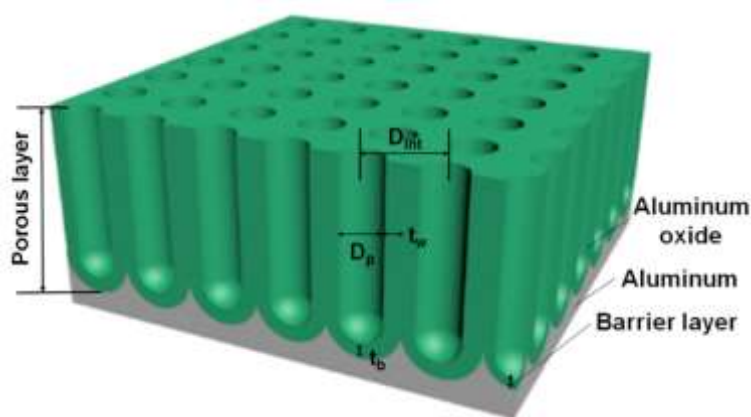


Figure 6. Schematic structure of porous anodic aluminum oxide (AAO).

One of the great advantages of porous AAO is that the structures of the nanopores are easily tunable by controlling the anodization conditions. The features such as anodization time, types or concentrations of electrolytes, and temperature play great roles for the formation of pores. The anodization time controls the depth of pores, which is proportionally grown with the total charge, and the types of electrolytes determine the diameter of pores, as shown in Figure 7.

Figure 7 a and 7 c show the top and side view of a porous AAO anodized in oxalic acid (0.3M, $\sim 5^\circ\text{C}$) and 7 b and 7 d show a porous AAO anodized in phosphoric acid (1.0wt%, $\sim 0.5^\circ\text{C}$). The use of oxalic acid results in smaller and narrower pores than for phosphoric acid, and the diameters of pores are $\sim 30\text{ nm}$ and $\sim 180\text{ nm}$, respectively. Since oxalic acid condition leads to smaller pores, the aspect ratio of pores between diameter and length increases rapidly for these pores than for those anodized in phosphoric acid.

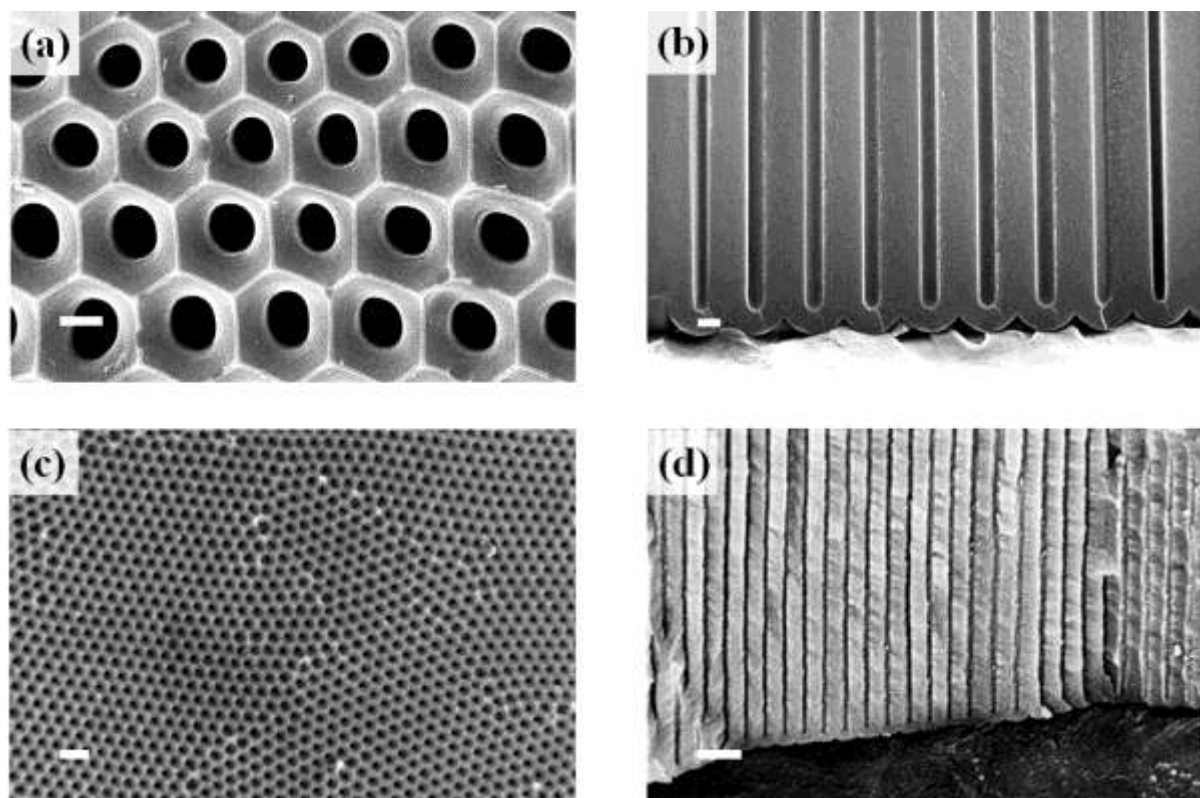


Figure 7. SEM images of porous AAOs anodized in phosphoric acid electrolyte (a and b) and in oxalic acid electrolyte (c and d): (a) top view and (b) side view SEM images of AAO anodized in phosphoric acid, and (c) top view and (d) side view SEM images of AAO anodized in oxalic acid (scale bar: 200 nm).

1.2.3 Experimental Set-up

The experimental set-up used for the fabrication of AAO templates is shown in Figure 8. It consists of a copper plate, a PVC cell for holding Al chips and electrolytes, and a metal lid containing a stirrer and a woven Pt wire net. The complete cell is placed on a cooling plate, which is connected to an external cooling pump. Two to six aluminum chips (diameter: 2cm) are placed between the copper plate and the PVC cell, which is then tightened with screws. A rubber O-ring is used for the complete sealing to prevent the leakage of electrolyte. After the electrolyte is poured into the PVC cell, the lid is covered to stir the electrolyte continuously and the electrolyte is cooled down to the required temperature for anodization. Both the copper plate and the woven Pt wire net are connected to the anode and the cathode of power supply, respectively for anodization process. Depending on the desired dimension of AAO, different kinds of electrolytes, mainly phosphoric acid and oxalic acid, are used and specific voltage is applied by a geared program.

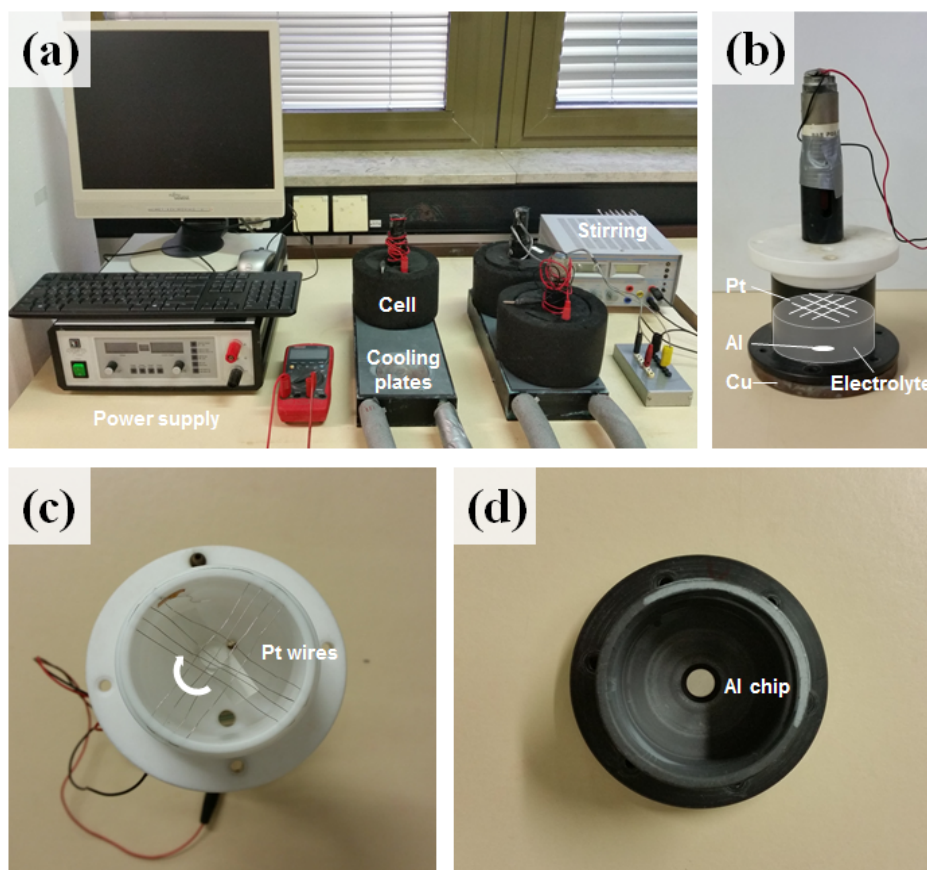


Figure 8. Anodization set-up for the fabrication of AAO: (a) overall set-up; (b) the components in one cell; (c) Pt-wires as cathode; (d) PVC cell to hold an electrolyte and Al chip that is anodized.

Figure 8 shows the exact set-up and the individual components. In general, the set-up consists of two electrodes that are connected to the power supply and the cell containing the aluminum chips and the electrolyte. A self-designed computer program is used to control the conditions of anodization such as anodization time and voltages. The current and the applied voltage are recorded in an Excel file. The cells are continuously cooled down by cooling water circulating the plates and by vigorous stirring. The present set-up can produce multiple numbers of AAO templates - up to 16 templates –at once and with a precise quality.

1.3 AAO Template-Assisted Fabrication of Nanostructures by template wetting

The special properties of AAO templates such as the well-ordered pore structures, large surface area, and controllable dimensions of pores and surface chemistry are main reasons that AAO templates have been used for enormous number of applications.^{8,23,24} In addition, the templating method provides a cost-effective alternative to conventional lithographic techniques, which require sophisticated and expensive equipment and are very time-consuming.

AAO templates having the highly ordered pore arrays have been used as a shape-defining mold for the fabrication of various nanostructured materials such as nanorods, nanowires, and nanotubes, and many different materials such as metals²⁵, polymers^{26–28}, nanoparticles²⁹, and inorganic semiconductors³⁰ have been applied. In relative terms, the templating method has little restriction to the materials that can be used, therefore, various nano-objects with different materials in a well-defined structure can be fabricated as required. Since, Martin and coworkers first introduced the concept of “template synthesis”³¹, many researchers such as Wendorff^{32,33}, Steinhart^{34,35}, Russell^{36,37}, and several others have studied and developed the template synthesis method. The most often used methods for an infiltration of materials into AAO templates are chemical vapor deposition, electrochemical deposition³⁸, sol-gel deposition³⁹, and wetting of precursors of polymers.

In general, nanostructured polymeric materials can be obtained by infiltration of a polymer melt or solution or by “in-situ” polymerization of a monomer. Steinhart and coworkers described the template synthesis method with polymer melts or solutions of polystyrene and polytetrafluoroethylene using AAO templates and found that the different wetting phenomena were caused by the respective conditions of infiltrated materials.⁴⁰ The wetting is achieved by the difference of surface energies between the infiltrated materials and the oxide surface of the pores. Commonly, the pore surface of AAO templates has high surface energies, whereas the surface energy of polymer melts or solutions are one order of magnitude lower⁴¹; therefore, polymer melts or solutions having a low viscosity tend to spread on the pore surfaces to minimize the interfacial energy. For this reason, polymer nanotubes can be obtained by controlling the conditions of the infiltrated materials. The tubular structures formed by wetting the pore surfaces can be used as a nanochannel that can be developed into sensors⁴² or separating filters^{43,44}. The applicability of nanochannels increases steadily.

The infiltration of polymer melts is also carried out by capillarity. In a regime where the temperature is only slightly above the glass transition temperature, the melts cannot form a fluid melt film; however, the melts tend to wet the pore surfaces because they still have a low surface energy. Therefore, the melts are infiltrated into the pores, and the melts are not only wetting the surfaces, but also filling the whole pores. This causes the formation of solid nanorod or nanowire whose shape is unlike that of nanotubes. In addition, the polymer molecular weight plays an important role for the wetting transition temperature. Zang and coworkers observed a transition point, where the wetting is completed by increasing the temperature, and the results showed that the wetting transition temperature was dependent on the polymer molecular weights.³⁶

Solution wetting infiltration is one of the most frequently used methods to prepare polymer nanostructures. The AAO templates can be immersed in the polymer solutions and the pores of AAO can be completely or partially filled, depending on the concentration of the solutions. This method can be a great alternative for polymers having a high glass transition temperature. Wendorff and coworkers described the solution wetting infiltration and they found a correlation between the polymer molecular weights and the morphology of the resulting nanostructures.³³

The infiltration method can be classified as shown in Figure 9, and this method has been frequently used to prepare polymeric nanostructures. Depending on the desired nanostructure, the suitable infiltration methods can be varied; for instance, melt wetting is recommended for the reproducible fabrication of nanofibers and nanotubes, since it has less solvent-related problems, and solution wetting is suggested to obtain nanotubes because the wall thickness of nanotubes can be controlled by the solvent concentration or by the quality of the solvent. In addition, precursor film wetting and melt capillary infiltration can be used to prepare the solid polymer nanofibers and methods based on additional forces, such as vacuum-induced infiltration, can be used to fabricate nanofibers containing nanoparticles.

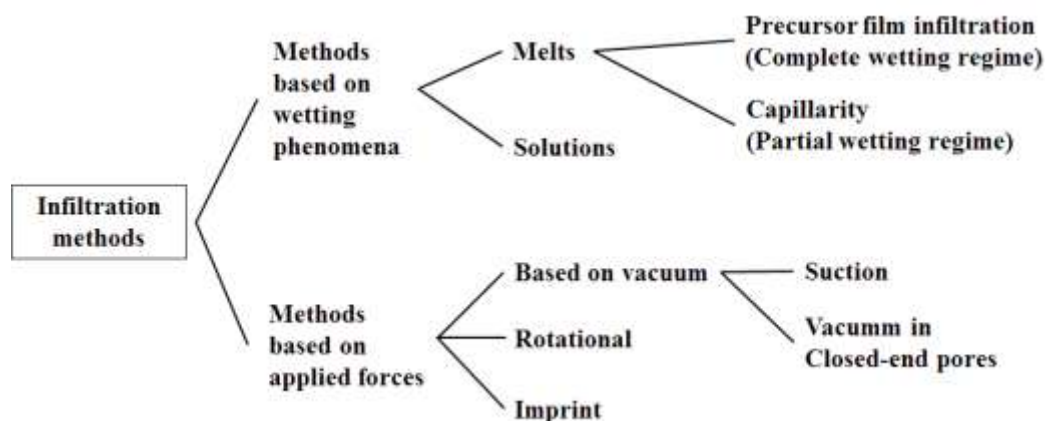


Figure 9. Summary of infiltration methods for the hard-templating methods. Reproduced with permission from Ref.⁴⁵, Copyright 2012, Elsevier Ltd.

As an alternative method for the preparation of versatile polymeric nanostructures, an “in-situ” polymerization in the nanocavities of AAO templates can be conducted. By using a polymerization technique, various monomers can be directly polymerized in the confined space. For instance, Mijangos and coworkers demonstrated the free radical polymerization of styrene and methyl methacrylate in the confinement of AAO templates.^{46,47} A small amount of thermal initiator, 2,2'-azobis-(isobutyronitrile) (AIBN), was added to styrene and methyl methacrylate and the solutions were casted on top of the AAO templates. The infiltrated monomer solutions with the initiator were then polymerized for a set of different temperatures and times. In both cases, after in-situ polymerization, polymers having a lower molecular weight and a lower dispersity were obtained, as compared to polymers synthesized in bulk.

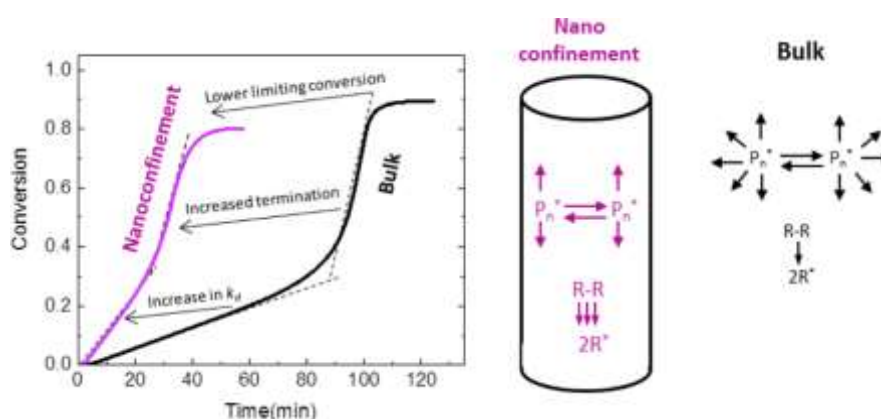


Figure 10. Scheme showing difference in reaction kinetics of methyl methacrylate polymerized in bulk and in nano-confinement (60 nm) at 60 °C. Copyright 2017 American Chemical Society.

This phenomenon can be explained by confinement effects and a catalytic effect, which is caused by native surface-bounded hydroxyl groups on the pore walls.⁴⁸ The catalytic effect occurs during the in-situ polymerization process in a nano-confined system and this catalytic effect induces an increased rate of initiator decomposition. The fast initiator decomposition leads to an increased rate of polymerization in the initial stages of polymerization. In addition, the movement of two radicals generated from the initiator decomposition is restricted under nano-confinement, as shown in Figure 10, and it causes higher termination rates, unlike bulk polymerization.^{49,50} As a result, lower molecular weight polymers having a low dispersity are obtained.

Via in-situ polymerization, copolymers also can be polymerized inside the pores of AAO templates. Cui and coworkers reported on the fabrication of poly(*N*-isopropylacrylamide)-*co*-(*N,N'*-methylenebisacrylamide) (PNIPAM-*co*-MBAA) nanotubes via surface-initiated atom transfer radical polymerization using the commercial AAO templates.^{51,52} By this direct grafting-from synthesis methods, copolymer nanotubes were produced, and the wall thicknesses of the nanotubes was controlled by the concentration of the monomer solutions, as shown in Figure 11.

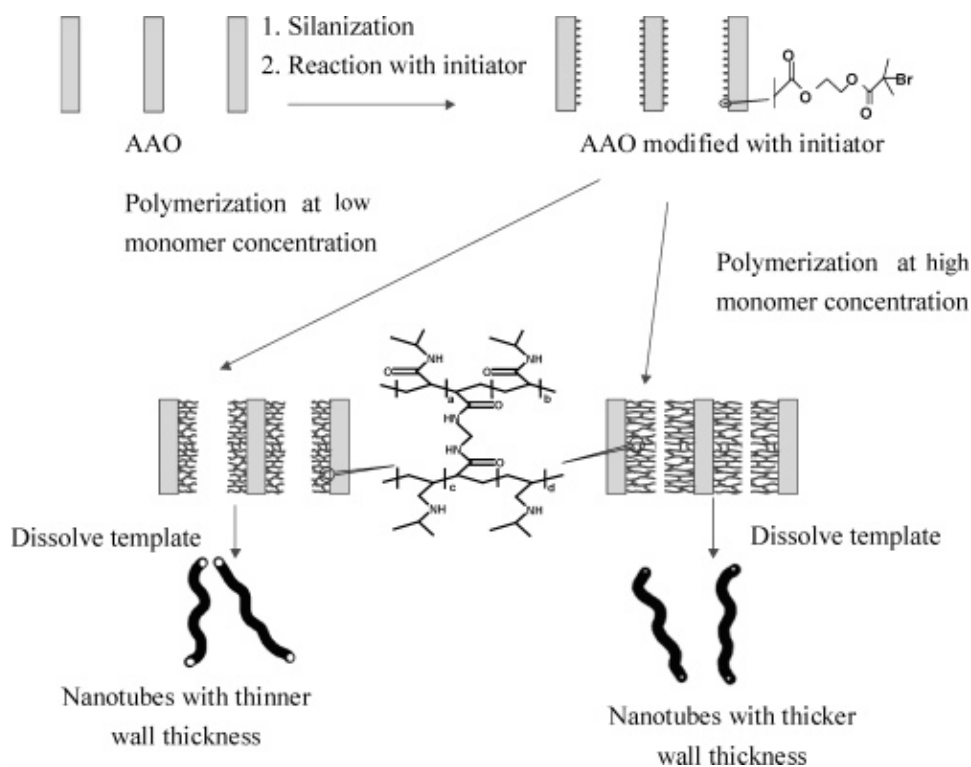


Figure 11. Schematic illustration in fabricating PNIPAM-*co*-MBAA nanotubes with different wall thicknesses in porous AAO membrane.⁵¹ Copyright 2006 American Chemical Society.

The polymerized nanopillars can be released from the templates by etching of the sacrificial templates. However, the prevention of a collapse or an aggregation of the nanopillars after the removal of the AAO template is a challenging key issue to obtain the initial shape of nanopillars. In contrast to inorganic materials, organic and polymeric materials have a low hardness; therefore, the bending or collapsing of nanopillars can occur. In general, the collapse of nanopillars is caused by adhesion forces between nanopillars⁵³ and capillary forces during the etching and drying processes.⁵⁴⁻⁵⁶ While the wet chemical etching process of the templates is conducted, the nanopillars are inevitably brought into contact with aqueous solutions, and capillary forces exert a great influence upon the lateral collapse of nanopillars.

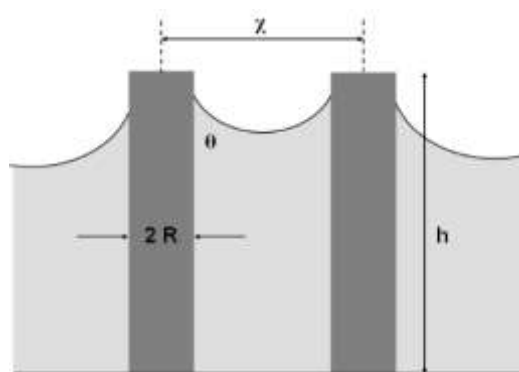


Figure 12. Schematic illustrations of two pillars partially immersed in a liquid. Reproduced with permission from Ref. ⁵⁷, Copyright 2009, American Chemical Society.

The capillary interaction energy (W_c) of two pillars, when the pillars are partially immersed in a liquid with surface energy (γ) and a contact angle (θ), can be described as:⁵⁷

$$W_c = -2\pi\gamma R^2 \cos^2\theta \ln\left(\frac{l_c}{x + \sqrt{x^2 - 4R^2}}\right) \quad (9)$$

where, $l_c = (\gamma/\rho g)^{1/2}$ is the capillary length of the liquid (ρ is the density and g is the gravitational acceleration) and the radius of nanopillars (R), the interpore distance between two pillars (x) shown in Figure 12.

Accordingly, the capillary force (F_c) between the two pillars can be written as:

$$F_c = -\frac{dW_c}{dx} = -\frac{\pi\gamma R^2 \cos^2\theta}{\sqrt{(x/2)^2 - R^2}} \quad (10)$$

The capillary force increases proportionally to the surface tension of the liquid and the contact angle at the liquid/pillar interfaces; therefore, the liquid which comes into contact with the

nanopillars plays an important role in the capillary force. To reduce the capillary forces and prevent the lateral collapse of the pillars, solvents having a low-surface tension such as methanol or isopropyl alcohol can be used or the supercritical freeze drying technique can be applied.^{58,59} Especially, the freeze drying method prevents the high-aspect-ratio nanopillars from collapsing after rinsing. The procedure of freeze-drying is extraordinarily simple. After washing the nanopillars released from the AAO templates with water, the wet samples containing the nanopillars are connected with a freeze-drying machine and the water surrounding the nanopillars is sublimed. Due to the sublimation, the nanopillars can keep their initial shapes without being exposed to the influence of the capillary force caused by liquid between the pillars.

Figure 13 shows the free-standing nanopillars without and with freeze-drying treatment, and one can see clearly that the nanopillars preserve their shapes without collapsing after freeze-drying process.

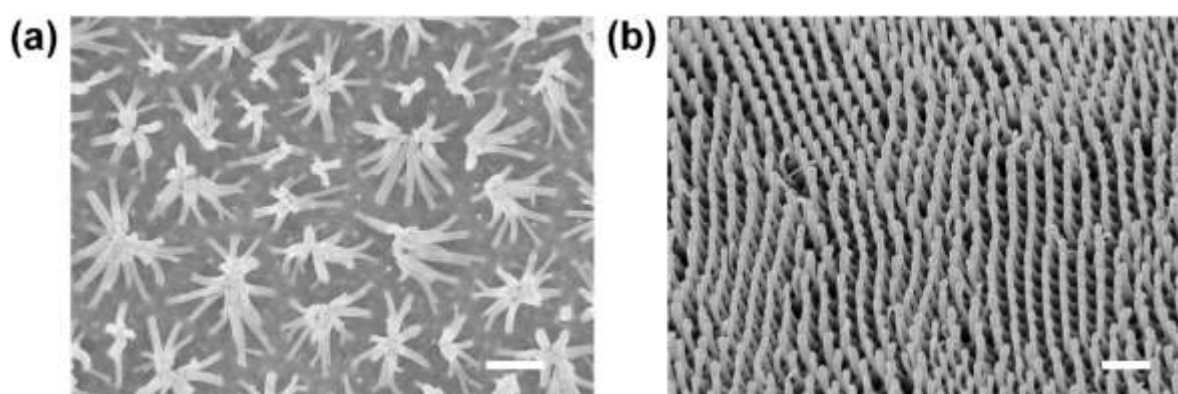


Figure 13. Freestanding polymeric nanopillars without freeze drying (a) and after the freeze-drying process (b) (scale bar: 1 μm).

AFM images of nanopillars also prove that the nanopillars stand in most of the area without undergoing a critical collapse, unlike the nanopillars affected by the capillary force during the drying step.

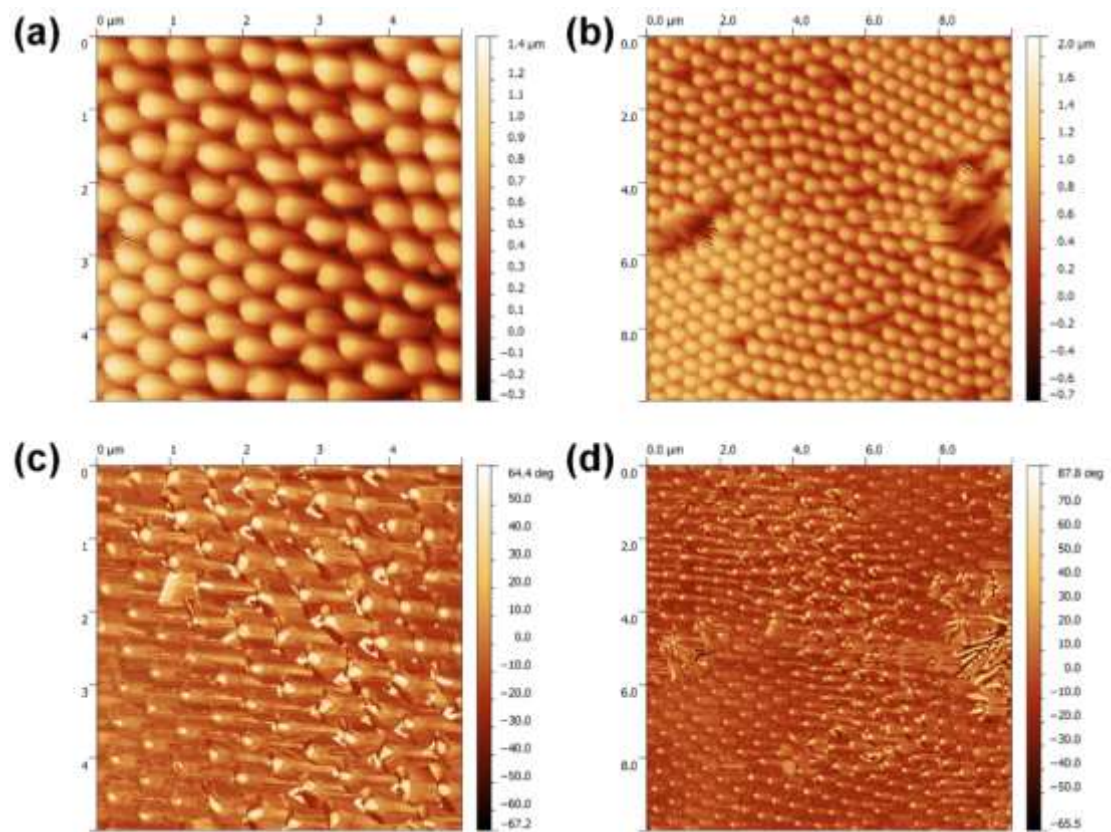


Figure 14. AFM images of free-standing polymeric nanopillars: topology of a small area (a) and a large area (b), and the phase images of the small area (c) and the large area (d).

1.4 Stimuli-responsive polymers

A smart polymeric system is capable of a physiochemical change upon internal or external stimuli and has received great interest.⁶⁰ A large variety of stimuli-responsive polymers with well-controlled composition and different stimuli-responsiveness has been synthesized and widely investigated. The changes of structure and property at the macromolecular level can be mainly caused by physical, chemical, or biological stimuli (Figure 15).⁶¹ Stimuli-responsive polymers undergo dramatic changes with external stimuli such as physical stimuli (e.g. temperature, light, magnetic, and electricity, etc.), chemical stimuli (e.g. pH, ionic strength, and solvent, etc.), and biological stimuli (e.g. enzymes and receptors, etc.). These stimuli-responsive polymers can be potentially applied in many applications; for instance, biocompatible stimuli-responsive polymers are useful in drug delivery and bio-applications^{62–64}, and temperature or light responsive polymers can be utilized as sensors and actuators, and surface grafted stimuli-responsive polymers can be used to control the interface wettability.⁶⁵ Stimuli-responsive polymers can be classified depending on material states, number of responsibility, and stimuli. Further discussion on the stimuli-responsive polymers will be based on the type of stimuli (temperature, light, and pH) that are mostly applied in previous studies.

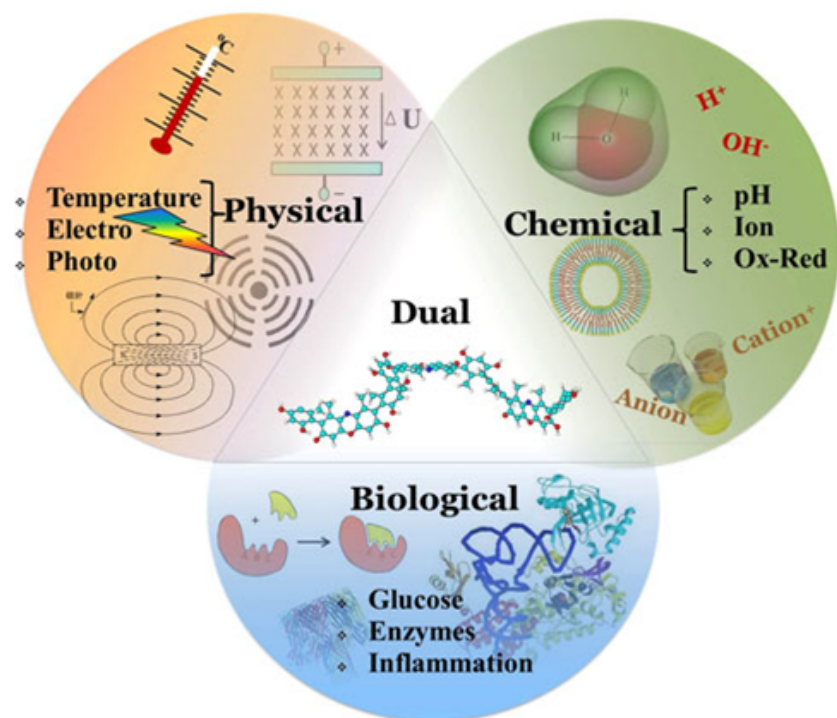


Figure 15. Classification of stimuli of stimuli-responsive polymers. Reproduced with permission from Ref. ⁶¹, Copyright 2012, BioMed Central Ltd.

1.4.1 Temperature responsive polymers

Thermo-sensitive polymers as one of representative stimuli-responsive polymers have been intensively studied. The main feature of thermo-sensitive polymers is a critical solution temperature, which is a temperature where the interaction between the polymeric chains and the aqueous media rapidly changes. Below or above this point, the intra- and intermolecular interactions such as electrostatic and hydrophobic interactions are adjusted and the polymeric chains are collapsed or expanded. This point is called a lower critical solution temperature (LCST) and an upper critical solution temperature (UCST). Thermo-sensitive polymers featuring LCST become miscible and immiscible below and above of LCST, respectively, and UCST polymers exhibit the opposite behaviors that the polymers are immiscible and miscible below and above of UCST, respectively, as shown in Figure 16. Based on physical changes or phase separation, the LCST can be considered superficially as an inverse of the UCST; however, the theoretical physical foundations of LCST and UCST are quite different.

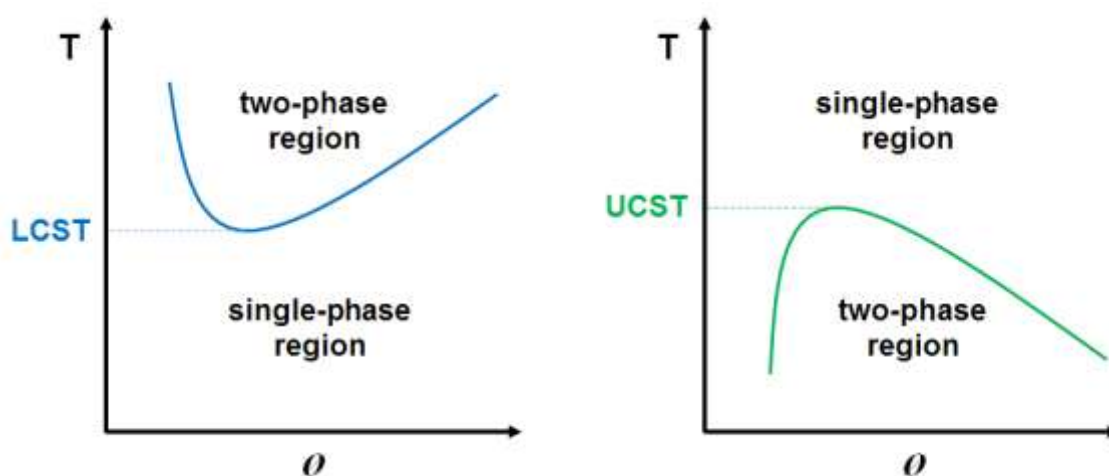


Figure 16. Schematic illustration of phase diagrams: (a) lower critical solution temperature (LCST) behavior and (b) upper critical solution temperature (UCST) behavior (T : temperature, ϕ : polymer volume fraction). Reproduced with permission from Ref. ⁶⁶, Copyright 2011, *Polymers*.

According to Flory and Huggins theory, the phase separation only occurs with unfavorable enthalpy interaction between polymer and solvent.^{67,68} In such a case, the mixing entropy still can outbalance the unfavorable enthalpy and make the polymer miscible with solvent. For

instance, a very small amount of polymer can be dissolved in a large amount of solvent and keep the single phase at the thermodynamic equilibrium.

Unconventionally, LCST phase separation is driven by unfavorable entropy of mixing, which originates from a strong polar interaction or hydrogen bonding between polymer and aqueous solution.^{69–71} Below LCST, the water molecules form hydrogen bonds with the amide groups in the polymer and form the solvation shell around polymer. Due to the hydrogen bonding, the entropy of water becomes unfavorable but the mixing enthalpy becomes favorable, which makes the system mono-phasic. In contrast, above LCST, the water molecules that form the hydrogen bonding with polymers are released into bulk water; therefore, the overall entropy increases and the mixing enthalpy becomes unfavorable. As a result, the phase separation occurs and the transparent homogeneous solution becomes cloudy inhomogeneous solution.

Numerous LCST-type polymers exhibit a phase separation upon heating in aqueous solution. Prominent examples of LCST-type polymers are poly(*N*-isopropylacrylamide) (PNIPAM), poly(*N,N*-diethylacrylamide) (PDEAM), poly(*N*-vinylcaprolactam) (PVCL), and poly(2-isopropyl-2-oxazoline) (PIOZ).⁷² Figure 17 illustrates the chemical structures of these thermo-responsive polymers featuring LCST.

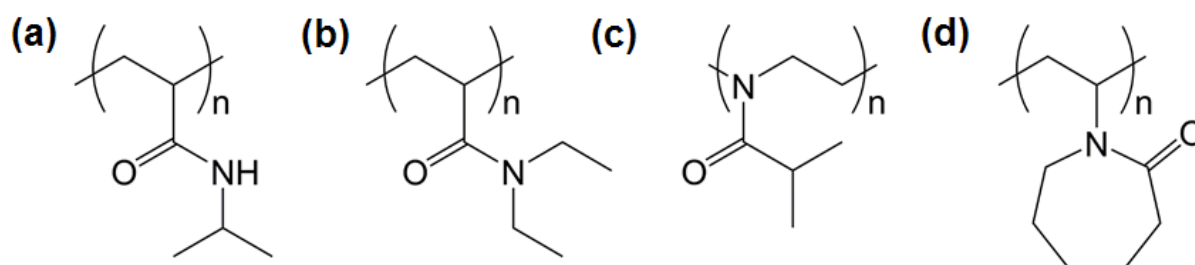


Figure 17. Thermo-responsive LCST-type polymers: (a) poly(*N*-isopropylacrylamide) (PNIPAM), (b) poly(*N,N*-diethylacrylamide) (PDEAM), (c) poly(2-isopropyl-2-oxazoline) (PIOZ), and (d) poly(*N*-vinylcaprolactam) (PNVCL).

PNIPAM, a well-known temperature-responsive polymer, has a sharp transition at 32°C upon heating.⁷³ However, in a few cases, a LCST hysteresis upon heating and cooling can be observed, depending on the heating and cooling rates, the viscosity and a formation of intra- and inter-molecular hydrogen bonds during phase separation.⁷⁴ Figure 18 shows an example of LCST hysteresis curves of PNIPAM. A PNIPAM solution in water was heated and cooled with a slow rate (0.1 °C min⁻¹) after temperature stabilization. By increasing the temperature above

LCST, the intra- and inter-chain hydrogen bonds form between NH-groups and $-C=O$ groups, while PNIPAM undergoes the structural transition from a coiled to a globular structure.⁷⁵ At the initial stage of cooling, these intra- and inter-chain hydrogen bonds cannot be completely disassembled, and this causes the LCST hysteresis, as shown in Figure 18.

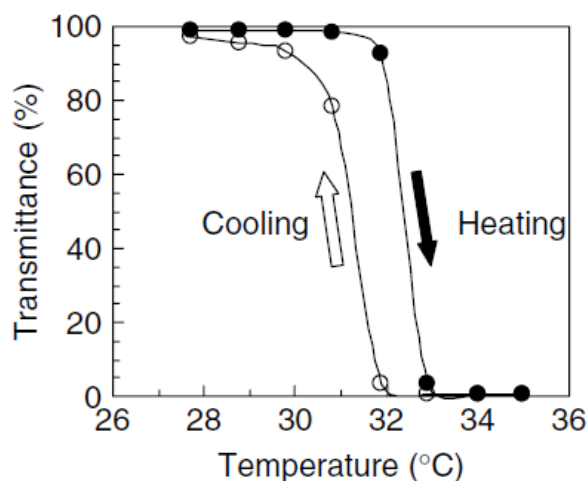


Figure 18. LCST curves of PNIPAM upon heating and cooling. Reproduced with permission from Ref. ⁷⁴, Copyright 2008, Society of Chemical Industry.

PVCL, a water soluble temperature-responsive polymer, features a low toxicity. In case of PVCL, the nitrogen in a cyclic amide is directly attached to the polymer backbone; therefore, the amide by-products are not generated upon hydrolysis. This feature makes PVCL as an attractive candidate material for the various bio-applications.⁷⁶⁻⁷⁹

These LCST of polymers is dependent on the molecular weight (MW) and solution concentration; for example, the increase of MW causes a shift of LCST to lower values, and the addition of salts or surfactant decrease or increase the LCST due to the disruption in the polymer-water interaction.^{69,80,81} These tunable properties can be used to control the LCST.

Temperature-responsive polymers featuring UCST, on the other hand, show different behaviors upon the change of temperature. Upon cooling, the mixing entropy decreases gradually and the unfavorable enthalpy which causes the phase separation increases; therefore, the solution becomes turbid below UCST. Zwitterionic polymers containing positively and negatively charged moieties in the repeating units have been mainly studied as the UCST type polymers in water.⁸² Due to the charges of repeating units, a strong intermolecular attraction is generated and resulted in the UCST behavior. UCST thermo-responsive polymers show a great potential for broad application in various fields.

1.4.2 Light responsive polymers

Light-responsive polymers contain photochromic moieties which undergo a reversible or irreversible structure isomerization upon light irradiation at a specific wavelength. Upon the light irradiation, the structure of photochromic moieties changes and this structural change is usually accompanied by changes of color, polarity, and solubility of the polymer. The transition is rapid and sharp; therefore, the reactivity of light-responsive polymers can be precisely controlled by regulating the irradiation time and location. Due to this advantage, light-responsive polymers have been widely applied in controlled drug delivery systems and reversible wettability.^{72,83–85}

Light-responsive polymers can be either reversible with structural change or irreversible with chemical bond breakage. Especially, the reversible light-responsive polymers have been intensively studied during the last decade. Azobenzene, spiropyran, dithienylethene, and *N*-salicyliden-aniline, are well-known photo-induced structure-isomerization units, which have been thoroughly studied and whose chemical structures are shown in Figure 19.^{83,86–89}

Azobenzene is one type of photochromic molecules which has a reversible photoisomerization from *trans* to *cis* or *cis* to *trans* upon UV- or visible light irradiation, respectively (see Figure 19 (a)).^{90–93} By the irradiation, the molecular structure of azobenzene is rapidly altered within picoseconds, and the wettability of surface covered by azobenzene is also rapidly changed. The wettability can be reversibly switched by change of the irradiated wave length. For instance, Lim and coworkers used 7-((trifluoromethoxyphenylazo)phenoxy)pentanoic acid as a photo-switch and successfully fabricated a nano-porous organic-inorganic hybrid multilayer film that is reversibly switchable between a superhydrophobic and superhydrophilic state upon light irradiation. Another group developed a material that features a reversible adhesion by combining azobenzene with sugar alcohol derivatives.^{85,94} Besides that, an azobenzene-functionalized amphiphilic dendritic polymer (polyethylenimine-steric ester-azobenzene) was developed as photo-switchable nano-carriers, and it showed the potential that azobenzene can contribute to the development of bio-applications.⁹⁵

Photochromic spiropyrans can be reversibly switched between a closed spiropyran form and an open merocyanine form upon light irradiation as shown in Figure 19 (b).^{89,96–101} This photo-switching is accompanied by a notable color change which proves the transition of forms, and it is accepted in general as the most recognized feature of photo-switches. In addition,

spiropyran exhibits a large change in its dipole moment, which affects the surface-free energy during the transition; therefore, it can be used for a switching of the wettability.

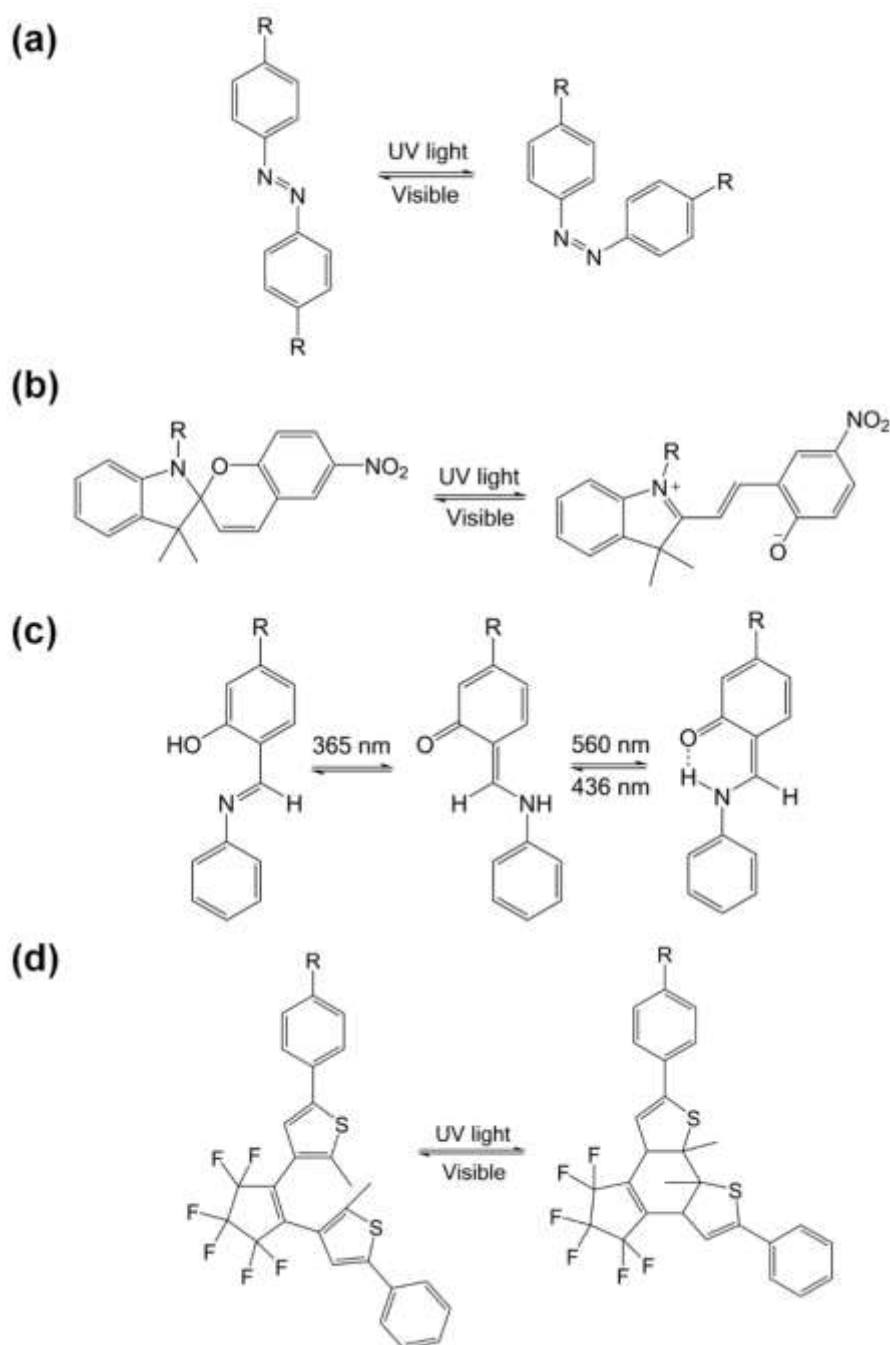


Figure 19. Light-responsive polymers with reversible photochromic moieties: (a) azobenzene, (b) spiropyran, (c) *N*-salicyliden-aniline, and (d) dithienylethene.

Locklin and coworkers fabricated photochromic spiropyran polymer brushes, which can reversibly control the wetting property of surfaces by exposure to light. The photo-induced isomerization between the spiropyran form and the merocyanine form caused a reversible

change of the contact angle up to 15°, and the change of contact angle was enhanced up to 35° by adding the metal ions.⁹⁶ Theato and coworker investigated and described photo-switchable surfaces based on polysilsesquioxanes and compared the wettability of azobenzene, salicyliden-aniline, and spiropyran-immobilized surfaces.⁹⁹ The maximum change of contact angle of a spiropyran-immobilized surface reached almost 30° and the change of wettability was switchable multiple times upon UV light and visible light irradiation. Spiropyran was also used for the formation of micelles, which can be potentially used as a drug carrier. By the synthesis of spiropyran-containing block copolymers, a photo-responsive nanocarrier can be produced and an encapsulated drug within the nanocarrier can be released by UV light irradiation.¹⁰² In addition, spiropyran is added to printing inks and is also used for daily products, such as T-shirts and toys.¹⁰³

1.5 Post-Polymerization Modification

Controlling the synthesis process of functional polymers to obtain a defined molecular weight, composition, and architecture is still a great challenge. For the synthesis of functional polymers, a protected monomer can be used; however, an additional deprotection step is mandatorily required and the deprotection process is in general not completely performed. Therefore, it is preferable to directly polymerize the monomers bearing functional groups.

Post-polymerization modification is an attractive alternative method offering the possibility to overcome the problems associated with conventional polymerization techniques (e.g., additional deprotection step, high temperature, and use of organic solvents, etc.).^{104,105} Post-polymerization modification, also called as polymer analogous reaction, was first reported in 1840 by Hancock and Ludersdorf independently, and since then, many researchers have studied these methods to fabricate various functional materials.^{106,107} Although the applicability of post-polymerization modification was proven, the number of chemical reactions available for this method was relatively limited until the early 1990s. However, the evolution of controlled (living) radical polymerization methods and several chemo-selective coupling reactions allowed the enormous growth in the use and adaptability of post-polymerization modification.¹⁰⁸ The representative controlled radical polymerization methods are atom-transfer radical polymerization (ATRP), nitroxide-mediated polymerization (NMP), and reversible addition-fragmentation chain transfer (RAFT).^{109–111} As common coupling reactions,

copper-catalyzed azide/alkyne cycloaddition (CuAAC), thiol-ene/-yne addition, activated esters, and many others, which are generally referred to click reactions, have been intensively applied.^{112–116}

In contrast to the traditional living polymerization, the controlled radical polymerization has the advantage of providing a higher tolerance towards functional moieties and of maintaining their functionality during the synthesis process.^{109,117,118} In addition, the post-polymerization modification method has a number of advantages, one of them being that the libraries of chemical reactions and monomers that can be applied in this method are various and another one being that the method can be applied on a variety of surfaces and interfaces which can be limited when using conventional direct polymerization.

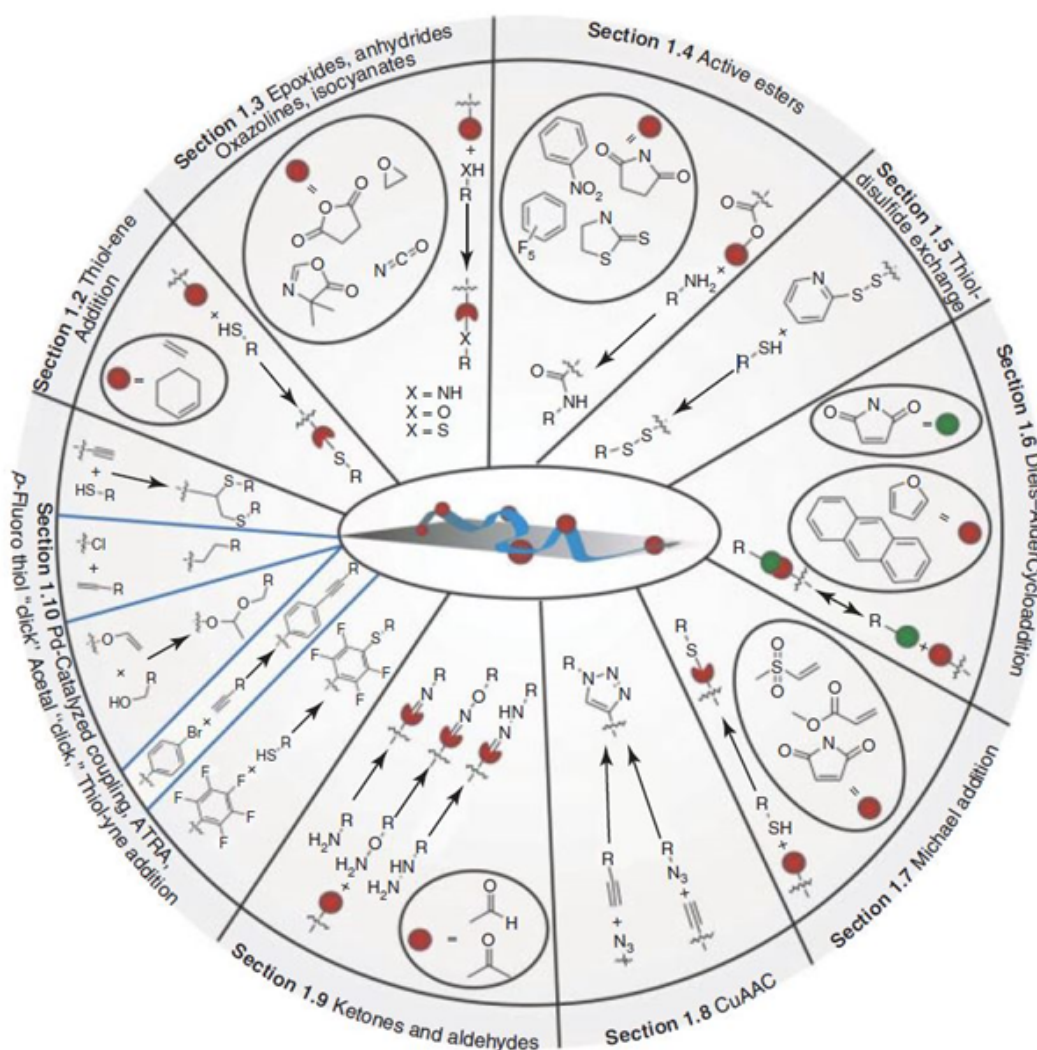


Figure 20. Classifications of post-polymerization modification methods. Reproduced with permission from Ref. ¹⁰⁸, Copyright 2013 Wiley-VCH Verlag GmbH & Co. KGaA.

As shown in Figure 20, the range of chemical reactions that can be used for post-polymerization modification is extremely broad. It shows the rapid and great development of post-polymerization modification methods and the potential that the methods can be expanded in the future. Active research on the development of new methods and applications with post-polymerization modification is continuously conducted.

1.5.1 Post-Polymerization Modification via Activated Esters

Activated esters belong to one of several representative groups that are able to covalently link with amines and result in stable amide bonds via post-polymerization modification. Since Ringsdorf and Ferruti reported polymers bearing activated ester groups in 1972, activated esters have been intensively studied and applied in a broad range of applications over the past decades.^{119,120}

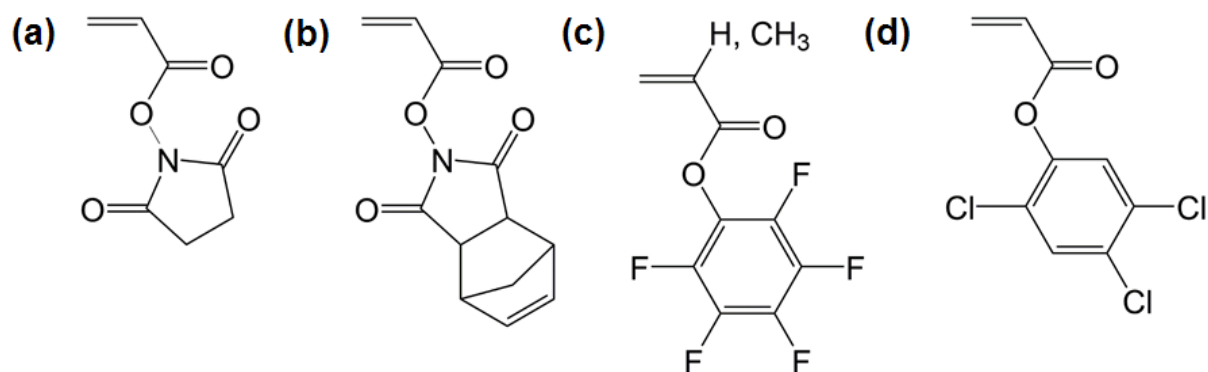


Figure 21. Activated ester monomers: (a) *N*-hydroxy succinimide acrylate (NHSA), (b) *endo-N*-hydroxy-5-norbornene-2,3-dicarboxyimidacrylate (NorbNHSA), (c) pentafluorophenyl acrylate (PFPA) and pentafluorophenyl methacrylate (PFPMA), and (d) 2,4,5-trichlorophenyl acrylate (TCP).

Some of the most frequently used well-suited activated ester monomers that have been deployed for the post-polymerization modification are shown in Figure 21: *N*-hydroxy succinimide acrylate (NHSA) (also called *N*-acryloxysuccinimide or *N*-succinimidyl acrylate), *endo-N*-hydroxy-5-norbornene-2,3-dicarboxyimidacrylate (NorbNHSA), pentafluorophenyl acrylate (PFPA), and pentafluorophenyl methacrylate (PFPMA), and 2,4,5-trichlorophenyl acrylate (TCP).^{99,104,121–125} NHSA has been used comprehensively as a macromolecular precursor for synthesis and polymerized to poly(*N*-hydroxy succinimide acrylate) (PNHSA),

which can react with amines and produce functionalized polyacrylamides. However, PNHSA has a limited solubility in only a few organic solvents; therefore, to improve the solubility of activated ester polymers, either copolymerization or the use of alternative activated ester was chosen.¹²⁶

As a replacement for the NHSA group, TCP, NorbNHSA, and PFP ester groups have been studied, and especially the PFP ester group shows great advantages. Poly(pentafluorophenyl acrylate) (PPFPA) and poly(pentafluorophenyl methacrylate) (PPFPMA) have an excellent solubility in general organic solvents, and the conversion with amines is generally quantitative without side reactions. In addition, the conversion reactions can be monitored by in-situ ¹⁹F NMR spectroscopy. One of the greatest advantage of PFP ester group is that the conversion occurs under mild conditions without a metal catalyst at r.t. Due to their noticeable advantages, activated ester polymers have been broadly applied broadly in polymer chemistry and material science.

1.5.2 The Use of Post-Polymerization Modification on Nano-Objects

1.5.2.1 Reactive Polymeric Nanorods

Polymeric nano-objects in 2D or 3D structures have been intensively studied and used for various applications.¹²⁷⁻¹³⁰ In addition, the fabrication methods have been improved and varied to meet the individual requirements. One of the most commonly used methods is a templating method deploying AAO templates.^{131,132} Various organic materials can be infiltrated into the pores of AAO templates by wetting of the desired materials or by precursors in melt or solution states. Due to the advantage of the AAO templates that the pore dimension can be easily tuned, the size and structures of the corresponding polymeric nano-objects can be varied by controlling the conditions of the AAO templates. Various researchers have comprehensively investigated the template wetting method for the fabrication of functional nano-objects.^{40,133-135}

In particular, Theato and coworkers introduced a new route for the fabrication of stimuli-responsive nanorods by combining of the template wetting technique with post-polymerization modification.¹³⁵ A highly concentrated activated ester monomer solutions with cross-linker and initiator were drop-casted onto the AAO templates and cross-linked by either UV light or heat,

depending on the type of initiator. Three kinds of activated ester monomers, namely PFPA, PFPMA, and pentafluorophenyl 4-vinyl benzoate (PFPVB) as well as two kinds of initiator, namely azobisisobutyronitrile (AIBN) as a thermal initiator and Lucirin TPO as a photo-initiator were used to produce the chemically modifiable nanorods. The resulting cross-linked activated ester nanorods were obtained by etching the sacrificial AAO templates with phosphoric acid. It is noteworthy that the hydrolysis of the ester which is unfavorable for the post-polymerization modification was observed when the etching of the AAO templates was conducted under basic conditions; therefore, phosphoric acid was used for further modification. The released bundles of activated ester nanorods were modified with isopropylamine via post-polymerization modification, and afterwards the temperature-responsive PNIPAM nanorods have been obtained. Due to the LCST property of PNIPAM in water, the dramatic changes in the size of the nanorods were observed in water, which were reversible upon heating above LCST or cooling below LCST of PNIPAM. These results show the great potential the stimuli-responsive nanorods have for their use as a drug delivery system, which is aimed at achieving an efficient reversible phase transition.

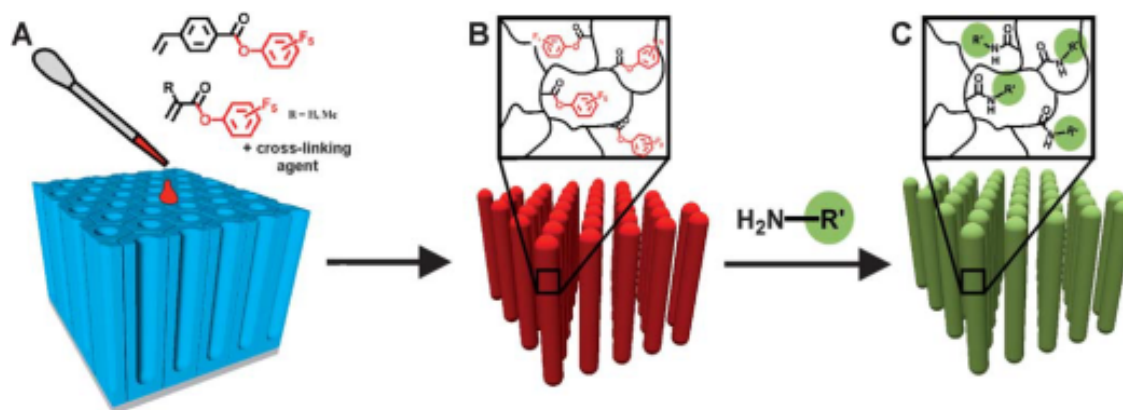


Figure 22. Schematic diagram of the template wetting method for the fabrication of reactive nanorods and their post-polymerization modification. Reproduced with permission from Ref.¹³⁵, Copyright 2011 Royal Society of Chemistry.

1.5.2.2 Functionalized Nanoparticles

Nanoparticles are one of the most studied nanostructure due to their accessible surface and the applicability in biological systems. Nanoparticles have been intensively studied for their usage as nanocarriers, and the nanocarriers have been improved to give an easily tunable architecture. Metallic nanoparticles can be tailored with polymer brushes through either a “grafting to” or a “grafting from” approach, and its covalent immobilization provides a robust attachment between the nanoparticle and the polymer brushes. In general, through the “grafting to” method, the desired polymer brushes can be densely grafted onto the surface of nanoparticles, and the different chemical functionalities, which are able to be chemically modified, can be applied.

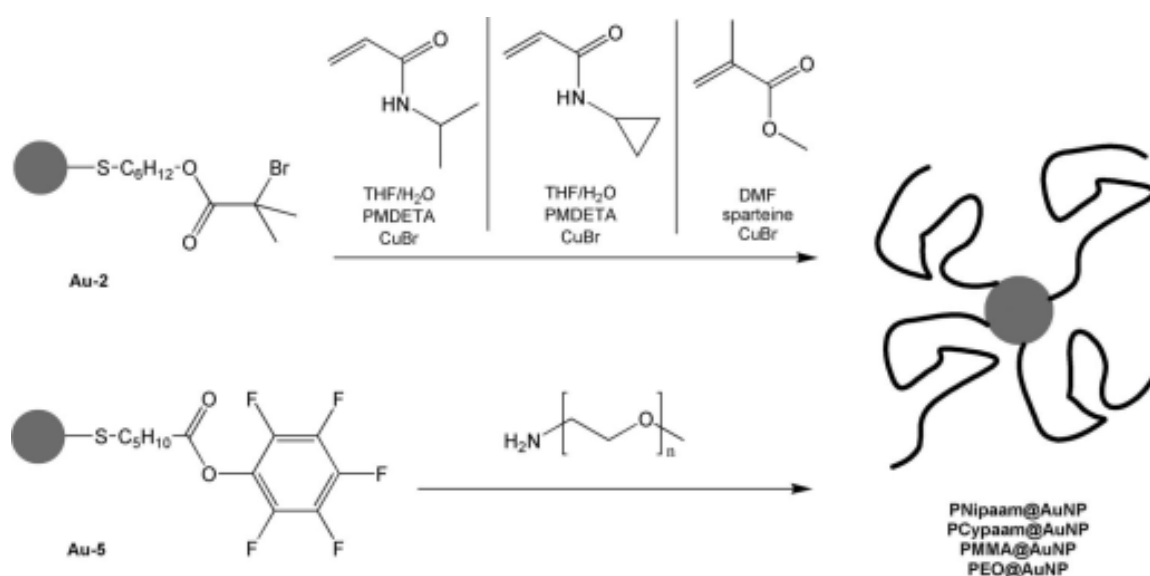


Figure 23. Schematic images of a grafting-from polymerization of NIPAM, CYPAM, and MMA from AuNPs stabilized with bis(6-hydroxyhexyl) disulfide bis(2-bromoisobutyl) ester; a grafting-onto polymerization of amino end-functionalized PEO onto AuNPs stabilized with bis(5-carboxypentyl) disulfide bis(pentafluorophenyl) ester. Reprinted with permission from Ref. ¹³⁶, Copyright 2008 American Chemistry Society.

As one example to be discussed here, Theato and coworkers fabricated chemically functionalized gold nanoparticles (AuNPs), and the prepared AuNPs were modified with amine via a post-polymerization modification method.¹³⁶ AuNPs were synthesized in an organic solvent (ethyl acetate and water) by a two-phase reduction method using disulfide and ester as stabilizing ligands.¹³⁷ Due to the disuse of the phase transfer agent for the preparation of AuNPs,

the AuNPs could be mildly reduced and the ligands could be grafted onto the surface of the AuNPs, resulting in a functionality suitable for the post-polymerization modification. Thus, for instance, the AuNPs using bis(5-carboxypentyl) disulfide bis(pentafluorophenyl) ester resulted in the pentafluorophenyl esters-functionalized AuNPs which were able to be modified with amine. Amino end-functionalized poly(ethylene oxide) (PEO) ($M_n = 550\text{g/mol}$) could be successfully grafted onto the pentafluorophenyl esters-functionalized AuNPs. Since the grafted PEO is hydrophilic, the AuNPs completely transfer from the organic phase to the water phase, and the transformation can be observed with the naked eyes. In the same manner, by employing bis(6-hydroxyhexyl) disulfide bis(2-bromoisobutyl) ester, the resulting AuNPs allow a surface-initiated atom transfer radical polymerization (ATRP) of methyl methacrylate (MMA), *N*-isopropylacrylamide (NIPAM), and *N*-cyclopropylacrylamide (CYPAM) on the surface of nanoparticles. The resulting stimuli-responsive polymer gold hybrids exhibited the plasmonic band of the gold core and the LCST property of the grafted polymer shell.

1.5.2.3 Functionalized Electrospun Polymer Fibers

Electrospinning is a well-known technique for the preparation of the multifunctional polymeric nanofibers.¹³⁸ By applying a high voltage between the syringe containing the polymer solution and the conductive collector, polymeric nanofibers can be collected on the surface of the collector. The spinning condition and the polymer concentration cause variations in the results regarding the morphology and the mechanical properties of polymeric fibers. The synthetic methodology has been developed and varied to meet the demands for various applications. Especially, the surface modification of nanofibers by grafting or interfacial polymerization has gained great attention due to its applicability and controllability on the surface. The surface modification can be conducted with different techniques, such as surface coating and grafting.

Theato and coworkers performed a thiol-ene post-polymerization modification on electrospun polybutadiene fibers.¹³⁹ In general, polymers having a higher glass transition temperature (T_g) than r.t. are readily solidified during the spinning process. In contrast, rubbery polymers, such as butadiene rubber, which has a low T_g typically below 0°C , do not form stable fibers under ambient conditions and there is the possibility that the fibers are chemically modified. In that manner, a solution of polybutadiene rubber containing cross-linker and photo-initiator in a

THF/DMF mixture was electrospun into a methanol solution containing 1% sodium chloride under *in situ* UV light irradiation. The resulting polybutadiene rubber fibers were chemically modified with 2-mercaptoethanol or thioglycolic acid after the complete purification of the resulting fibers. The carbon double bonds contained in the fibers reacted with thiol-groups via a thiol-ene click reaction, and this caused the change of wettability. A dramatic change of the static contact angle was observed on the chemically modified polybutadiene rubber fibers from 135° (electrospun polybutadiene rubber fibers) to 0° (modified fibers).

2. Scope and Objectives

The aim of this thesis is to fabricate various stimuli-responsive and chemically tunable nano-objects and nanostructured thin films by the template-assisted replication method using nanoporous AAO templates for surface engineering and for a drug delivery system. The main task is to develop a novel method for the fabrication of various shapes of nanostructures and to provide these nanostructures with advanced functionalities, such as stimuli-responsiveness or chemical modifiability. As shown in the introduction, the template-assisted replication method is highly advantageous for the fabrication of well-ordered functional nano-objects.

A modification of the anodization method should be performed in order to vary the shapes of templates and to produce their various replicated nanostructures, and a proper infiltration method should be chosen to successfully prepare the nanostructures which are to undergo further modification. For an effective infiltration, various methods, such as spin-coating, dipping, and a vacuum-assisted method should be applied and compared, and the choice of the proper solvent for a precursor solution should be considered. Consequently, the nanostructures should be released from the AAO templates by the wet etching method without causing structural damage. The post-polymerization modification should result in a change of functionality of the nanostructures so that the modified nanostructures react to an external stimulus.

Stimuli-responsive nanostructured thin films, which are selectively responsive to a specific stimulus, are desired to be obtained in order to control the wetting properties of surfaces or to release dye or drug by an external trigger. The feasibility of the concept should be verified by applying these stimuli-responsive nanostructures as a light-sensitive nanostructured surface or a drug delivery medium in surface engineering or bio-application. Moreover, the efficiency and capability of the concept should be compared with the one of non-structured objects, and the reusability of samples should be also tested.

3. Results and Discussion

3.1 Fabrication of Chemically Tunable, Hierarchically Branched Polymeric Nanostructures by Multi-branched AAO Templates*

*) This chapter is reconstructed based on a publication.¹⁴⁰

For decades, the fabrication of asymmetric polymeric nanopillars has gathered great attention due to their potential to control the wettability and adhesive properties of surfaces, which can be controlled by varying the shapes of nanostructures on the surfaces. Especially, biomimetic surfaces such as superhydrophobic surfaces¹⁴¹⁻¹⁴³, gecko-mimicking¹⁴⁴⁻¹⁴⁶, and dry adhesive surfaces¹⁴⁷⁻¹⁴⁹ have been studied intensively. In particular, the hierarchical nanopillars play an important role in adjusting the wettability and adhesive properties of surfaces. The complexity of structures causes a great change of wetting and adhesive properties of materials. Previous studies have shown that the nanostructures replicated from the complex, hierarchical AAO templates make the surfaces superhydrophobic.^{150,151} Various methods have been demonstrated to fabricate hierarchical nanopillars; however, these methods were limited to mimicking biological surfaces or variation of physical structures of nanopillars only.

In this study, chemically modifiable hierarchical poly(pentafluorophenyl acrylate) (PPFPA) nanostructures were fabricated by the template-assisted method with hierarchically branched AAO templates. A post-polymerization modification was applied subsequently to modify the surface of nanopillars with a light responsive molecule. Depending on the structures of the AAO templates, various corresponding shapes of PPFPA nanostructures, such as raspberry shape, flower shape, or branch shape, were fabricated and the individual hierarchical structures showed significantly differing wettability properties. Dynamic contact angle measurements were used to analyze the wettability properties.

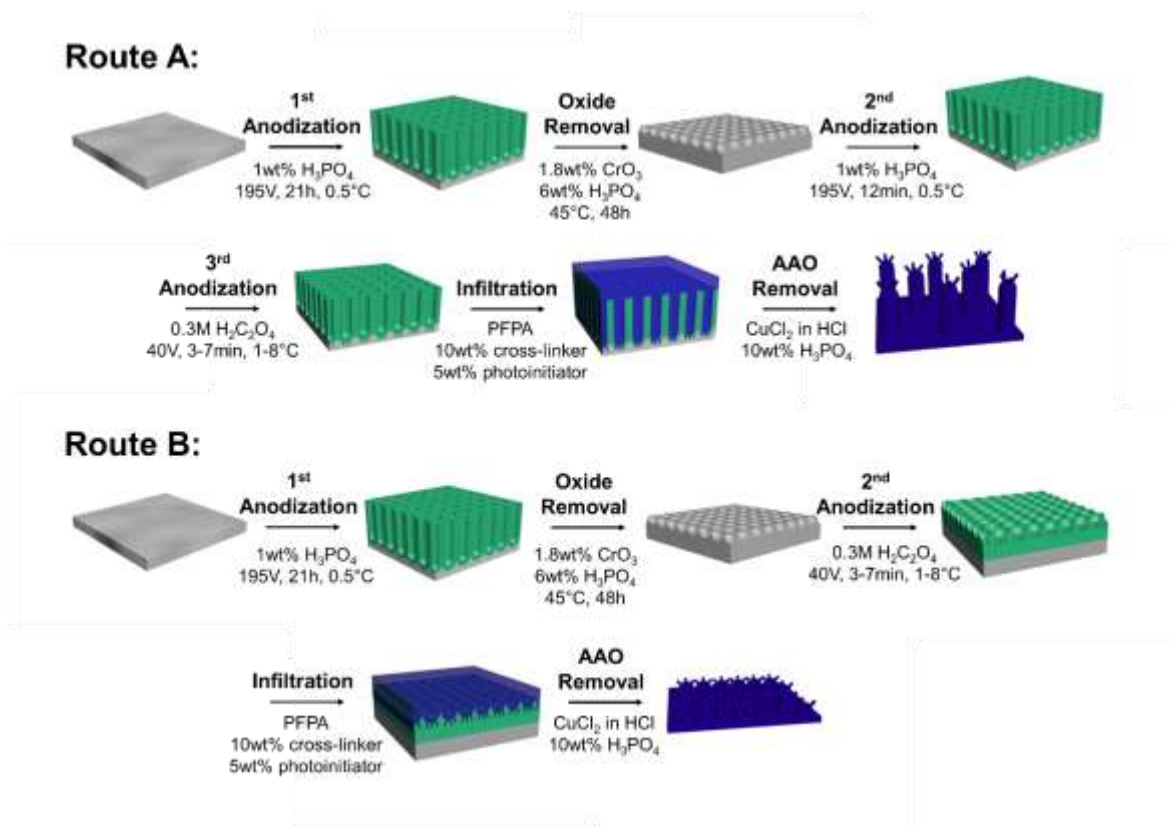


Figure 24. Schematic illustration of the fabrication of hierarchically branched polymeric nanostructures.

Chemically modifiable hierarchical PPFPA nanostructures were fabricated by the template-assisted method as shown in Figure 24. Two different routes were used to produce the different shapes of templates, which basically determined the structures of PPFPA nanopillars. Multi-branched AAO templates were fabricated by three successive anodization processes. Briefly, an asymmetric anodization was conducted via either route A or B on textured aluminum substrates, which had resulted from a first anodization step. To pursue route A, the second anodization was conducted in 1 wt% phosphoric acid electrolyte solution at 195 V for 12 min, and the barrier layer was subsequently thinned out by consecutive reduction of the applied voltage. To conduct further the anodization, the barrier layer was additionally thinned out by 10 wt% phosphoric acid solution under ambient conditions for 1 h. Figure 25 shows the side view of the templates before and after the thinning out processes, and it clearly shows that the barrier layer becomes thinner after the thinning out processes from ~140 nm to ~110 nm.

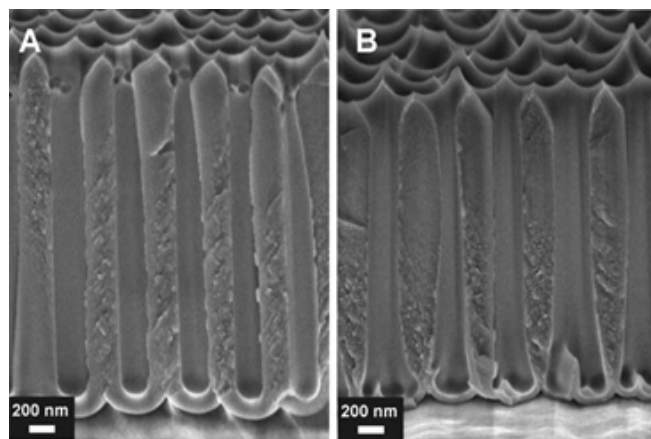


Figure 25. Cross-section SEM images of AAO templates before (A) and after (B) the thinning out procedure.

To produce the secondary branched pores, a third anodization was conducted in 0.3 M oxalic acid electrolyte solution at 40 V for 3 – 7 min. The resulting AAO templates exhibited secondary pores with a pore diameter of ~ 40 nm, as shown in Figure 26 (e). Afterwards, a PFPA monomer solution containing cross-linker (1,6-hexanediol diacrylate) and photoinitiator (TPO) was drop-casted onto the resulting hierarchically branched AAO templates and vacuum was applied to assist the infiltration of the PFPA monomer solution. The top of the templates was then covered by a surface-modified supporting substrate, and subsequently UV light (365 nm) was irradiated to photo-polymerize the PFPA monomer. As a last step, aluminum and aluminum oxide of the sacrificial AAO templates were removed by a 0.02 M $\text{CuCl}_2 \cdot \text{HCl}$ solution with an ice bath and 10 wt% phosphoric acid solution at 45 °C for 1 h, respectively. The released PPFPA nanostructures were then freeze-dried to prevent undesired aggregation or collapse of the polymeric nanostructures.

For route B, the second anodization step was conducted instead in 0.3 M oxalic acid electrolyte solution at 40 V for 3 – 7 min. The smaller subordinated pores (pore diameter of ~40 nm) were formed on hemispherical concaves (with a diameter of ~ 500 nm), as shown in Figure 26 (g). To support the infiltration of monomer solution, an additional pore widening process was conducted in 5 wt% phosphoric acid solution at r.t. prior to infiltration.

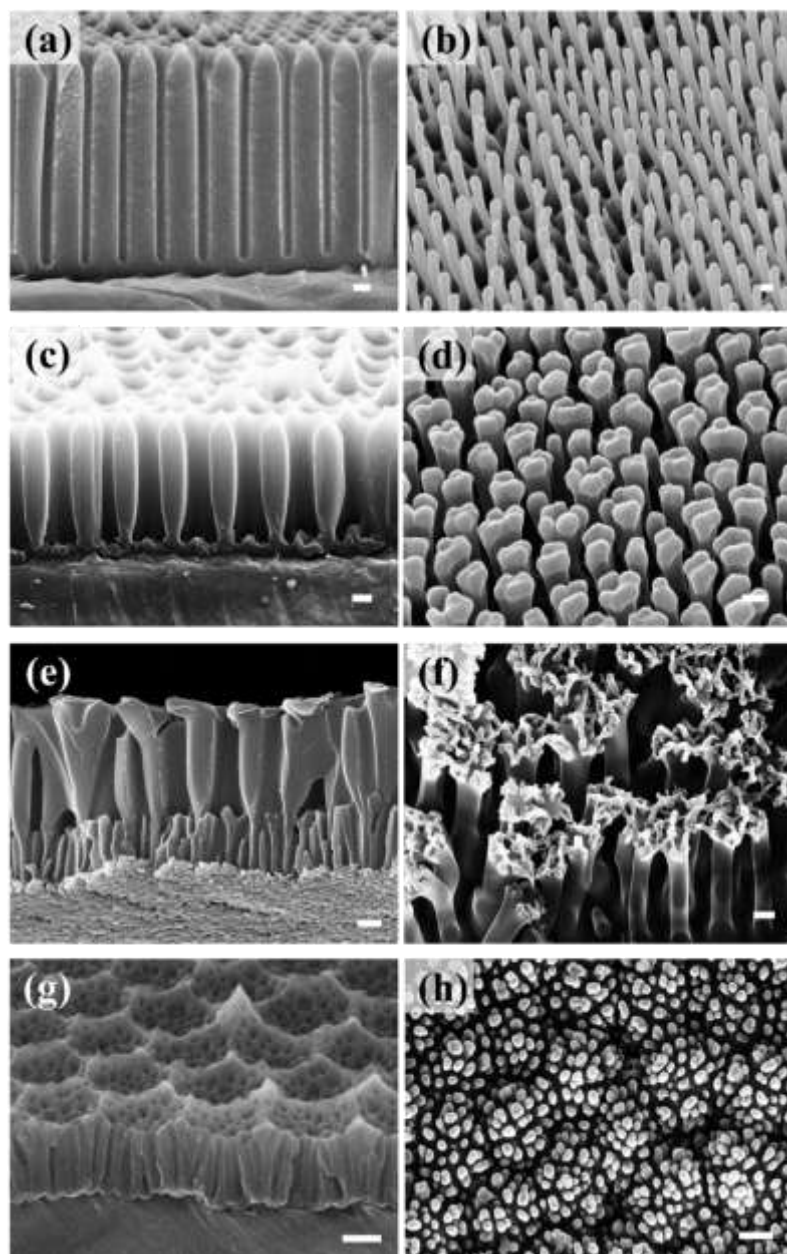


Figure 26. SEM images of standard and hierarchically branched AAO templates and the corresponding polymeric nanostructures: (a) standard AAO template, (b) free-standing regular PPFPA nanopillars, (c) branched AAO template fabricated via route A, (d) flower-shaped of PPFPA nanopillars, (e) two-tiered branched AAO template fabricated via route A, (f) branch-shaped of PPFPA nanopillars, (g) hierarchically patterned AAO template fabricated via route B, and (h) raspberry-like PPFPA replication (scale bar: 200 nm).

Various hierarchically branched AAO templates were successfully produced via these two different pathways. Either branch-shaped templates or raspberry-shaped templates were obtained via route A or B, respectively. Figure 26 shows the different shapes of AAO templates

and the resulting shapes of PPFPA nanostructures. As a reference structure, a conventional AAO template was fabricated by two-step anodization without further asymmetric anodization, and the free-standing PPFPA nanopillars (with a diameter of ~ 180 nm and a length of $1 - 2$ μm) were prepared (Figure 26 a and b). Just as the hierarchically branched nanostructures, the free-standing PPFPA nanopillars also underwent a freeze-drying step, which sublimates the water between the pillars and prevents the collapse of the pillars that is generally caused by the capillary forces of water. The hierarchically branched AAO templates via route A resulted in a flower shape (Figure 26 c) or a branched shape (Figure 26 e) of AAO templates by conducting the third anodization at 40 V and $1 - 8$ $^{\circ}\text{C}$ for 3 and 7 min, respectively. Furthermore, a raspberry shape (Figure 26 g) AAO template was prepared via route B by performing the second anodization at 40 V for 5 min. The PPFPA monomer solution was infiltrated into the resulted hierarchically branched AAO templates and photo-polymerized, followed by in situ polymerization. The corresponding PPFPA nanostructures are shown in panels d, f, and h of Figure 26. Depending on the shape of the templates, various shapes of nanostructures were successfully fabricated. It is worthy to note that different nanostructures can be fabricated using the same type of templates but varying the time of the asymmetric anodization. Figure 27 shows the replicated PPFPA nanostructures from the raspberry shape AAO templates, and the images show that the resulting shapes of nanostructures can be diverse by applying different lengths of anodization time.

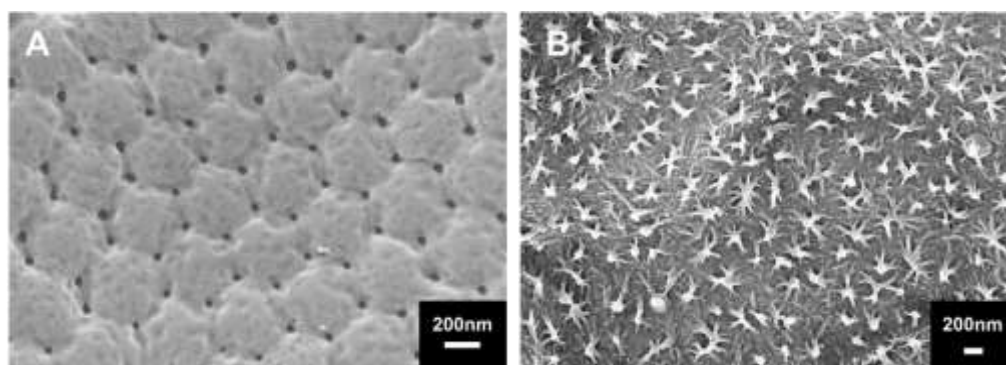
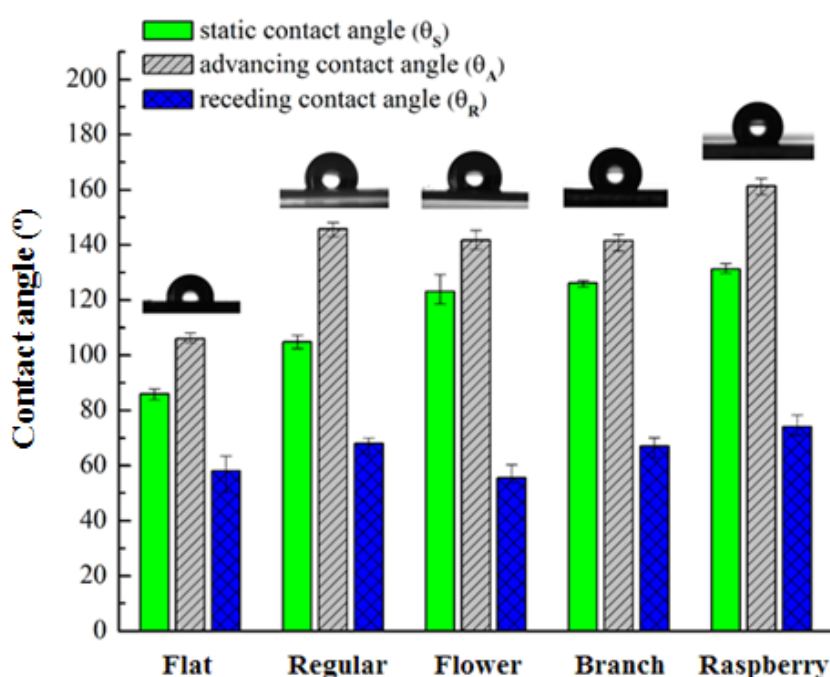


Figure 27. SEM images of PPFPA nanostructures produced by the AAO template fabricated via route B: (a) second anodization for 3min at 40V and (b) second anodization for 7min at 40V.

The surface wettability of hierarchically branched PPFPA nanostructures was investigated by dynamic contact angle measurement with water droplets, since the surface roughness and heterogeneity could cause a contact angle hysteresis, advancing and receding contact angles

were measured to precisely study the surface properties. It is known that the domains hinder the motion of water droplets and cause an increase in the advancing contact angle and a decrease in the receding contact angle.¹⁵² Hence, for the characterization of the dynamic wetting, the advancing contact angle θ_a and the receding contact angle θ_r which indicate the maximum expanding and contracting angles of the water droplets were measured. For instance, flower-shaped of PPFPA nanopillars show the advancing contact angle (141.7°) and the receding contact angle (55.6°), while the static contact angle is 123.1°.



	Flat	Regular	Flower	Branch	Raspberry
Static CA (deg)	86.0	104.9	123.1	126.3	131.3
Increment from Flat surface (%)	0	22.0	43.1	46.8	52.7
Advancing CA (deg)	106.0	145.9	141.7	141.6	161.4
Receding CA (deg)	58.0	68.0	55.6	67.1	74.0
CA hysteresis (deg)	47.9	77.9	86.1	74.5	87.4

Figure 28. Static, advancing and receding contact angles for the PPFPA thin film and the PPFPA nanostructures shown in Figure 26 (b), (d), (f), and (h), including the photographs of a water droplet on the respective surfaces.

The results of dynamic contact angle measurements showed that the shapes of nanostructures determine the contact angles, and the changes of the contact angles were dramatic. Compared to a smooth PPFPA thin film, the nanostructured surfaces having different morphologies generally had higher contact angles. A prominent contact angle hysteresis, which depicts the

difference between the advancing angle and the receding angle, was observed for the hierarchically nanostructured surfaces due to their roughness. Wenzel's hydrophobicity mode can explain this phenomenon, because the increment of surface roughness increases the contact interface area and causes the hindrance of the movement of water droplets and hence the increase of the contact angle hysteresis.¹⁵³ The raspberry shape of the nanostructures shows the largest hysteresis ($87.4 \pm 7^\circ$) and the highest static contact angle ($131.3 \pm 3^\circ$) among the various shapes of nanostructures, and the static contact angle increases even up to $\sim 53\%$ compared to the contact angle of a flat surface (Figure 28).

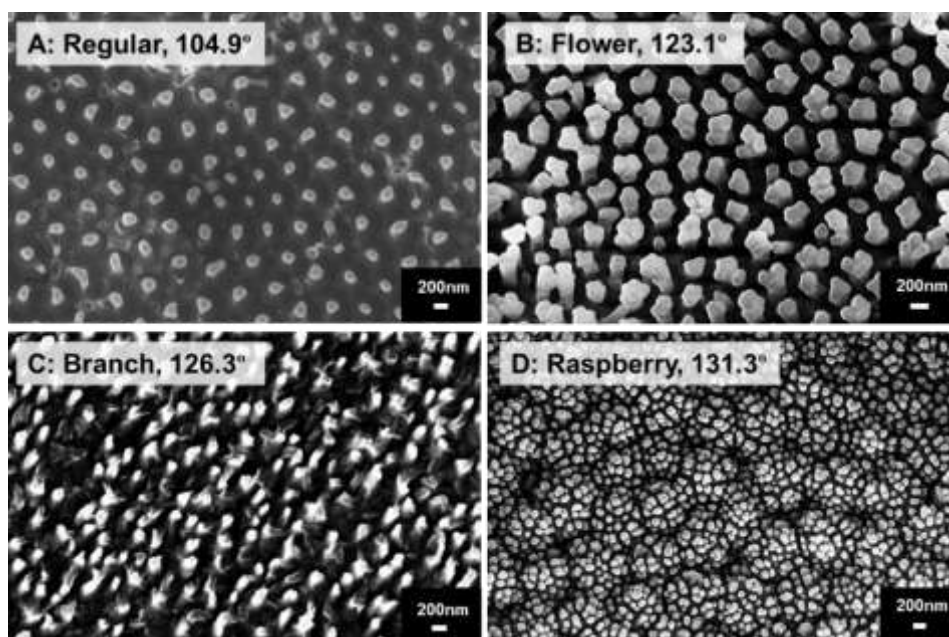


Figure 29. Top view SEM images of surface of the nanopillars: (a) free-standing nanopillars, (b) flower shape nanopillars, (c) branched shape nanopillars, and (d) raspberry shape nanopillars with the corresponding static contact angle.

To evaluate the correlation between the surface roughness and the wetting properties, the top view SEM images of each structure and the corresponding structure's static contact angles are compared. As shown in Figure 29, the contact angle increases with the roughness of the surface which fits the expectation that the nanostructures induce the surface to be more hydrophobic. The branched shape of nanostructures having thinner secondary pillars on the top surface of the nanopillars shows a higher static contact angle ($126.3 \pm 2^\circ$) compared to the free-standing nanopillars ($104.9 \pm 5^\circ$) and the flower shape nanopillars ($123.1 \pm 10^\circ$), where no secondary pillars are formed on the head of the nanopillars. The result supports the fact that the advancement of the structural complexity makes the surfaces more hydrophobic.

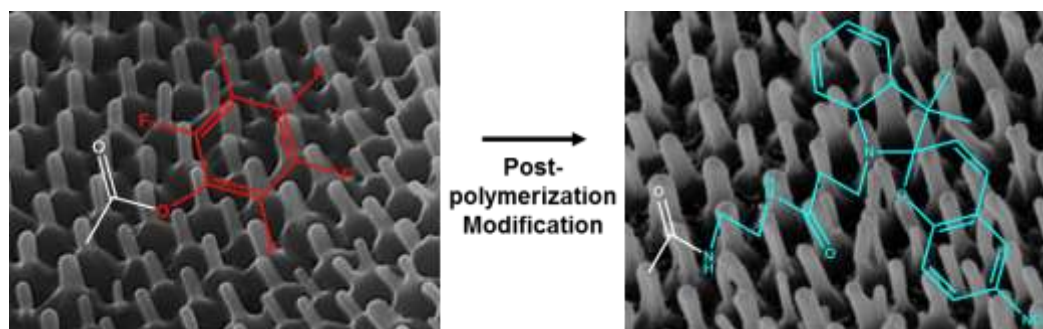


Figure 30. Schematic illustration of post-polymerization modification with activated ester to spiropyran-amine, and the SEM images of nanostructures before and after modification.

All of the PPFPA nanostructures were then chemically modified via the post-polymerization modification method. Based on the established activated ester – amine chemistry, the pentafluorophenyl ester group (PPFPA nanostructures) was substituted with the amine group of a UV light responsive spiropyran amine, as shown in Figure 30. In this experiment, a UV light-responsive spiropyran amine as a photochromic dye was used, because the light-responsive surfaces can easily convert their surface properties without water contact which can cause the collapse of nanopillars.

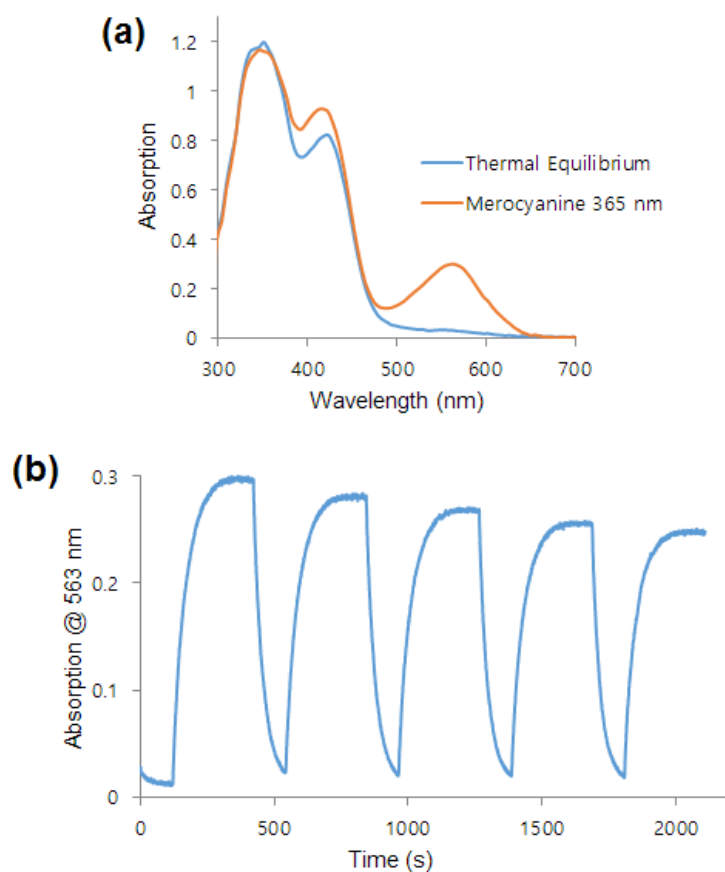


Figure 31. (a) UV-vis spectrum of spiropyran-amine before and after UV light irradiation at 365 nm, and (b) absorbance change of spiropyran-amine (0.1 mM) at 563 nm upon alternating irradiation with UV light (365 nm) and visible light (563 nm).

The reactivity of spiropyran amine upon UV light was studied as well as its switching behavior. As shown in Figure 31 (a), relatively nonpolar spiropyran converted into a polar, zwitterionic merocyanine form upon UV light irradiation at 365 nm, and a characteristic absorption peak of merocyanine was observed at 563 nm. In addition, a stable and reversible photo-switching behavior of spiropyran amine was observed, as shown in Figure 31 (b).

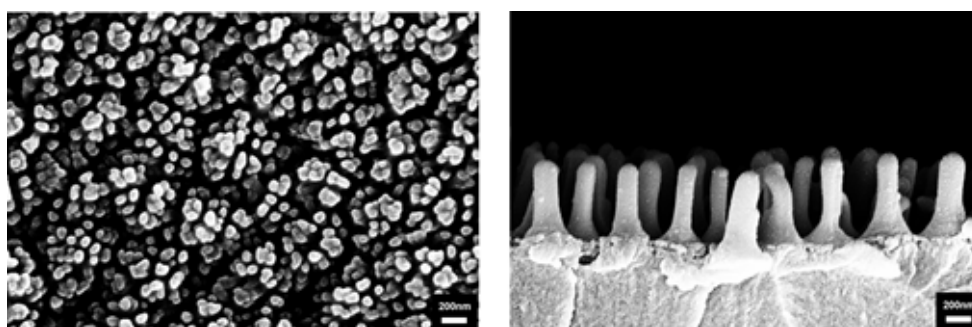


Figure 32. Top-view SEM images of spiropyran-modified raspberry shape nanostructures and cross-section SEM image of spiropyran modified regular nanopillars (scale bar: 200 nm).

Post-polymerization modification was conducted by immersing the PPFPA nanostructures in 5 wt% spiropyran amine solution in methanol for 18 h at r.t. SEM images in Figure 32 show that the nanopillars have the same structure as in the initial state, even after the modification step. To eliminate the capillary force effect, all the samples were freeze-dried after post-polymerization modification.

To prove the conversion of the pentafluorophenyl ester group into the spiropyran-bound amide group, FT-IR spectroscopy was measured. As shown in Figure 33, the FT-IR spectra displayed the decrease of the PFP ester signal at 1783 cm^{-1} and also the increase of the N – H bending vibration signal and the C = O amide stretching vibration signal at 3306 and 1650 cm^{-1} , respectively. The FT-IR spectra show an incomplete conversion. It was assumed that the PPFPA nanostructured thin film which was chemically bound to a PET film was not able to be fully swollen and it caused the incomplete conversion. The chemical change could also be observed with the bare eyes by color changes from yellow to violet under UV light irradiation at 254 nm. The inserted pictures in Figure 33 show the color changes of a sample before and after irradiation. To induce the photo-isomerization of spiropyran on the nanopillars, UV light at 254 nm was used instead of 365 nm according to the procedure described in the literature.^{154–156} It was found that the photo-isomerization was induced at both wavelengths.

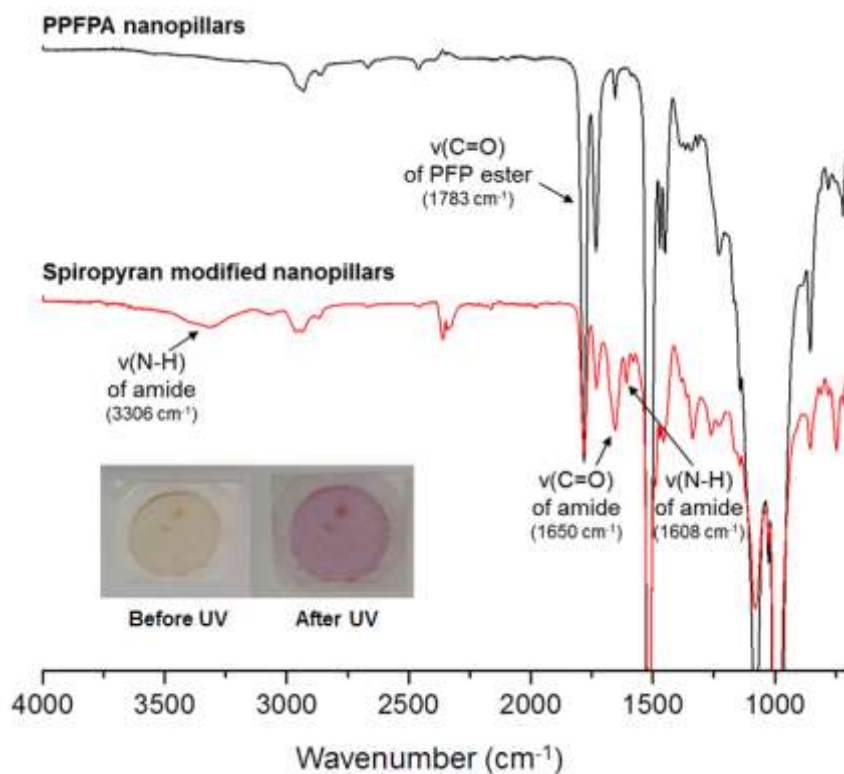


Figure 33. FT-IR spectra of free-standing nanopillars before and after post-polymerization modification.

As shown in Figure 34, the contact angles of all shapes of nanostructures decreased after post-polymerization modification due to the substitution of surface-bound functional groups from the hydrophobic pentafluorophenyl groups to relatively hydrophilic spiropyran amine groups. Moreover, the contact angles decreased further as a result of the photo-isomerization of spiropyran by UV light irradiation at 254 nm. In general, photo-induced isomerization accompanies a large change of dipole moment that affects surface free energy. As a result, change of wettability of functionalizing surfaces with photochromic dyes is caused. The free-standing spiropyran-modified nanopillars showed the greatest change of contact angles from $101.2^\circ \pm 10^\circ$ to $87.3^\circ \pm 10^\circ$ which is a 15.92% reduction of the values before and after UV light irradiation.

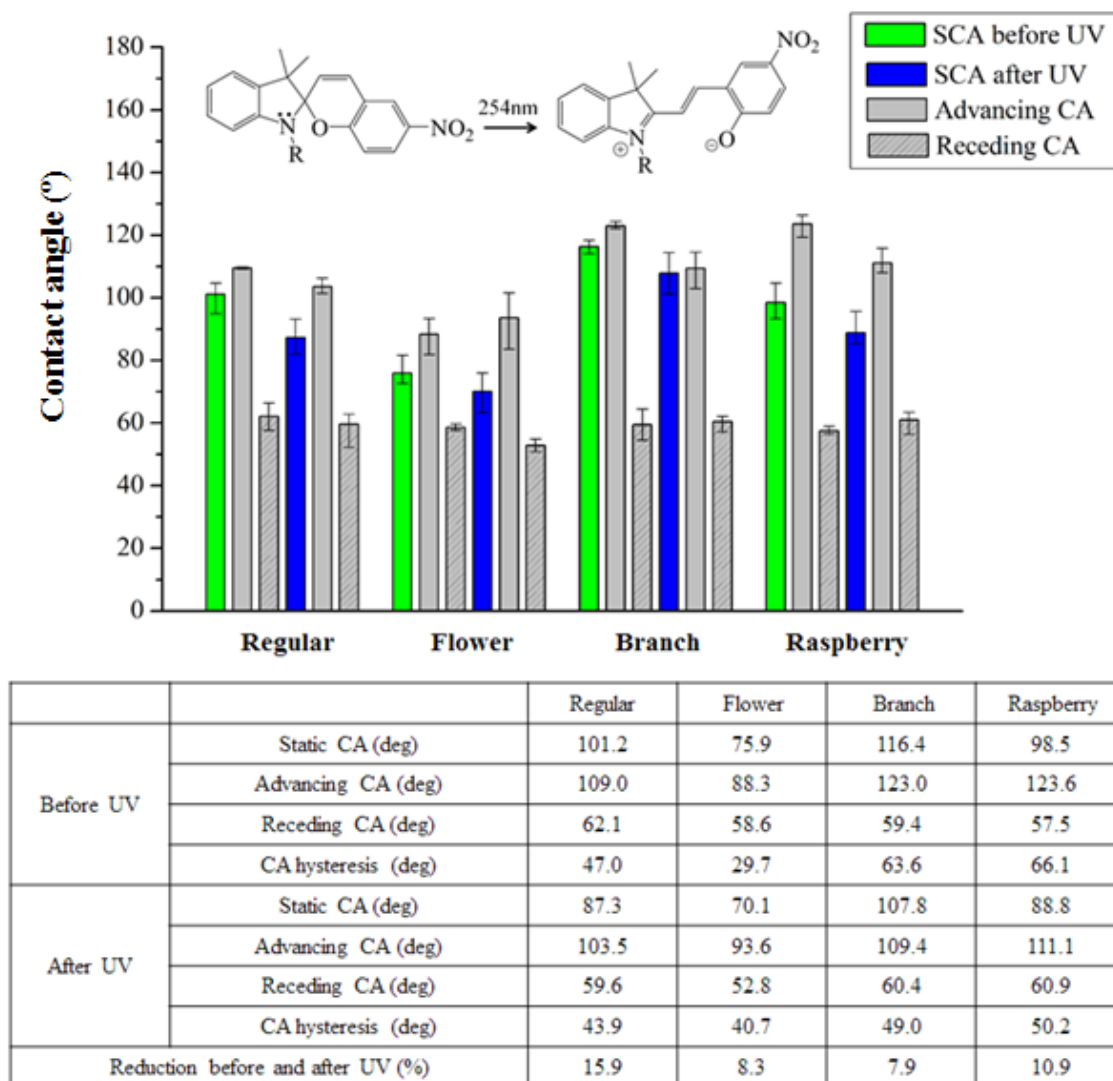


Figure 34. The static, advancing, and receding contact angles of spiropyran modified nanostructures before and after UV light irradiation and the reduction percentage of static contact angles before and after UV light irradiation. The change of the chemical configuration of spiropyran upon UV light irradiation is presented as an insert.

To verify the effect of surface modification on the surface wetting, the raspberry shape PPFPA nanostructured film was modified with isopropylamine via post-polymerization modification to generate a temperature-responsive surface. Identical raspberry shape of samples were fabricated simultaneously, to eliminate any structural effect. The raspberry shape PPFPA nanostructured film was immersed into a 3wt% isopropylamine solution in dry methanol for 5min and washed with sufficient methanol. FT-IR spectroscopy was conducted to confirm the chemical modification. As shown below, the amide band from the substituted isopropylamine group appeared and the PFP ester band decreased. This proved that PPFPA had been converted

into temperature-responsive poly(N-isopropylacrylamide), although the conversion was not fully completed. It was assumed that the reason for the incomplete conversion was the same as in the PPFPA nanostructured thin film when it was modified with spiropyran amine.

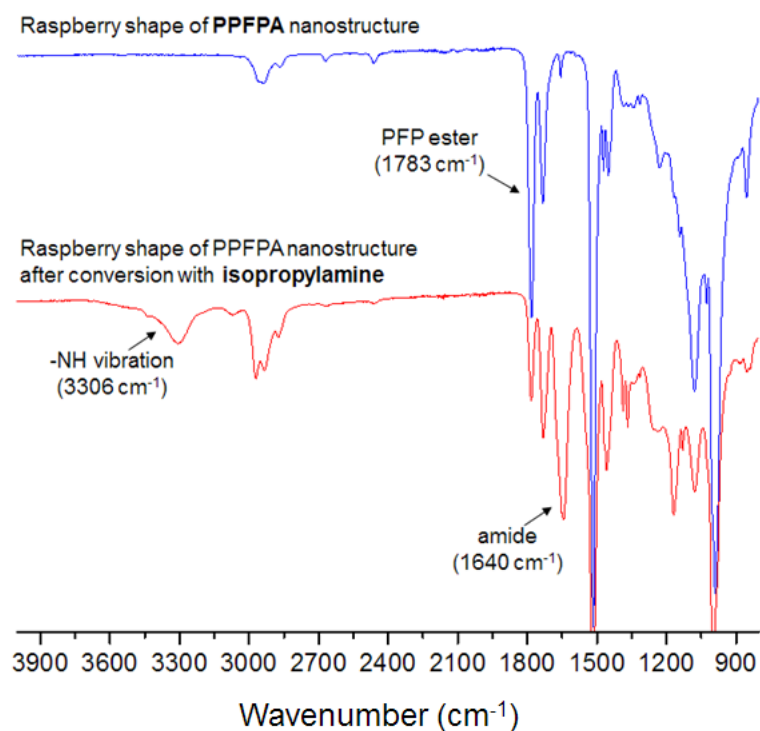


Figure 35. IR spectrum of raspberry shape of PPFPA nanostructure before and after post-polymerization modification with isopropylamine.

It is known that the surface covered by PNIPAM becomes hydrophobic by heating it up to a temperature above the LCST of PNIPAM. The raspberry shapes of the PNIPAM nanostructures on a surface showed the same trend, namely that the static contact angle increased by heating it up to a temperature of 50 °C which is an arbitrary temperature above the LCST of PNIPAM (~ 32 °C).

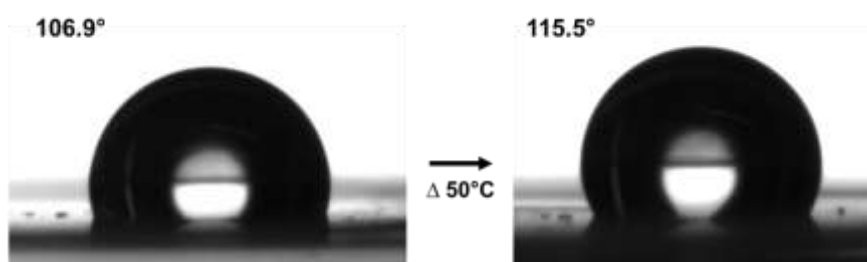


Figure 36. Static contact angle of the raspberry shape PNIPAM nanostructure before and after heating.

It was observed that the static contact angle decreased after post-modification since the hydrophobic pentafluorophenyl group was substituted with hydrophilic isopropylamine (PPFPA 131.3° to PNIPAM 106.9°). However, the contact angle increased to 115.5° by heating due to the chemical nature of PNIPAM. This result is contrary to the results of spiropyran, which becomes hydrophilic upon stimulation. This shows that the chemical surface modification affects the wetting property of surfaces. As a result, both the surface structure and the surface modification have a significant influence on the wetting property of surfaces. The increase of the complexity of the structure enhances the hydrophobicity, and the surface modification alters the chemical nature of the structure and makes the wetting property tunable.

It is already known that spiropyran can be switched back to the initial state by visible light irradiation at a wavelength range of 400 – 700 nm, heating, or keeping the sample in the dark (cessation of UV light).^{154,157,158} To verify the retention of spiropyran, the static contact angles were measured repeatedly after UV light irradiation and keeping the sample in the dark for 24 h. As shown below, the contact angle decreased by UV light irradiation and increased after recovering in the dark (cessation of UV light).

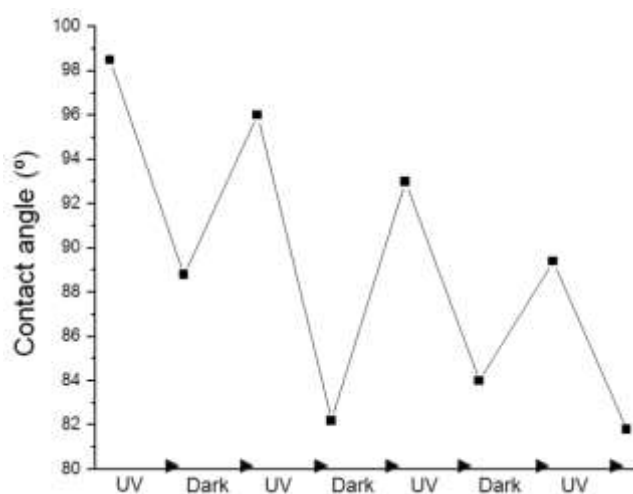


Figure 37. Wettability switching cycles upon UV light irradiation and the cessation of UV light (20min irradiation with $\lambda = 254\text{nm}$; 24 h in the dark).

As shown in Figure 37, the wettability was switched upon UV light irradiation and the cessation of UV light; however, it was found that the wettability was not fully recovered. This phenomenon is called a photofatigue.^{89,156} Due to the undesired hydrolysis of merocyanine form, hydrolytic degradation is caused and the wettability cannot be fully recovered. An acute photofatigue is observed in this case, and it was assumed that the numerous repetitions of the

contact angle measurement caused the photofatigue. While measuring contact angles, the sample cannot avoid the contact with water. Especially, the contact of merocyanine and water after the isomerization is critical. Nonetheless, the visible switching behavior could be observed for the short cycles. All these results showed that the wetting properties of the surfaces containing various nanostructures can be controlled by applying the post-polymerization modification method, even on complex structures, and it shows the great potential of our approach which can be extended to a wide range of stimuli-responsive materials.

3.2 Drug Releasable Nanostructured Poly(*N*-vinylcaprolactam) Thin Films

Stimuli-responsive polymers have been widely applied in the biomedical applications, such as controlled drug delivery systems and bio-sensing application.^{61,159–163} In specific, the polymers reactive to pH or temperature have gathered a great attention because human body has different pH along the body and a specific body temperature.¹⁶⁴ Thermosensitive polymers, such as poly(*N*-isopropyl acrylamide) (PNIPAM) and poly(*N*-vinylcaprolactam) (PNVCL), have their critical temperature close to human body temperature, therefore these polymers have been applied for drug delivery systems. However, PNIPAM can only be used to a limited extent, since PNIPAM produces toxic amine compounds via hydrolysis.^{76,165} Unlike PNIPAM, PNVCL generates no side products and shows biocompatibility and low toxicity.^{166,167} Due to these properties, various drug delivery systems have recently adopted PNVCL in their systems.^{78,168,169} However, most of studies have been conducted using PNVCL in the forms of hydrogel without a confined structure. In this study, thermosensitive nanostructured PNVCL thin films were fabricated as a drug delivery medium with an advanced complexity and a significantly larger area, thereby improving the effectiveness of drug delivery.

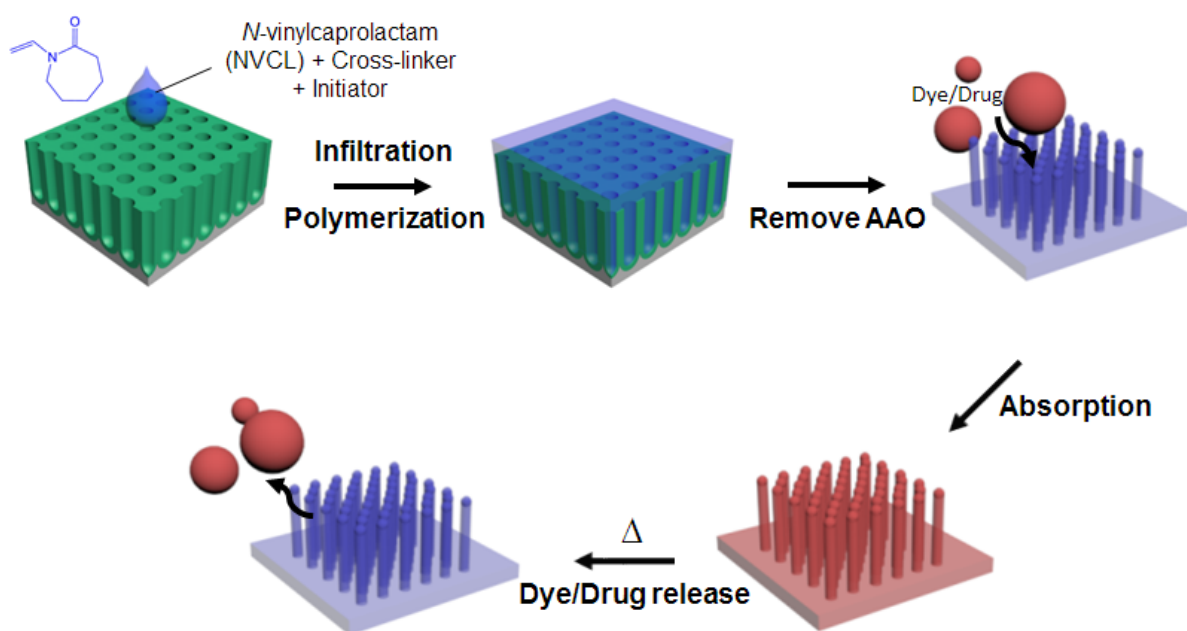


Figure 38. Schematic illustration of the fabrication of dye or drug releasable nanostructured PNVCL thin films.

The template replication method using AAO templates was used to prepare nanostructured PNVCL thin films. As shown in Figure 38, an NVCL solution containing cross-linker (1,6-hexanediol diacrylate) and photo-initiator (TPO) was infiltrated into an AAO template fabricated by a conventional two-step anodization and polymerized by UV light (365 nm). Subsequently, the sacrificial AAO template was removed by acidic solution. The prepared nanostructured PNVCL thin films were then tested to adsorb either a fluorescent dye (rhodamine B) or a potent drug (aspirin) under ambient conditions. The thin films were immersed into the dye or drug solutions, and the adsorption of the respective solution was monitored for up to 24 h. Afterwards, the thin films were gently washed with DI-water in order to remove any residue that might have been left on the surface of thin films and submersed in pure DI-water to observe the release of dye or drug upon heating.

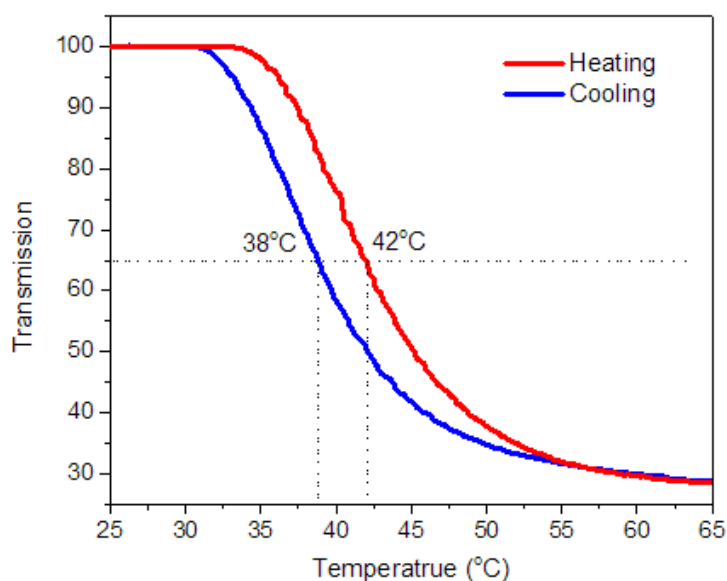


Figure 39. LCST hysteresis curves of PNVCL.

It is well-known that PNVCL has LCST which can be used as a trigger to release a drug upon heating.^{168–170} To analyze the range of temperature that could release dye or drug, the LCST of PNVCL was measured. An NVCL solution containing only photo-initiator (TPO) was spin-coated and polymerized on an identical aluminum chip, which was used for the fabrication of AAO templates. Subsequently, PNVCL was dissolved in DI-water with the support of sonication, and the obtained solution was heated up to 65 °C. As shown in Figure 39, the

PNVCL solution (conc. 1 mg / 3 mg in DI-water) shows an LCST around 42 °C and the range of temperature, in which PNVCL is responsible, ranges from 35 to 65 °C. To verify the applicability of the nanostructured PNVCL thin films as drug delivery medium, the release of dye or drug was observed at an average human body temperature (36 °C) and at a high temperature (50 °C).

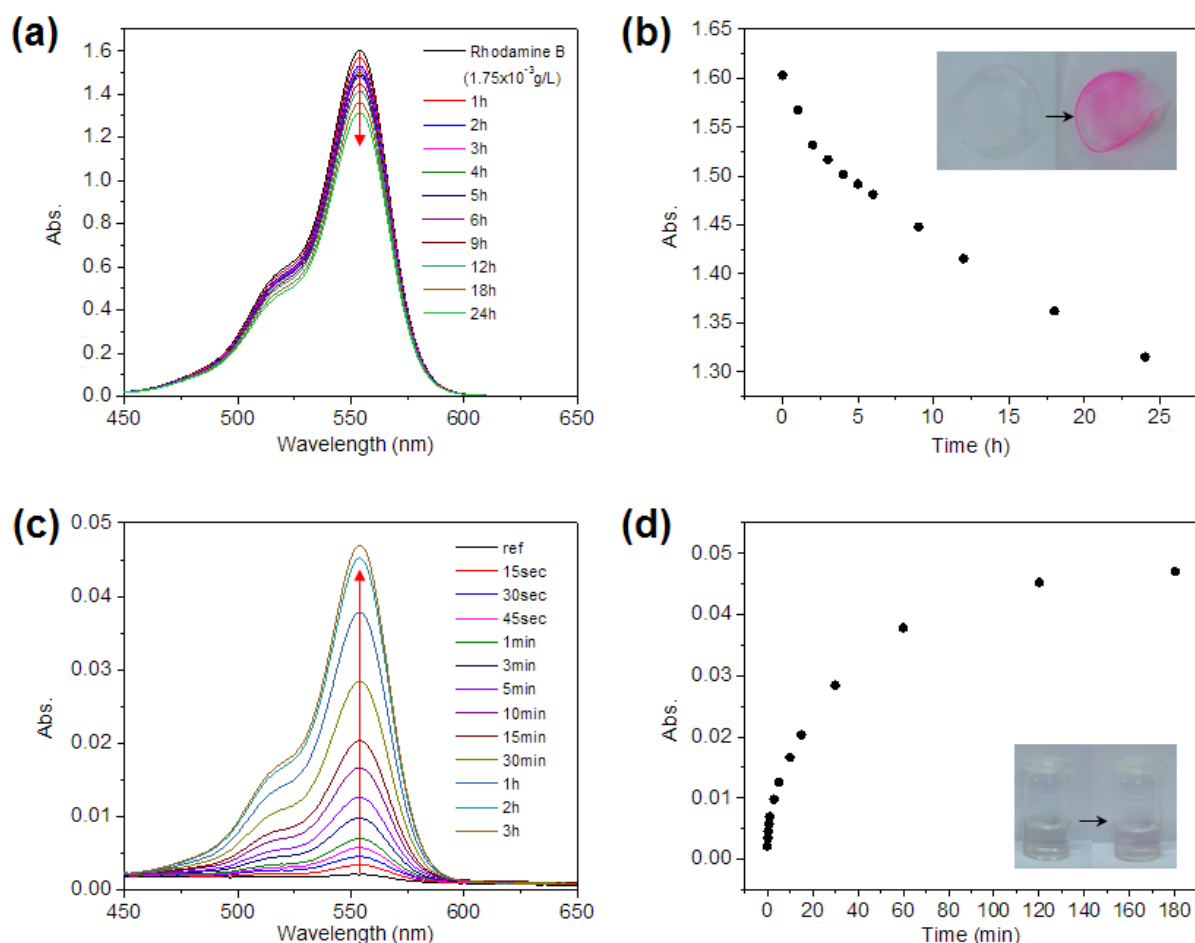


Figure 40. UV-vis spectra for time-dependent (a) adsorption and (c) release of rhodamine B under ambient conditions and when heated to 36 °C, respectively. Extracted adsorption (b) and release (d) peaks at 554 nm wavelength. Inset: photographs of the PNVCL thin film before and after adsorption of rhodamine B, and the DI water solution before and after the release of rhodamine B.

The adsorption of rhodamine B was monitored by UV-vis spectroscopy and recorded as shown in Figure 40. The nanostructured PNVCL thin film was submerged in an aqueous solution of rhodamine B (conc. 1.75×10^{-3} g/L) and vigorously stirred at r.t. The UV-vis spectra show a characteristic absorption peak of rhodamine B at 554 nm and the decrease of this

absorption peak, since the PNVCL thin films adsorb the dye with time. Figure 40 (b) exhibits the extracted points at 554 nm which clearly show the decrease and a distinct color change of the PNVCL thin film from transparent to pink. After the adsorption of dye for 24 h, the PNVCL thin film was gently washed and dipped into pure DI-water. Subsequently, the water containing the PNVCL thin film was heated to 36 °C, and the release of rhodamine B from the thin film to water was recorded. It was observed that the hydrophilic rhodamine B tended to be released from the thin film to water, since PNVCL converted to a hydrophobic state upon heating due to its LCST. As a consequence, the increase of absorption peak of rhodamine B at 554 nm was observed, and the color of water was also changed to pink due to the release of rhodamine B. These results apparently show the potential of the nanostructured thin film as a drug delivery medium that can load the potent drug and release it at a target point.

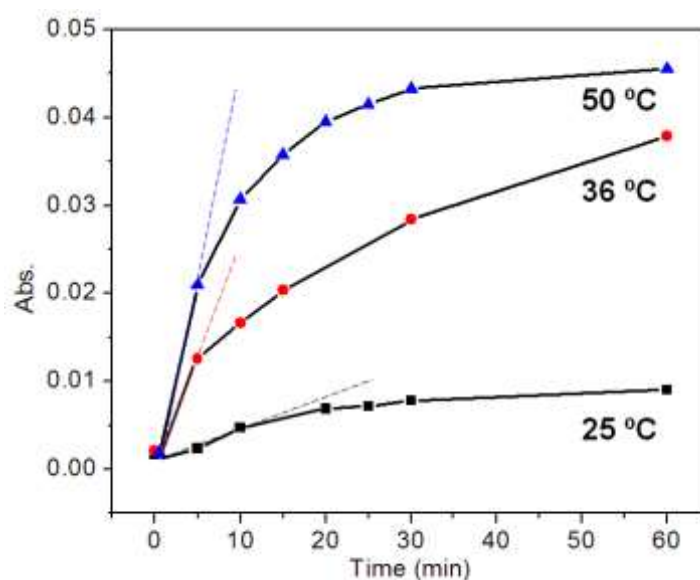


Figure 41. Comparison of the amount of released dye upon heating at different temperatures.

The nanostructured PNVCL thin films with the adsorbed dye were heated at different temperatures to compare the amount of dye released. As a reference, the release of dye was observed at r.t. without heating. As shown in Figure 41, the absorption peaks increased upon heating with accumulation of the amount of dye released to DI water, unlike the reference sample showed an inferior increment. The thin film heating at 50 °C showed a larger gradient in the initial state of heating compared to the one heated at 36 °C or to the one without heating due to the greater change of polarity. The result also showed that the absorption peaks increased with reducing speed until a saturation point. It might be because of an intrinsic problem that

the thin film releases a small amount of dye without heating or due to relatively high cross-linking density of the thin film.

Moreover, an enhancement of the adsorption and release of dye by increasing the surface area was verified by the comparison in the nanostructured PNVCL thin film and the non-structured flat PNVCL thin film. A flat PNVCL thin film was fabricated on the round aluminum chip (d: 1.3 cm), followed by spin-coating and polymerization of the NVCL solution. To precisely compare the nanostructured surface and the non-structured surface, the area of both surfaces were calculated. In case of the non-structured thin film, the surface area should be equal to the one of the aluminum chip, therefore, the equation for the area of a circle (πr^2) was applied and the area of the non-structured thin film was calculated to be **1.327 cm²**. For the calculation of the area of the nanostructured thin film, the overall surface area of the nanostructures should be considered, thus, the surface area of the individual nanostructures was summed up and added as follows.

Pore density of the AAO template fabricated by phosphoric acid: **5 x 10⁸ pores/cm²**

Surface area of the aluminum substrate (d=1.3cm): **1.327 cm²**

From these, the number of pores that one AAO template has can be calculated:

$$5 \times 10^8 \text{ pores/cm}^2 \times 1.327 \text{ cm}^2 = \mathbf{6.633 \times 10^8 \text{ pores.}}$$

The open surface area of one nanopillar standing on a surface (radius: 20nm, length: 200nm) = $2\pi rh + \pi r^2 = \mathbf{2.638 \times 10^{-10} \text{ cm}^2}$.

Therefore, the total surface area of nanostructured thin film can be calculated as follows.

The area of aluminum substrate + {(the number of pores) x (the surface area of one nanopillar)} – the overlapped surface area below the nanopillars = $1.327 \text{ cm}^2 + \{(6.633 \times 10^8) \times (2.638 \times 10^{-10} \text{ cm}^2)\} - \{(6.633 \times 10^8) \times (0.126 \times 10^{-10} \text{ cm}^2)\} = \mathbf{1.494 \text{ cm}^2}$.

The results of these experiments clearly show that the nanostructured thin film has a larger surface area (1.494 cm²) than the non-structured thin film (1.327 cm²). The bigger area of surface allowed the nanostructured thin film to have an improved adsorption and release of dye, as shown in Figure 42.

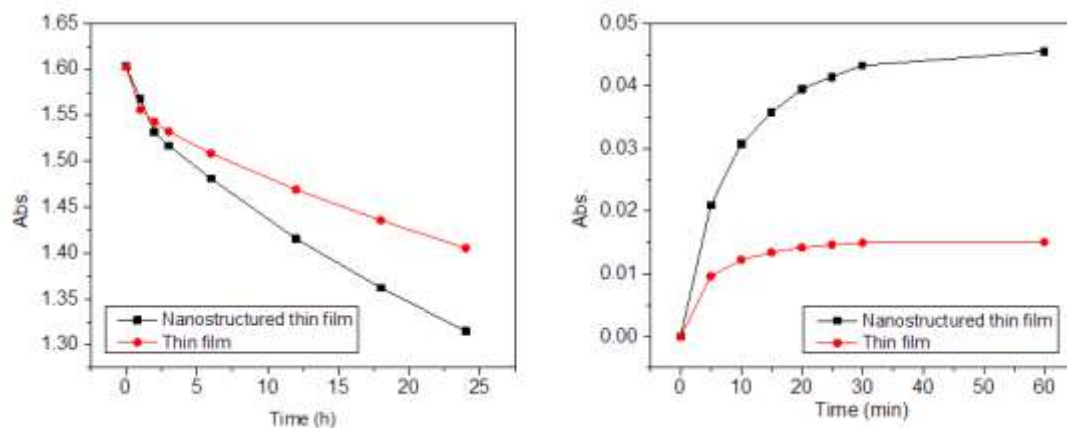


Figure 42. Comparison of adsorption (a) and release upon heating at 50 °C (b) of rhodamine B between the nanostructured PNVC thin film and the non-structured PNVC thin film.

Furthermore, a study on the adsorption and release of dye depending on the extent of cross-linking of thin films was conducted to compare the effect of cross-linking. A highly cross-linked nanostructured PNVC thin film was fabricated using the identical method by which the other thin films were fabricated by applying twice the amount of cross-linker (30 wt%), and their adsorption and release of dye were compared with a less cross-linked nanostructured PNVC thin film (15 wt%), as shown in Figure 43. The less cross-linked thin film showed an improved adsorption and release, which are more desirable in the drug delivery system; therefore, the less cross-linked thin films are utilized as the drug delivery medium in the following experiments.

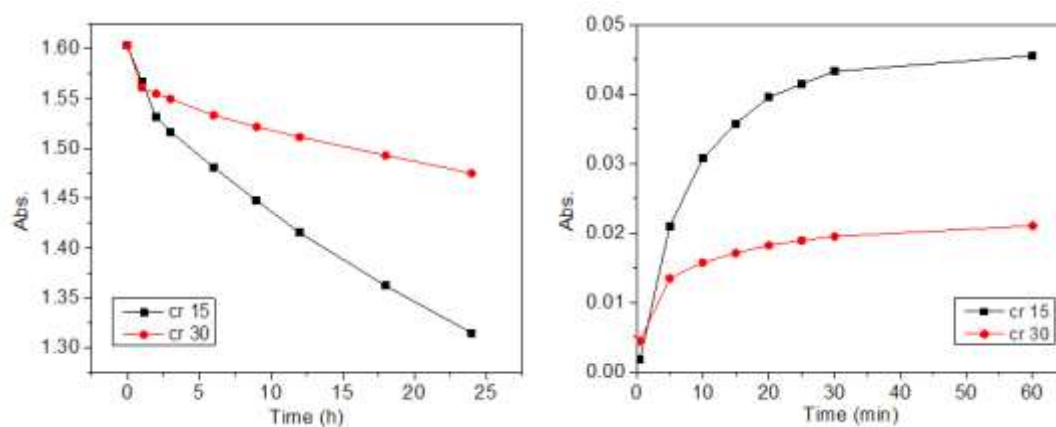


Figure 43. Comparison of adsorption (a) and release upon heating at 50 °C (b) of rhodamine B between the nanostructured PNVC thin film fabricated by 15 wt% cross-linker and 30 wt% cross-linker.

Aspirin, also known as acetylsalicylic acid, is a common medication used to moderate pain, fever, and inflammation. As a potent drug, aspirin was used to investigate the use of a nanostructured PNVCL thin films as a drug delivery medium. Although, aspirin is a hydrophobic nonpolar compound, a small amount of aspirin can be dissolved in water (3.333 mg/mL at 25 °C).¹⁷¹ The nanostructured PNVCL thin film was submersed in an aspirin solution (conc. 0.25×10^{-3} g/L) for 24 h with vigorous stirring in the same manner with rhodamine B and was then gently washed to remove excess aspirin. Subsequently, the release of drug upon heating at human body temperature (36 °C) was monitored for 6 h and recorded by UV-vis spectroscopy. As shown in Figure 44 (a), a characteristic absorption peak of aspirin at 298 nm increased with time, which proves that the nanostructured PNVCL thin film can successfully release aspirin at human body temperature. This result shows the great potential of the presented work, which can be used to produce the biocompatible and effective drug delivery materials having an enhanced performance.

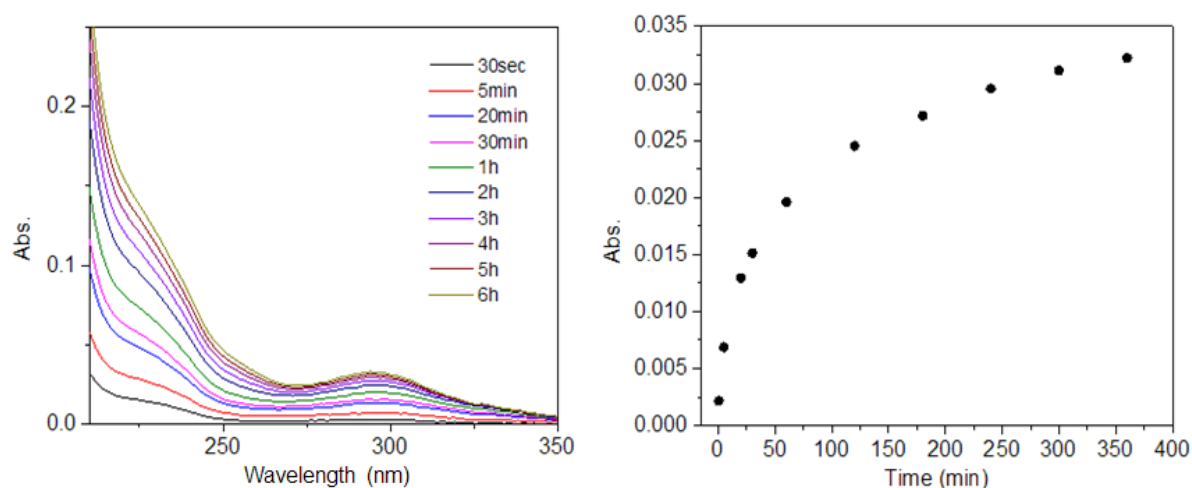


Figure 44. (a) UV-vis spectra for time dependent release of aspirin and (b) extracted peaks at 298 nm wavelength.

In addition, it was found that the nanostructures on the surface of the PNVCL thin film had not been damaged over the usage, as shown in Figure 45. Although the surface of nanostructures became rough due to the numerous repetitions of the transition between the swollen and the shrunken state, the overall structures had kept their initial shape.

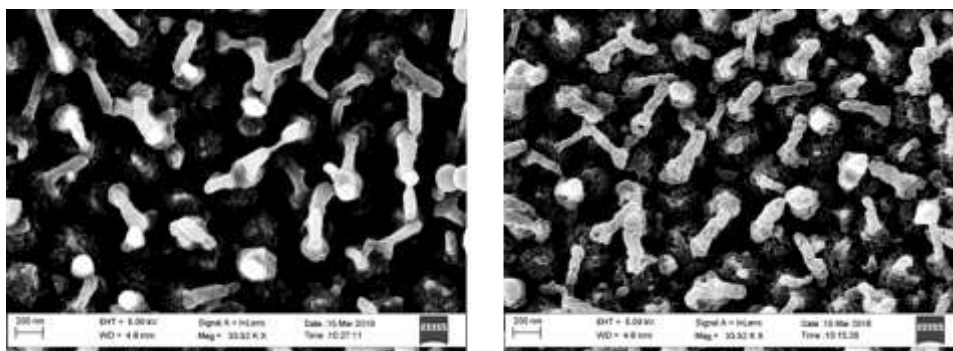


Figure 45. SEM images of the nanostructures before and after adsorption and release of dye.

Furthermore, the reusability of the nanostructured PNVCL thin film was investigated by repeating the process 4 times. The nanostructured PNVCL thin film was immersed in the aqueous solution of rhodamine B (conc. 1.75×10^{-3} g/L) for 24 h, and the resulting dye-adsorbed thin film was then heated for 1 h at 50°C after washing and transfer to pure DI water. The adsorption and release of rhodamine B were monitored by UV-vis spectroscopy, as shown in Figure 46. The upper blue box shows the decrease (1 to 2) of the absorption peak of rhodamine B at 554 nm which is caused by the adsorption of rhodamine B onto the thin film and the lower violet box shows the increase (3 to 4) of the absorption peak of rhodamine B at 554 nm which proves the release of rhodamine B. The result clearly shows that the thin film can be reused with reasonable performance.

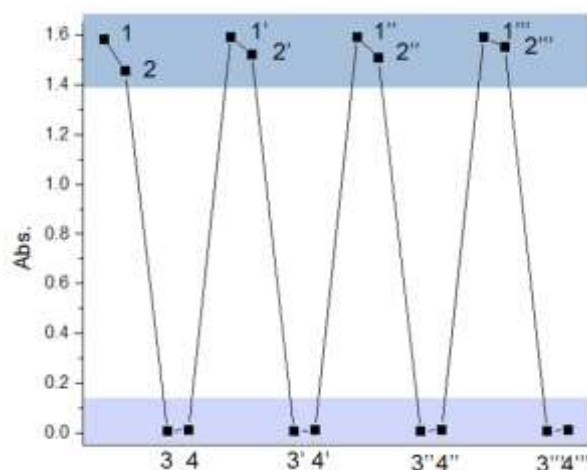


Figure 46. Test for the reusability of the PNVCL thin film.

3.3 Fabrication of Temperature Responsive Block-like Nanorods

The construction of responsive self-assembled structures has been intensively demonstrated due to their broad applicability. Particularly, the responsive behavior of nanoscopic molecular amphiphiles, which can induce a change in morphology, such as from micelles to vesicles upon external stimulation, has gathered great attention.^{172–174} However, the synthesis of polymeric, amphiphilic nanorods or nanowires with a length scale of several hundred nanometers and their assembly into microscopic structures with defined morphologies has not yet been intensively studied. The polymeric nanorods amphiphiles can be prepared by a hard-templating approach and can be regarded as block-like nanorods, with the two individual blocks consisting of chemically different polymer networks. By variation of their respective volume fraction, i.e. block length, as well as the chemical nature of the polymers, different self-organized structures are expected to be formed, similarly to the various self-assembled structures of small-molecule amphiphiles. Moreover, one block will be designed as being stimuli-responsive and thus a selective swelling or deswelling of one of the blocks can be induced upon external stimulation. As a result, the occupied volume of the stimuli-responsive part will change and thus may trigger a change in the morphology of the self-assembled structure. Consequently, changes from a vesicular to a micellar structure can be expected. These morphological changes from giant vesicles to micelles are envisioned to be used as delivery vehicles, which can encapsulate a small molecule and release it in a controlled manner upon application of the specific stimulus, or as compartments for catalytic reactions.

The key to the preparation of nanoscopic block-like rods is the access of hard templates that allow size variations. For this purpose, AAO templates were prepared as a frame for the nanostructures. For the experiments, phosphoric acid was used as an electrolyte, and a relatively high voltage (195V) was applied for varying periods of time. As a result, the templates, which had a diameter of ~180nm and various lengths ranging from nano-scale to micro-scale, were fabricated.

As a first approach, physically bonded block-like nanorods were fabricated, as shown in Figure 47. 20 wt% styrene monomer solution in ethanol containing cross-linker (1,6-hexanediol diacrylate) and photo-initiator (TPO) was infiltrated by spin-coating in prepared AAO templates (diameter: ~ 180 nm, length: ~ 1.5 μm) and subsequently polymerized by UV light irradiation to fabricate the non-responsive blocks. To eliminate one half of the polystyrene

(PS) nanorods, oxygen plasma treatment under a relatively high power (990 W) and high pressure (0.6 mbar) was conducted. Over the etched PS nanorods, 40 wt% *N*-isopropylacrylamide (NIPAM) precursor solution in methanol containing identical cross-linker and photo-initiator as in the styrene monomer solution was infiltrated and polymerized by UV light for 30 min to form the other stimuli-responsive blocks. The sacrificial AAO templates were etched away by the wet etching method using 10 wt% phosphoric acid solution at 45 °C for 1 h.

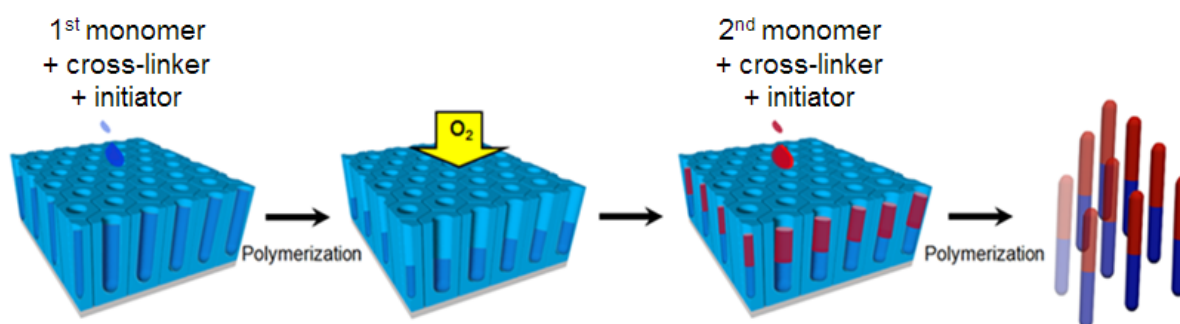


Figure 47. Schematic illustration of the fabrication of polymeric block-like nanorods.

Various weight percentages (20, 40, 60 wt%) of styrene precursor solutions in ethanol and a styrene solution without solvent were prepared for the infiltration, and spin-coated on the AAO templates with speed variance (1000, 2000, 3000, 5000 rpm), as shown in Appendix A. The result shows that the PS nanorods were well-formed above 2000 rpm with 20, 40, 60 wt% styrene precursor solution. Subsequently, all these samples received oxygen plasma treatment for 2 min, and the result showed that 20 wt% styrene precursor solution with 2000 rpm yielded the PS nanorod halves, as shown in Appendix B.

Figure 48 (a) shows the PS nanorods fabricated by using a 20 wt% styrene precursor solution in ethanol with the speed of spin-coating at 2000 rpm for 15 sec, and evenly infiltrated PS nanorods are observed. Subsequently, oxygen plasma treatment was applied to remove one half of the nanorods. To identify the etching ratio of nanorods to time, an AAO template containing the PS nanorods was cut into small pieces and the pieces were placed in an oxygen plasma chamber. Each piece was then removed from the chamber after a certain of time. As shown in Appendix C, the length of the PS nanorods decreased linearly by the longer oxygen plasma treatment, and the PS nanorods having a half size compared to the initial length were obtained after 2 minutes of treatment. Based on this result, oxygen plasma was conducted for 2 min on

the sample shown in Figure 48 (a), and the PS nanorods having half their original size were fabricated, as shown in Figure 48 (b).

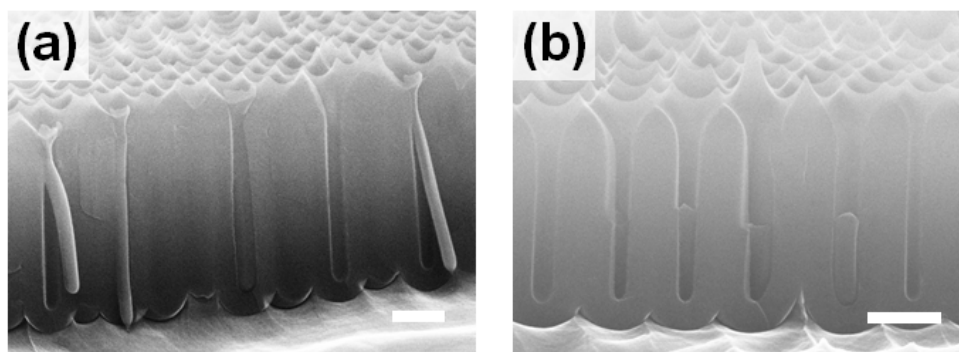


Figure 48. SEM images of (a) the PS nanorods in an AAO template and (b) the PS nanorods after oxygen plasma treatment (2 min, 990 W, 0.6 mbar) (scale bar: 500 nm).

For the fabrication of the stimuli-responsive blocks, NIPAM was chosen. In order to find the most suitable solvent which does not exceedingly swell the PS nanorods, a theoretical pre selection of solvents based on the Hansen theory was conducted. Hansen parameters consider three components: a dispersion component (δ_d), a polar component (δ_p), and a hydrogen bonding component (δ_h).¹⁷⁵⁻¹⁷⁷ These parameters are used to predict the solubility of polymers in solvents. Furthermore, Hansen used a three-dimensional model to plot the polymer solubility. Based on three coordinates of the component values (δ_d , δ_p , δ_h) of a polymer, a spherical volume of solubility can be defined in three dimensions, and the radius of this sphere indicates the interaction radius (R) of polymers. According to the Hansen theory, a polymer is presumably soluble in a solvent which has its Hansen parameters within the solubility sphere of the polymer. Therefore, the distance (R_a) between the coordinate of the solvent determined by the Hansen parameters and the center of the solubility sphere of the polymer (R_o) should be less than the interaction radius (R) of the polymer to meet the condition that the polymer is soluble in a specific solvent.

The distance (R_a) from the coordinate of the solvent to the center of the solubility sphere of PS (R_o) was calculated as follows.^{176,177}

$$R_a = [4(\delta_{dS} - \delta_{dP})^2 + (\delta_{pS} - \delta_{pP})^2 + (\delta_{hS} - \delta_{hP})^2]^{1/2}$$

where,

Results and Discussion

R_a = Distance between the coordinate of solvent determined by the Hansen parameters and the center of the solubility sphere of polymer

δ_{xS} = Hansen component parameter for solvent

δ_{xP} = Hansen component parameter for polymer

Table 1 shows the Hildebrand and Hansen solubility parameters of polystyrene and the solvents and the relative energy difference ($RED = R_a / R_o$) numbers that indicate the solubility between PS and the solvents.

Table 1. Hildebrand and Hasen solubility parameters, interaction radius, and RED number¹⁷⁸

	δ_d	δ_p	δ_h	R_a	RED (R_a/R_o)
Polystyrene	21.3 ^a	5.8 ^a	4.3 ^a	12.7* ^a	–
Methanol	15.1 ^b	12.3 ^b	22.3 ^b	22.80	1.80
Ethanol	15.8 ^b	8.8 ^b	19.4 ^b	18.92	1.49
Tetrahydrofuran	16.8 ^c	5.7 ^c	8.0 ^c	9.73	0.77
Chloroform	17.8 ^d	3.1 ^d	5.7 ^d	7.63	0.60
Toluene	18.0 ^c	1.4 ^c	2.0 ^c	8.26	0.65
Water	15.5 ^c	16.0 ^c	42.4 ^c	41.11	3.24

δ_d = dispersion component, δ_p = polar component, δ_h = hydrogen bonding component, R_a = interaction radius, * = the interaction radius (R) of polystyrene (^a Brandrup (2003)¹⁷⁹, ^b Hansen (2013)¹⁷⁵, ^c Barton Allan (1990)¹⁸⁰, ^d Miller (1998)¹⁸¹)

If the RED number is below 1 ($R_a < R_o$), the solvent presumably dissolves the PS, whereas if the RED number is above 1 ($R_a > R_o$), the solubility decreases. As shown in Table 1, for most of the solvents chosen in the preselection have the RED number is below 1, which indicates that the solvent will probably swell the PS. Among these solvents, methanol, which swells the PS less in most cases, was chosen for the preparation of the NIPAM precursor solution.

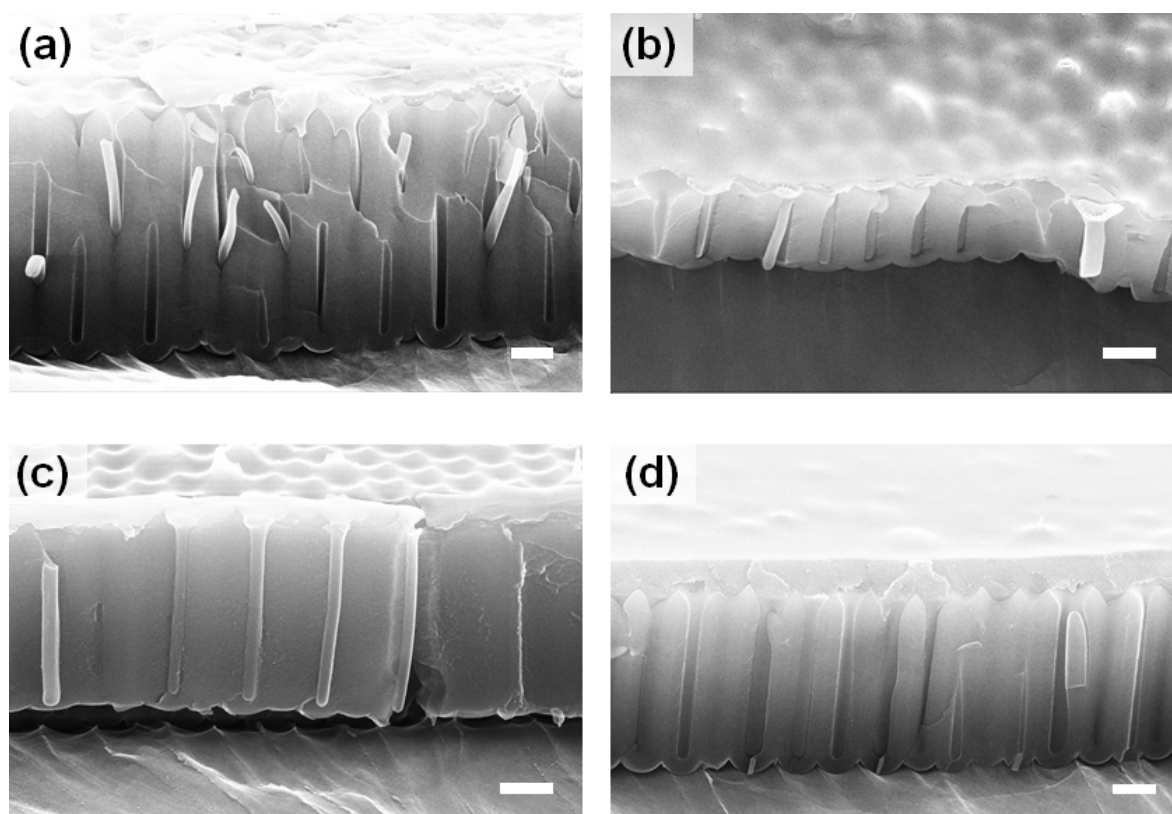


Figure 49. SEM images of the PNIPAM nanorods fabricated by using different weight percentages of NIPAM monomer solution: (a) 20 wt%, (b) 40 wt%, (c) 60 wt%, and (d) 80 wt% (scale bar: 500 nm).

Various NIPAM precursor solutions having different weight percentages (20, 40, 60, 80 wt%) of NIPAM, cross-linker (1,6-hexanediol diacrylate), and photo-initiator (TPO) in methanol were prepared and spin-coated on AAO templates with 2000 rpm for 30 sec. As shown in Figure 49, PNIPAM nanorods were fabricated inside the templates, regardless of the percentage of NIPAM, after the photo-polymerization for 30 min. However, an undesired polymer layer on top of the templates was also produced due to the low speed of spin-coating. Therefore, the speed of spin-coating was increased from 2000 rpm to 9000 rpm to avoid the deposition of a polymer layer, which would be an obstacle for the formation of the individual nanorods.

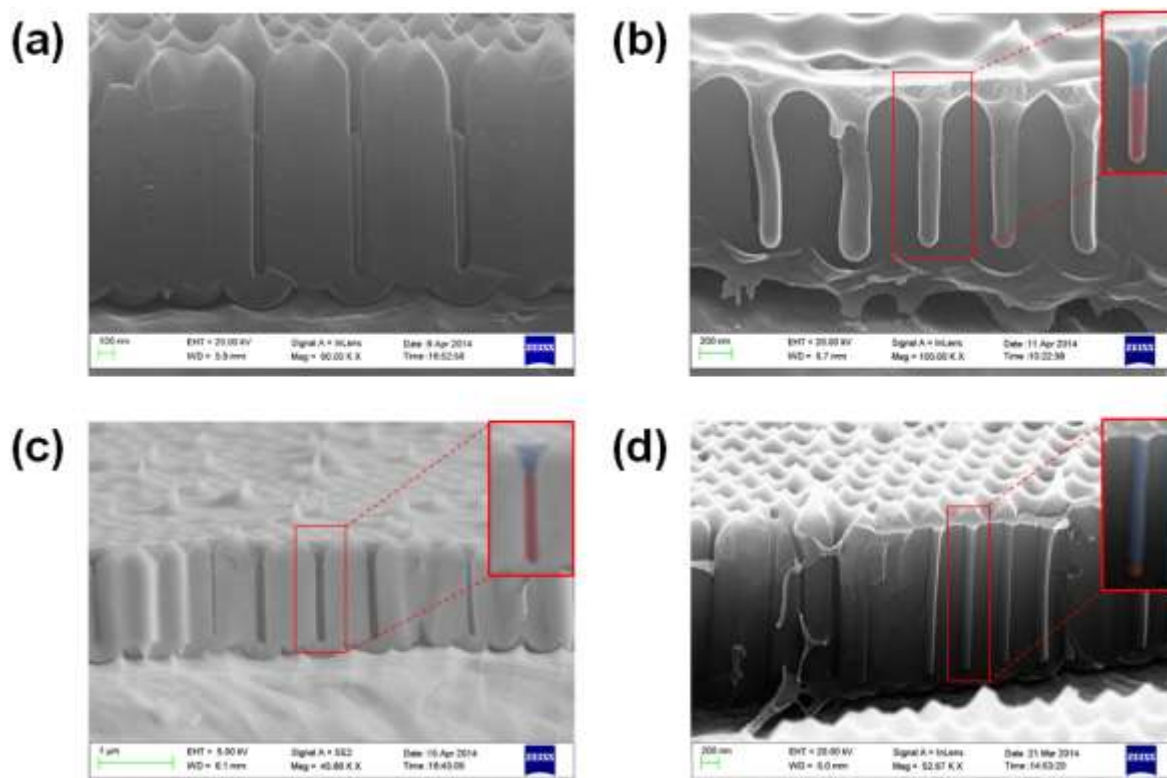


Figure 50. SEM images of the block-like nanorods. (a) PS nanorods after oxygen plasma irradiation for 7 min, (b) half PS-half PNIPAM nanorods, (c) long PS-short PNIPAM nanorods, (d) short PS-long PNIPAM nanorods (the red boxes show the junction of block-like nanorods).

Figure 50 shows the resulting PS nanorods and the block-like PS-PNIPAM nanorods with different ratios. 20 wt% styrene precursor solution in ethanol were spin-coated on the template with 2000 rpm for 15 sec and polymerized by UV light for 30 min. Oxygen plasma treatment was conducted for 7 min to remove one half of the PS nanorods. Over the resulting PS nanorods in Figure 50 (a), 40 wt% NIPAM precursor solution in methanol was spin-coated with 9000 rpm for 30 sec and polymerized by UV light for 30 min. Figure 50 (b) clearly shows the physically bonded block-like PS-PNIPAM nanorods having the same block length. Moreover, the block-like nanorods having a different block length were fabricated by controlling the time of the oxygen plasma treatment. Figure 50 (c) and (d) show the block-like nanorods having a long PS block – short PNIPAM block and a short PS block – long PNIPAM block. To fabricate these block-like nanorods, oxygen plasma treatment was conducted for 2 min and 12 min, respectively.

For an investigation of the temperature-responsiveness of the nanorods, the block-like nanorods were separated from the templates by removing the sacrificial AAO templates with

1wt% phosphoric acid solution at a temperature of 45°C for 1 h. Subsequently, the released nanorods were purified via dialysis to remove the acid and the elements from the templates. The transmittance of block-like nanorods in water was then measured upon increasing the temperature from 15 to 70 °C to verify the temperature-responsiveness of the nanorods. Before conducting the measurement, the exact volume percent of the nanorods in water was calculated as follows.

Pore density of the AAO template fabricated by phosphoric acid: **5×10^8 pores/cm²**

Surface area of the aluminum substrate (d=1.3cm): **1.327 cm²**

From these, the number of pores that one AAO template has can be calculated:

$$5 \times 10^8 \text{ pores/cm}^2 \times 1.327 \text{ cm}^2 = \mathbf{6.633 \times 10^8 \text{ pores.}}$$

After that, the volume of one pore was calculated by inserting the value of the diameter and the length of the pore, and its value was **0.028 μm³**. This value was multiplied with the number of pores to calculate the total volume of pores in one AAO template, and the value was **0.0743 cm³**. To increase the concentration of the nanorod solution, 0.0743 cm³ of block-like nanorods in 6mL of water underwent freeze drying, and the volume of water was reduced from 6 mL to 2 mL. Consequentially, the volume percent of the nanorods increased from 1.238 v% to **3.715 v%**. With the resulting concentrated solution, the turbidity was monitored by heating up the solution at a rate of 10°C/min.

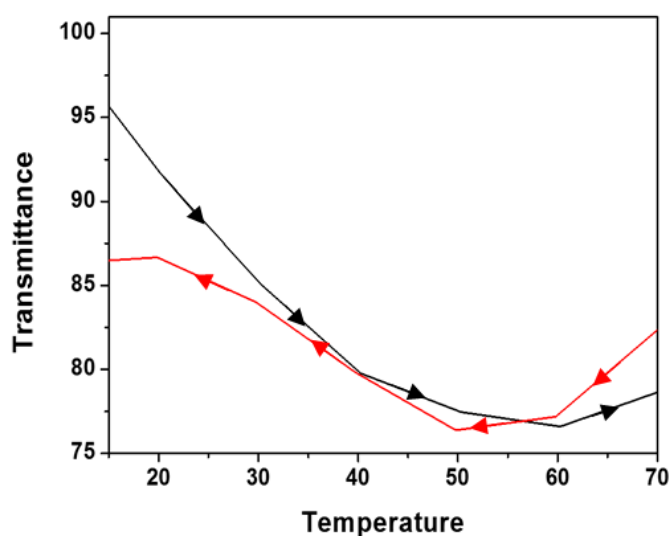


Figure 51. Turbidity of block-like nanorods (black: heating, red: cooling).

As shown in Figure 51, a smooth decrease of transmittance and an incomplete restoration of transmittance were observed upon heating and cooling, respectively. Although the complete transition of the solution from transparent to cloudy could not be observed due to the relatively low concentration of the nanorods, the measurement proved that the solution contained temperature-responsive PNIPAM blocks which caused the change of transmittance. However, the self-assembly behavior of the nanorods and their structural change could not be verified by this measurement. Therefore, dynamic light scattering (DLS) measurement was conducted to monitor the change in the size of block-like nanorods upon heating. Since PNIPAM has LCST, it is expected that the size of the block-like nanorods decreases upon heating. However, DLS data show that the average size of the block-like nanorods is ~ 320 nm at r.t. and ~ 380 nm at 40°C . In addition, the overall size of the nanorods was smaller than expected when considering the length of the block-like nanorods inside the AAO template (~ 1 μm). The result of DLS apparently showed an inconsistency in size of the block-like nanorods and its change of size upon heating. Furthermore, a fracture of the block-like nanorods was observed in the confinement even before removal of the template, as shown in Figure 52. These results led to the assumption that two blocks composed of block-like nanorods might be separated from each other during the fabrication process or during removal of the templates.

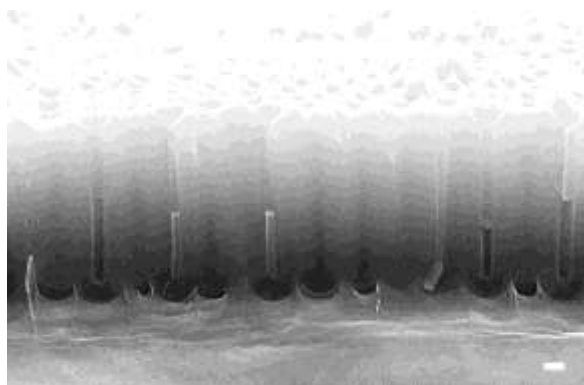


Figure 52. SEM image of the separated PS and PNIPAM blocks in the confinement of the template (scale bar: 200 nm).

To clearly verify the assumption, two different kinds of fluorescence dyes (rhodamine B and NBD-amine) were individually added to each block as a marker, and the emission from the block-like nanorods was observed by confocal microscopy. The hypothesis was that both emissions from two distinct dyes should be detected from the block-like nanorods, if both blocks connected as one.

For the experiment, NBD-amine and rhodamine B were added to the styrene solution and the NIPAM solution, respectively. NBD-amine shows a green emission when the dye is excited (maximum absorption at $\lambda_{ab} = 460$ nm, emission at $\lambda_{em} = 535$ nm), and rhodamine B shows an orange emission (maximum at $\lambda_{ab} = 555$ nm and the emission at $\lambda_{em} = 575$ nm) in water. The precursor solutions containing these fluorescence dyes were then used for the fabrication of block-like nanorods using the identical method by which the block-like nanorods without dye had been fabricated. Consequently, the solution containing the resulting nanorods was drop-casted between two glass slides for the confocal microscopy measurement.

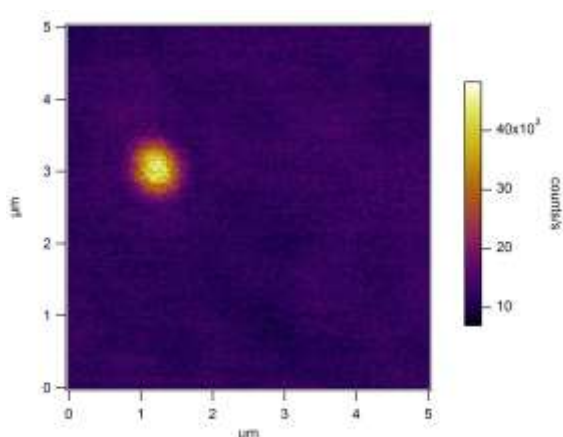


Figure 53. Confocal photoluminescence image of single block-like nanorod (532nm CW laser light, LP 532 filter, 500 nW, 10 sec).

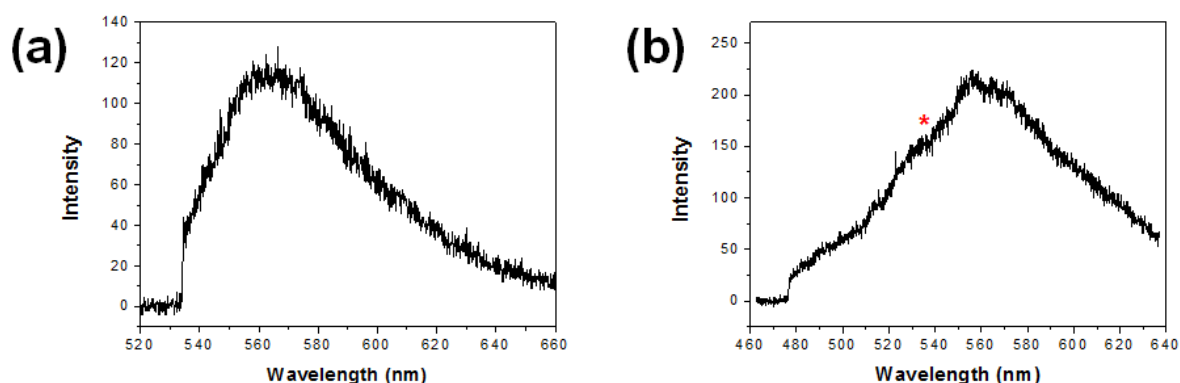


Figure 54. Photoluminescence spectra of single block-like nanorod with different excitation wavelengths (a) at 532 nm (CW laser light, LP 532 filter, 500 nW, 10 sec) and (b) at 440 nm (Ti:Sa laser in ML mode, LP 474 filter, 13 μ W, 1 sec).

As light sources, 532 nm continuous wave (CW) laser light from neodymium-doped yttrium orthovanadate (Nd:YVO₄) laser and 440 nm titanium-doped sapphire (Ti:Sa) laser were used

with a long pass (LP) 532 filter and a LP 474 filter, respectively. An object assumed to be a single block-like nanorod was observed in the confocal photoluminescence (PL) image, as shown in Figure 53. The size of the object was around 500nm, and the object strongly emitted at 570 nm with excitation at 532 nm, as shown in Figure 54 (a). Based on the excitation and emission wavelength, it is concluded that the object contains rhodamine B (λ_{ab} : 555 nm, λ_{em} : 575 nm). To verify the existence of NBD-amine (λ_{ab} : 460 nm, λ_{em} : 535 nm) in the object, 440 nm Ti:Sa laser in mode locking (ML) mode was used; however, the emission peak of NBD-amine (marked with a red star in Figure 54 (b)) did not appear.

These results also implied the fracture of the blocks which perhaps caused by the weak connection between the two blocks. To avoid the fracture and to enhance the stability of the block-like nanorods, a new approach to fabricate the chemically bonded block-nanorods was demonstrated by adding the reactive components in each block to bond them chemically.

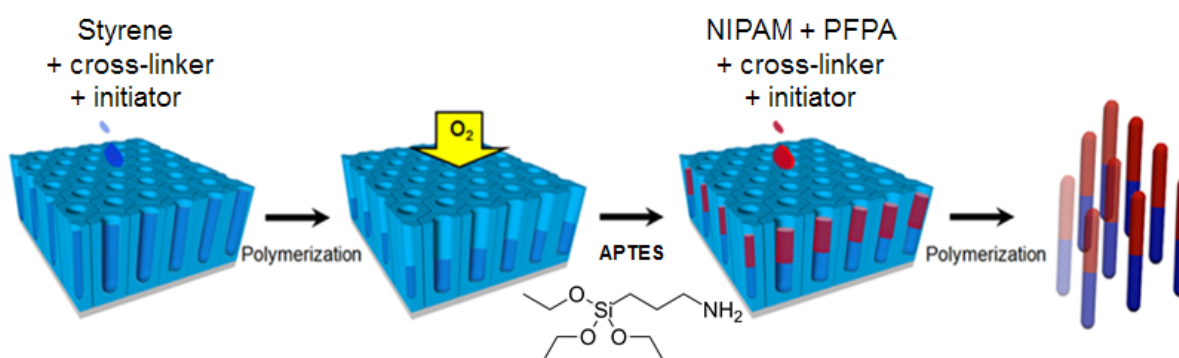


Figure 55. Schematic image of the fabrication of chemically-bonded block-nanorods.

An attempt was undertaken using aminopropyltriethoxysilane (APTES) as a linker to fabricate the chemically bonded nanorods. APTES is a well-known chemical for a self-assembled monolayer (SAM) and can be linked to oxide surfaces. Immediately after oxygen plasma treatment, the sample containing the PS nanorods was dipped into 0.4 wt% APTES solution in DI water for 15 min and dried under ambient conditions. Subsequently, the monomer solution in methanol having temperature-responsive NIPAM (40 wt%), linkable PFPA (20 wt%), cross-linker (1,6-hexanediol diacrylate), and photo-initiator (TPO) was drop-casted, and the AAO template was squeezed between two non-structured PDMS pads by a clip to support the infiltration. After the infiltration, the monomers were then polymerized by UV light for 30 min. As shown in Figure 56, APTES did not destroy the structure of the PS block; however, the second blocks were not infiltrated properly.

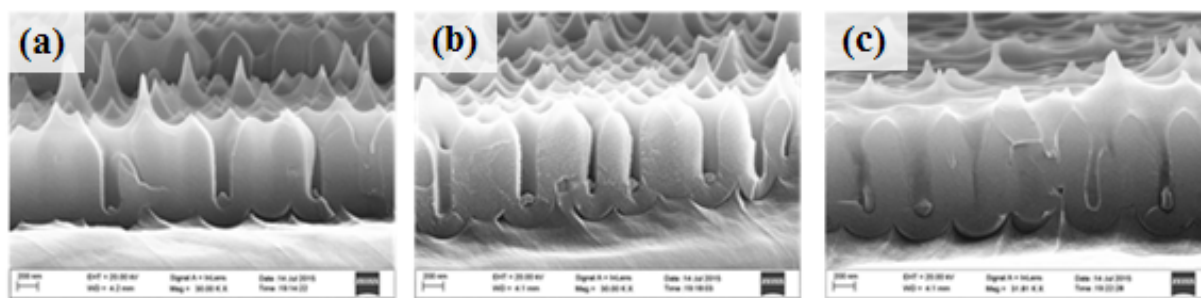


Figure 56. SEM images of PS nanorods (a), after the APTES modification (b), and after the polymerization of poly(NIPAM-r-PFPA) copolymer nanorods (c) (Scale bar: 200 nm).

Another attempt was made to use ethylenediamine (EDA) as an alternative linker. It was expected that one amine end of EDA would react with the pentafluorophenyl group from the first block and the other amine end would react with the pentafluorophenyl group from the second block. First, the first half blocks containing the inert styrene and the linkable pentafluorophenyl group were prepared from the mixed solution having 20 wt% styrene and 10 wt% PFPA, followed by the polymerization and the removal of half of the blocks via oxygen plasma treatment. Subsequently, the open surface of the first blocks was modified with EDA by dipping the samples into a 50 wt% EDA solution in methanol for 30 min. Afterwards, the second blocks containing the temperature-responsive NIPAM group and the linkable pentafluorophenyl group were fabricated.

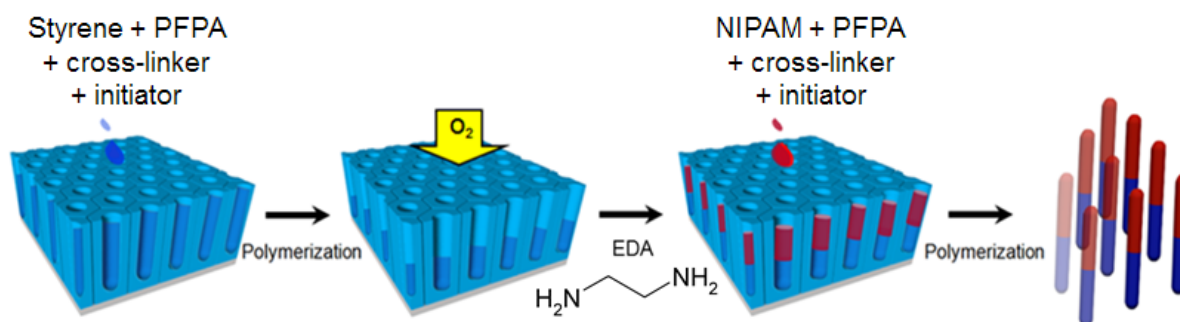


Figure 57. Schematic image of the fabrication of chemically-bonded block-nanorods.

As shown in Figure 58 (b), the shape of the first blocks was transformed after dipping the sample in the EDA solution. Although the second blocks were successfully formed, the deformation of the first blocks led to the fabrication of imperfect block-like nanorods.

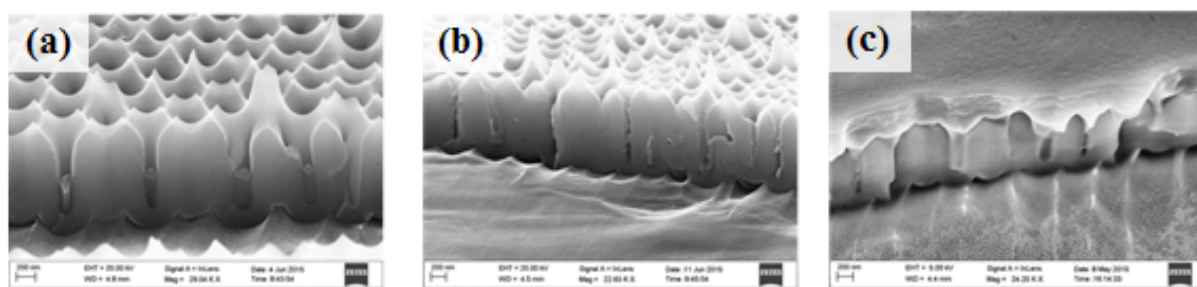


Figure 58. SEM images of poly(S-r-PFPA) copolymer nanorods (a), after the EDA modification (b), after the polymerization of poly(NIPAM-r-PFPA) copolymer nanorods (c) (Scale bar: 200 nm).

To overcome the problems of the previous trials, the amount of EDA and PFPA was reduced, and a single monomer was used for the fabrication of the second blocks. A styrene solution containing 1 wt% PFPA was used to fabricate the first blocks, and a 20 wt% EDA solution was used for the linking. After the modification with EDA, a PFPA solution was infiltrated into an AAO template by vacuum-assisted method. Followed by the polymerization and the removal of the sacrificial AAO template, the chemically bonded block-like nanorods containing the inert poly(styrene-r-PFPA) blocks and the chemically tunable PPFPA blocks were fabricated.

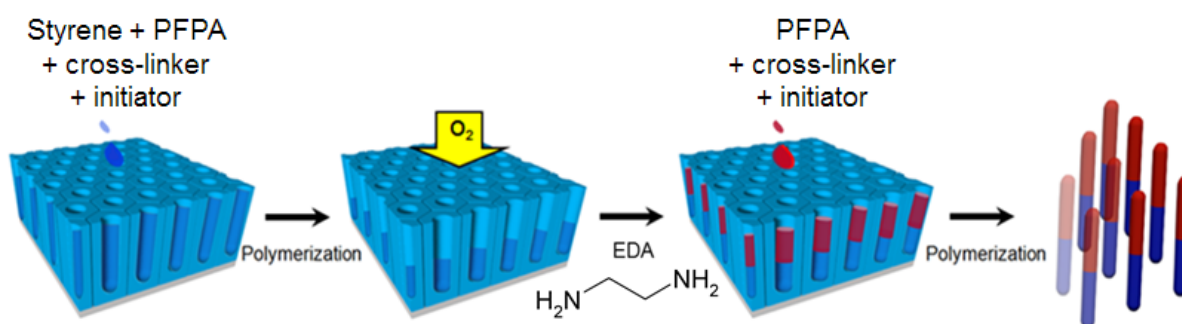
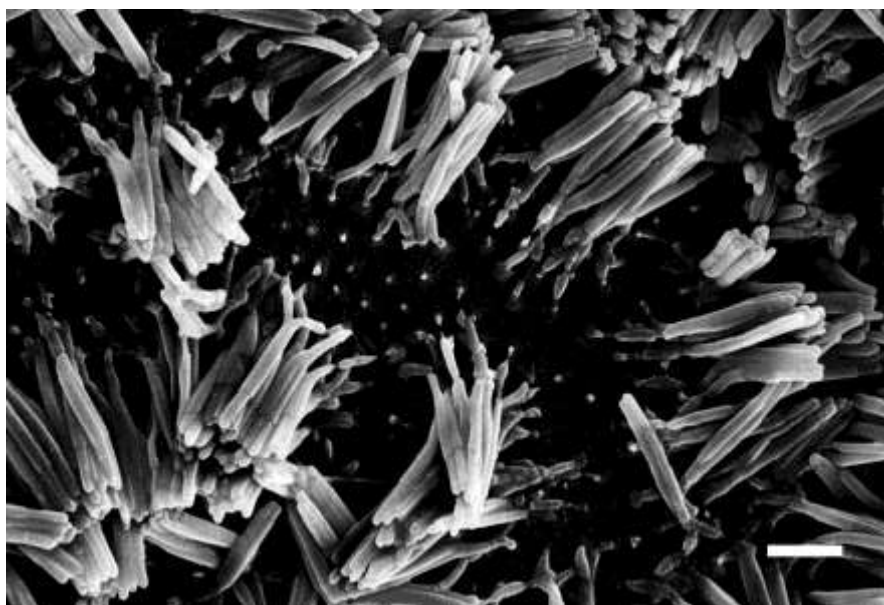


Figure 59. Schematic image of the fabrication of chemically-bonded block-nanorods.

Figure 60 clearly shows the chemically bonded block-like nanorods without any disconnection between the two blocks. By using EDA as a linker, the chemically bonded block-like nanorods containing the tunable blocks were successfully fabricated. However, the post-modification of the PPFPA blocks and the study on the assembly behavior of the block-like nanorods need to be further investigated in order to verify their potential to be used as a drug delivery medium. Although further investigation is needed, it is expected that the presented

method will contribute to the further development an effective fabrication method of stimuli-responsive amphiphilic nano-objects.



*Figure 60. SEM image of the chemically bonded block-like nanorods containing the poly(styrene-*r*-PPFA) blocks and the chemically tunable PPFA blocks (scale bar: 1 μm).*

3.4 Fabrication of Multi-functionalized Nanowires via Post-Polymerization Modification

A large number of studies on the template-assisted fabrication of polymeric nanomaterials have been reported;²⁴ however, studies on chemically tunable polymeric nanomaterials fabricated by the template-assisted fabrication have not been conducted extensively. Previously, the group of Theato reported a simple method for the fabrication of thermo-responsive nanowires via the template replication method and post-polymerization modification.¹³⁵ Post-polymerization modification was conducted with isopropylamine on the pentafluorophenyl ester nanowires which were prepared by the template replication method. The corresponding functionalized nanowires clearly showed thermo-responsive behavior and proved that the post-polymerization modification was well manageable. This result showed a great potential for the method to be applied in nanomaterials and to be used for the fabrication of stimuli-responsive nanomaterials.

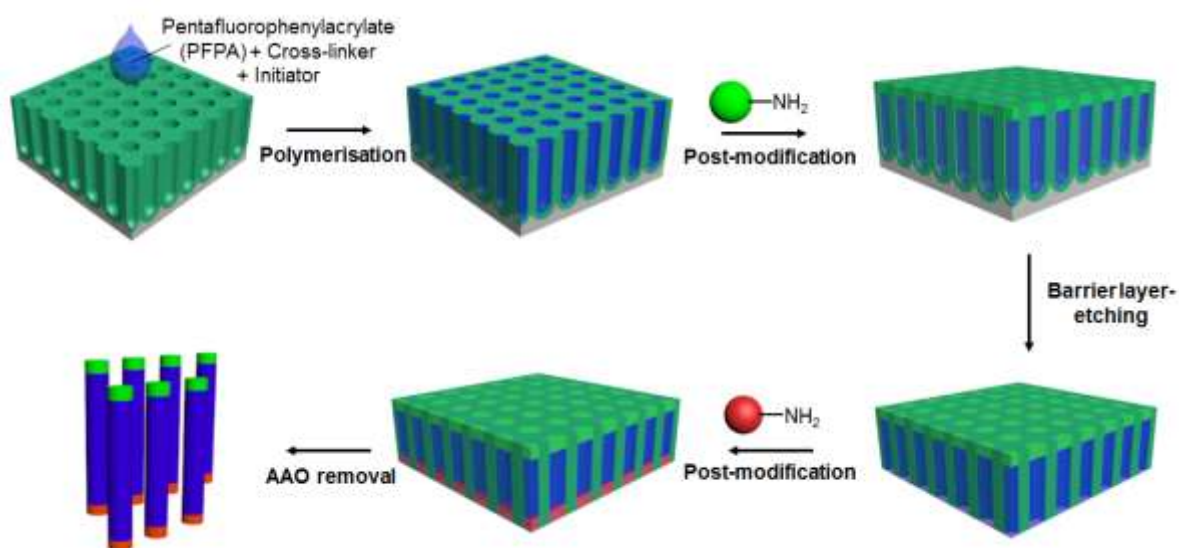


Figure 61. Schematic illustration of the fabrication of multi-functionalized nanowires.

As an extension of the method mentioned above, a method to fabricate the multi-functionalized nanowires was demonstrated via selective post-polymerization modification. Chemically tunable PPFPA nanowires were prepared by the vacuum-assisted infiltration method schematically shown in Figure 61. The AAO templates (diameter: ~ 40 nm, length: ~ 7 μm) were fabricated via the conventional two-step anodization process with oxalic acid as electrolyte. A PFPA monomer solution containing cross-linker (1,6-hexanediol diacrylate) and

photo-initiator (TPO) was infiltrated into the nanochannels of AAO with vacuum assistance, and the monomer solution was polymerized by UV light (365 nm) for 30 min. After the fabrication of the PPFPA nanowires, the open ends of the nanowires was modified with primary amine dye via post-polymerization modification. The whole AAO templates containing PPFPA nanowires were immersed in 0.01 wt% NBD-amine dye solution in methanol for 1 h and sufficiently washed afterwards. To modify the other ends of nanowires, a pore opening was necessary; therefore, the aluminum and the barrier layer (aluminum oxide layer) which were present at the bottom of the pores were removed by the chemical etching method or by the reactive ion etching method. The chemical etching method was carried out in different concentrations of phosphoric acid (5 or 10 wt%) and time to obtain the evenly opened pores¹⁸², and the reactive ion etching method was conducted by using CF₄ gas at 0.16 mbar with 180 W for 15 to 180 min. Subsequently, the other ends of the opened nanowires were modified with 0.01 wt% cresyl-violet dye solution in methanol to distinguish both ends with different emitting wavelengths. Finally, the AAO templates were removed by 10 wt% phosphoric acid solution at 45 °C for 1 h to separate the modified nanowires.

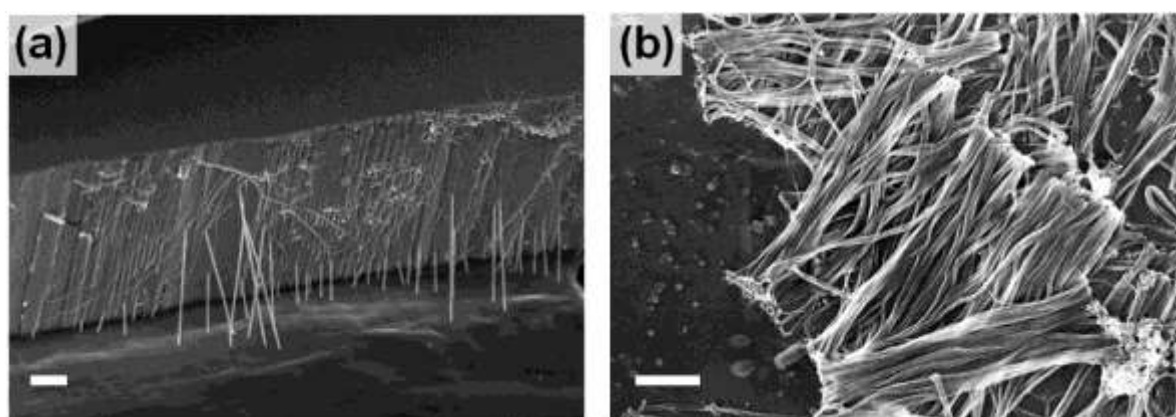


Figure 62. SEM images of chemically tunable PPFPA nanowires: (a) PPFPA nanorods formed inside the AAO template and (b) released PPFPA nanorods after the removal of the AAO template (Scale bar: 1 μ m).

The resulting PPFPA nanowires before and after removal of the AAO templates are shown in Figure 62. The PPFPA nanowires having an identical dimension of the AAO templates were observed either inside the AAO templates or after removal of the templates.

Prior to the post-polymerization modification of the resulting PPFPA nanowires, fluorescence spectroscopy was carried out to define the absorption and emission wave length of NBD-amine

and cresyl violet perchlorate dye. The result shown in Figure 63 exhibits the distinguishable ranges of wave length of the two dyes. NBD-amine had an absorption at 470nm and an emission at 550nm, and cresyl violet perchlorate had an absorption at 590nm and an emission at 640nm.

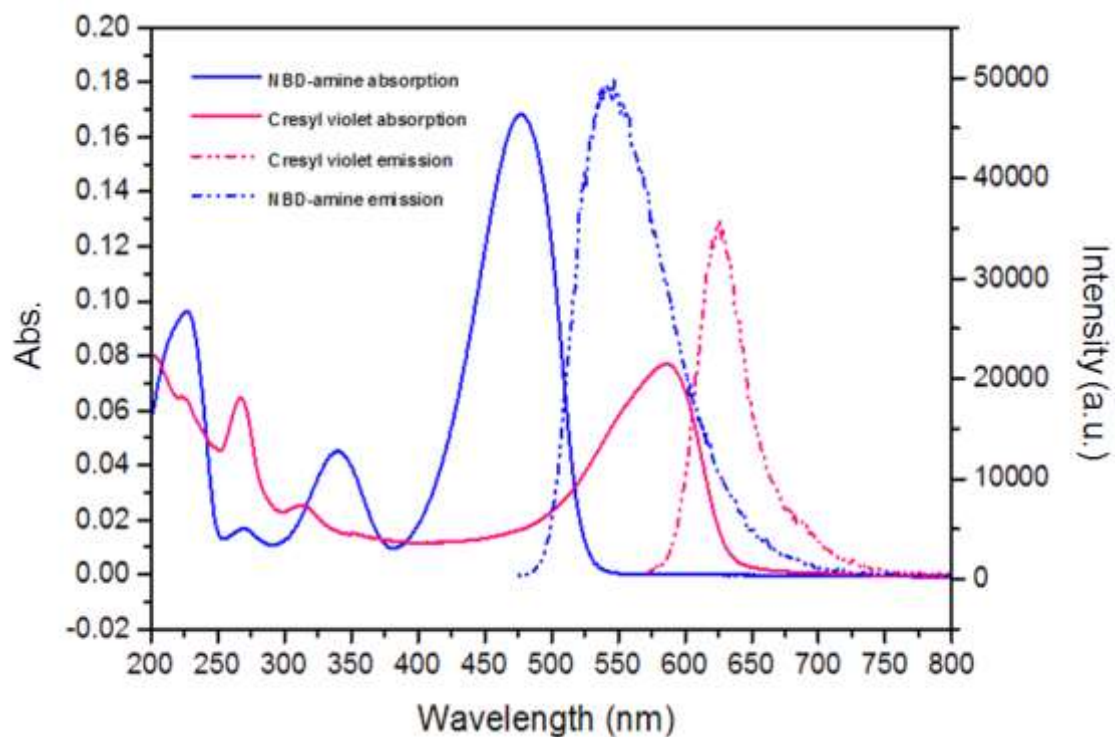


Figure 63. Absorption and emission spectra of NBD-amine and cresyl violet measured by Fluorescence spectrometer.

In addition, these two dyes were tested on the PPFPA thin films to confirm that the dyes could modify PPFPA via the post-polymerization modification method. As shown in Figure 64, the IR spectra of the PPFPA thin films show the increased -NH (3306 cm^{-1}) and amide (1533 cm^{-1}) bands and the dramatically decreased ester (1783 cm^{-1}) bands after the modification. It confirmed that the post-polymerization modification had been successfully conducted with NBD-amine and cresyl violet perchlorate dyes. It was also observed that the PFP ester band had not completely vanished after the modification. It is assumed that the cross-linked thin films were not swollen enough and consequently all of the PFP groups could not be modified; however, it was enough to show that these dyes could be applied for the post-polymerization modification of the nanowires.

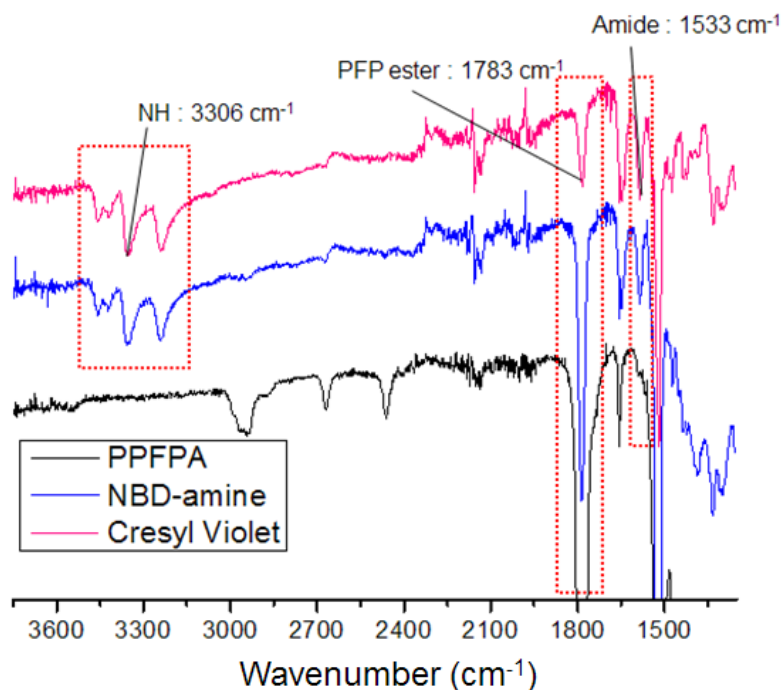
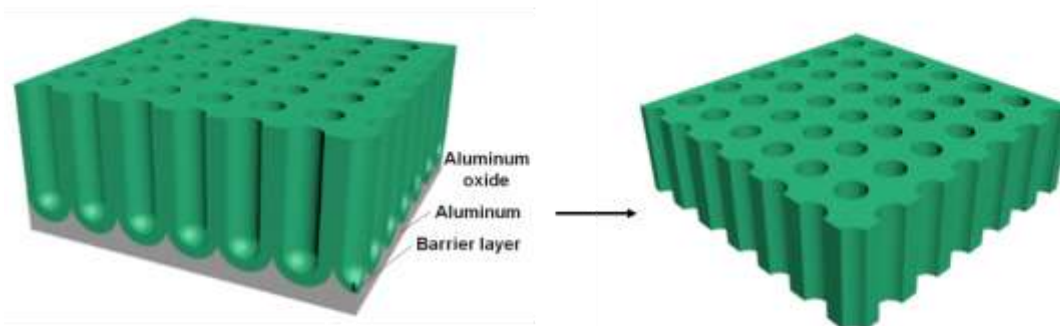


Figure 64. IR spectrums of the PPFPA thin films: without modification (black), after modification with NBD-amine (blue), and after modification with cresyl violet (red).

After the modification of the PPFPA nanowires with NBD-amine, the back side of the AAO templates was chemically or physically etched to open the other ends of the nanowires. For that, the aluminum layer was removed by $\text{CuCl}_2 \cdot \text{HCl}$ (0.02M) solution, and the barrier layer (aluminum oxide layer) which was revealed after removal of aluminum was etched by using one of two methods; reactive ion etching or wet chemical etching.



AAO	Method	Etchant	T [°C]	Time [min]
$\text{H}_2\text{C}_2\text{O}_4$	wet	5wt% H_3PO_4	30	30 - 50
H_3PO_4	wet	5wt% H_3PO_4	30	120 - 210
H_3PO_4	RIE	CF_4	N/A	30 - 180

Figure 65. Schematic illustration of AAO template before and after barrier layer etching and the etching parameters for barrier layer opening.

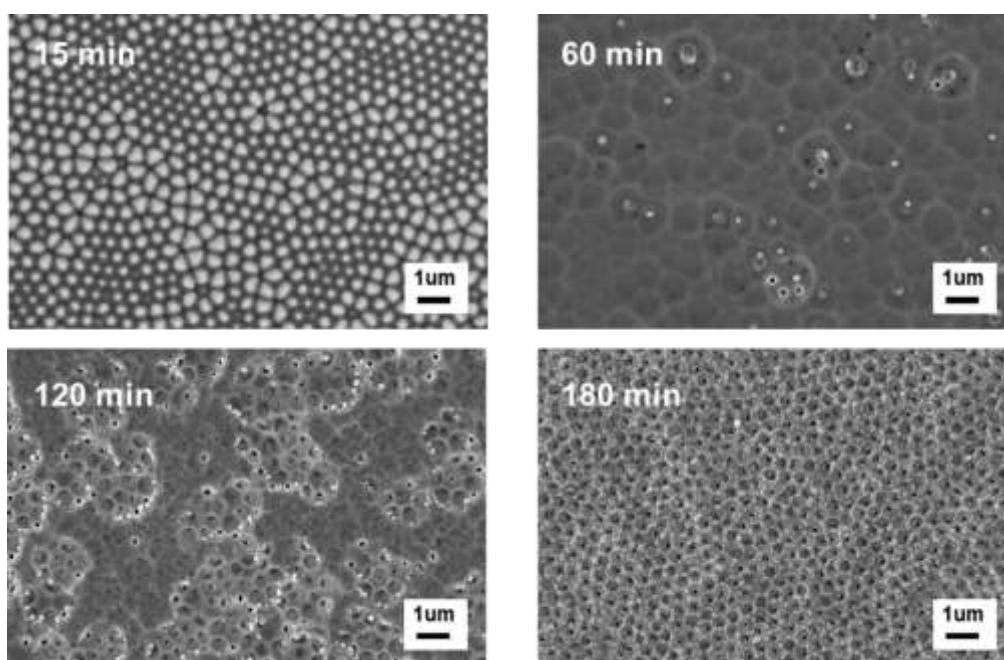


Figure 66. SEM images of the bottom surface of porous AAOs, showing the opening of the barrier oxide layer upon different reactive ion etching (RIE) times: (a) 15 min, (b) 60 min, (c) 120 min, (d) 180 min (Scale bar: 1 μm).

Figure 65 summarizes the conditions of the etching experiments. For reactive ion etching, CF_4 gas was used with various etching times, and the resultant morphology of the barrier layer of the AAO templates is shown in Figure 66. After 180 min, the barrier layer of the phosphoric acid (H_3PO_4)-anodized AAO template was uniformly etched away and the opened channels were exposed. The reactive ion etching was also applied on the AAO templates containing the PPFPA nanowires, however, the critical defect in the structure of PPFPA nanowires was found, as shown in Figure 67. It was assumed that the PPFPA nanowires was damaged by the high temperature inside the ion etching chamber. Although, the exact temperature inside the chamber was not able to be measured, it was expected over several hundred °C since the contact to the chamber was not available without protection from heat. To avoid this problem, a wet chemical etching method was explored.

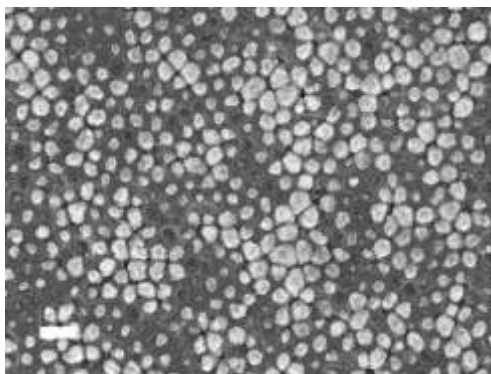


Figure 67. SEM images of the bottom surface of porous AAOs containing PPFPA nanowires, showing the opening of the barrier oxide layer by RIE etching for 30 min (Scale bar: 1 μ m).

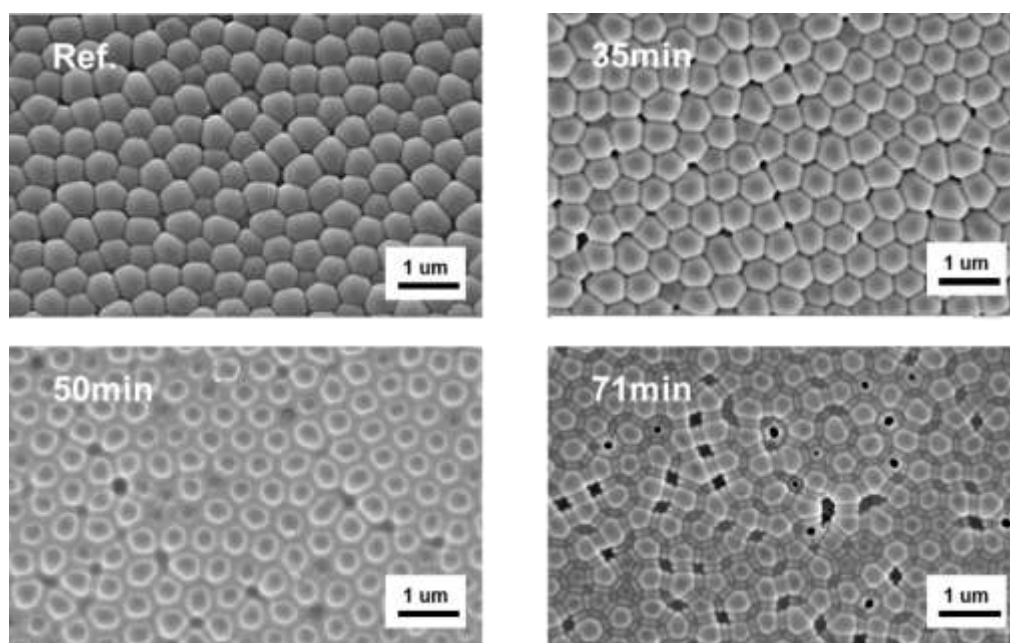


Figure 68. SEM images of the bottom surface of porous AAOs fabricated with phosphoric acid, showing the opening of the barrier oxide layer upon different wet-chemical etching times: (a) 0 min, (b) 35 min, (c) 50 min, (d) 71 min (Scale bar: 1 μ m).

The wet chemical etching was carried out in 5wt% aqueous phosphoric acid (H_3PO_4) at 30°C with various etching times. The channels of the H_3PO_4 -anodized AAO template started to open after 71 min, as shown in Figure 68; however, the opened channels were irregularly distributed and the diameters of the opened channels varied due to intrinsic defects such as an irregularity of the pore formation and the boundaries of the H_3PO_4 -anodized AAO template. Therefore, oxalic acid ($\text{H}_2\text{C}_2\text{O}_4$)-anodized AAO templates having less intrinsic defects were used.

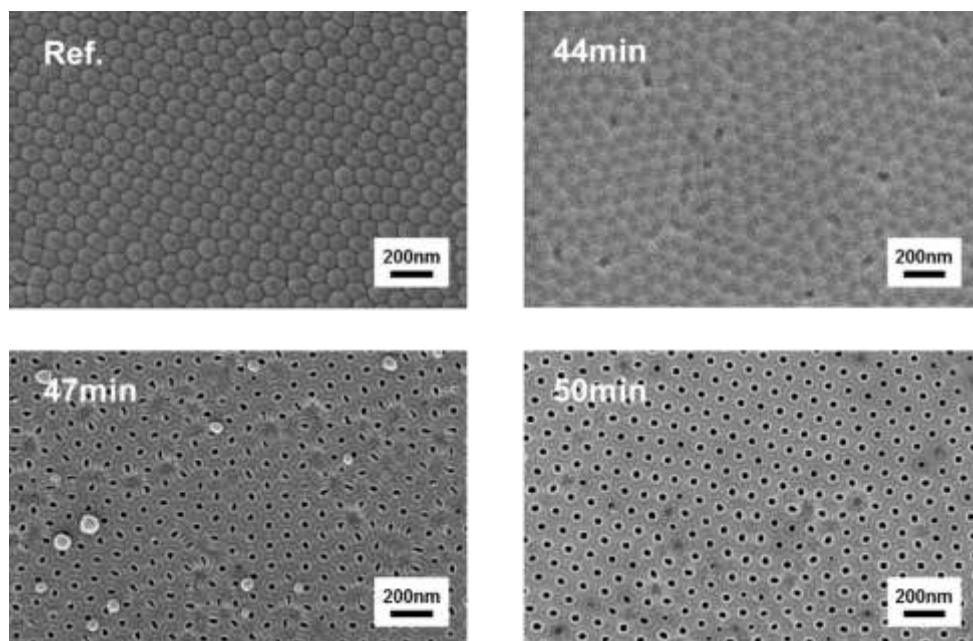


Figure 69. SEM images of the bottom surface of porous AAOs fabricated with oxalic acid, showing the opening of the barrier oxide layer upon different wet-chemical etching times: (a) 0 min, (b) 44 min, (c) 47 min, (d) 50 min (Scale bar: 200 nm).

Figure 69 shows the SEM images of an etched barrier layer of a $\text{H}_2\text{C}_2\text{O}_4$ -anodized AAO template with different etching times. The $\text{H}_2\text{C}_2\text{O}_4$ -anodized AAO template showed a regular and uniform etching in a large area, unlike the H_3PO_4 -anodized AAO template. After 47min of etching, the pores started to open, and the other side of the nanowires became accessible for further modification. In addition, side view SEM images shown in Figure 70 proved that both sides of the AAO templates were opened and no further pore widening happened; therefore, these conditions were applied for all of further experiments.

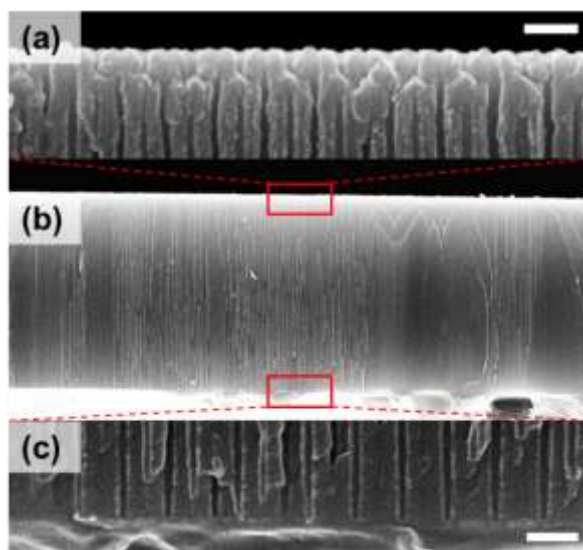


Figure 70. Side view SEM images of the opened $H_2C_2O_4$ -anodized AAO template etched by phosphoric acid: (a) initially opened pores, (b) overall view of the template, and (c) the opened pores after removal of the barrier layer (Scale bar: 200nm).

The unmodified ends of the nanowires that revealed by wet etching were then modified by cresyl violet perchlorate. Prior to the modification, the other side of AAO template was covered by a PET film and tapes to prevent that cresyl violet modified the side where was already modified with NBD-amine. Subsequently, the sample was immersed in 0.01 wt% cresyl violet solution in methanol for 1 h. After sufficient washing, the multi-functionalized nanowires were then released by removing the sacrificial AAO templates.

To verify the post-polymerization modification of PPFPA nanowires, fluorescence optical microscopy was conducted. As shown in Appendix D, many nanowires emitting green at both ends were found, and a phenomenon that one end emits brighter than the other end was also observed. Furthermore, this phenomenon was also observed in a close look at a multi-functionalized nanowires, as shown in Figure 71. It can be seen that the nanowire has two emitting ends with different intensity and the expected size of a nanowire fabricated from the AAO template having a length of 7 μm in length. To explain the phenomenon, the quantum yield of two dyes was calculated by comparing the gradient of the plot for the dyes and the gradient of the plot for rhodamine B as a reference dye. The gradient was determined by plotting maximum absorbance of the dyes in function of fluorescence intensity. As a result, it was found that NBD-amine has a higher quantum yield than cresyl violet; therefore, it was

assumed that the variation of emitting intensity was caused by the difference of the quantum yield between two dyes.

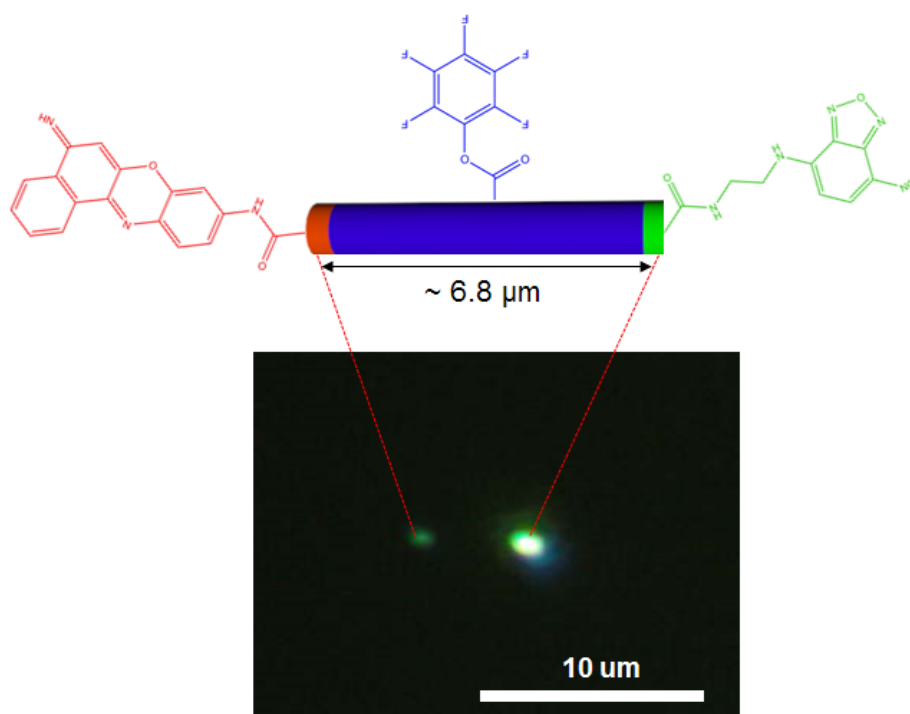


Figure 71. Illustration of a nanowire modified on both sides and fluorescence optical microscopy image of a multi-functionalized PPFPA nanowire.

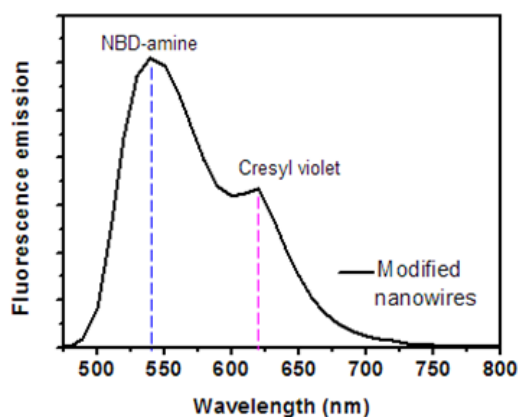


Figure 72. Fluorescence emission spectrum of the multi-functionalized nanowires.

Furthermore, fluorescence emission spectra were measured to confirm the presence of dyes with the multi-functionalized nanowires. As a reference, two dyes were dissolved in DI water and their solutions were measured. The NBD-amine solution was excited at 450 nm and emitted at 540 nm, and the cresyl violet solution was excited at 560 nm and emitted at 620 nm,

respectively. A solution containing the multi-functionalized nanowires was excited at 450 nm which could excite both dyes, and its emission was observed at 540 nm and 620 nm, which verified the presence of both dyes. From the results of the fluorescence optical microscopy and of the fluorescence spectrum, the successful fabrication of the multi-functionalized nanowires could be confirmed.

4. Conclusion and outlook

In summary, a facile method for the fabrication of the stimuli-responsive and chemically tunable nano-objects and nanostructured thin films was presented. Via the template-assisted replication method and the post-polymerization modification, various types of nano-objects were successfully produced, and these were applied in surface engineering and drug delivery system.

Multi-branched AAO templates were fabricated via the modified two-step anodization process. These templates were used to prepare various kinds of hierarchically branched PPFPA nanostructures. The hierarchically branched PPFPA nanostructures were then modified with spiropyran-amine via the post-polymerization modification, resulting in light-responsive nanostructures. Depending on the nanostructures, the distinct contact angles were shown, and the dramatic changes of the contact angles were observed upon UV light irradiation.

Biocompatible and thermosensitive nanostructured PNVCL thin films were prepared for a drug delivery system. The nanostructured PNVCL thin films adsorbed the fluorescent dye rhodamine B or the potent drug aspirin under ambient conditions and released them upon heating at around human body temperature. The nanostructured PNVCL thin film showed an improved adsorption and release of the dye compared to the non-structured PNVCL thin film. Furthermore, nanostructures on the film were not damaged after the release of dye, and the thin film was reusable without a deterioration of performance.

Block-like nanorods were produced by sequential infiltration of two types of monomer solution. By selecting the proper solvents for the monomer solution, physically bonded nanorods could be fabricated. Depending on the time of oxygen plasma treatment, different lengths of PS nanorods were prepared, and PNIPAM nanorods were formed on the PS nanorods sequentially. Using this method, various ratios of temperature-responsive block-like nanorods were successfully produced; however, it was found that the physically bonded nanorods were vulnerable to an external stimulus. To overcome this problem, the chemically bonded block-like nanorods were fabricated by several new methods. Using EDA as the linker between two blocks containing PFP group showed a great potential to prepare the chemically bonded block-like nanorods, and the structure of block-like nanorods was verified by SEM.

An innovative method to fabricate the multi-functionalized nanowires was demonstrated. PPFPA nanowires that can be modified with amines were prepared by the template-assisted replication method. The closed pores of AAO templates were opened by either RIE or the wet etching method to access both ends of the nanowires. Afterwards, both opened ends of the PPFPA nanowires were chemically modified with NBD-amine and cresyl violet perchlorate via the post-polymerization modification method. The fluorescence optical microscopy images and the fluorescence spectra confirmed that both ends of the PPFPA nanowires were successfully modified with the different fluorescent dyes.

The presented approaches are expected to expand the functionalities of nano-objects by applying various amines via post-polymerization modification, thereby the nano-objects obtain a complexity which is desired for an advanced nanoscience. Moreover, substituting the activated ester with particular stimuli-responsive amines allows the nano-objects or the thin films to react upon a specific stimulus. These stimuli-responsive materials can be applied in drug delivery application which requires a smart system to effectively release a drug, or in surface engineering which is used in the coating industry.

5. Experimental section

5.1 Characterization methods

The topographies of all samples were investigated by scanning electron microscopy (SEM, Sigma-Zeiss) after gold sputtering (Cressington sputter coater) onto the surfaces with a thickness of less than 3 nm. To measure the wetting properties of the nanostructures, contact angle measurements were conducted using a DataPhysics OCA 20. In general, a minimum of five data points on each sample were measured. The post-modified nano-objects and the thin films were investigated by a Nicolet iS10 FT-IR spectrometer. To investigate the nano-objects modified by the fluorescent dyes, fluorescence spectrometer and fluorescence optical microscope (Olympus BX51 with fluorescence illuminator, X-Cite series 120 Q - EXFO) were conducted. The adsorption and release of dye or drug were monitored by UV-vis spectroscopy (Jasco V-630 spectrophotometer). LCST measurement was performed with UV-vis spectroscopy using a Jasco ETC-717 peltier element with continuous stirring. The size of nano-objects was measured by DLS (Malvern Zetasizer Nano-ZS90) which is equipped with a He-Ne laser operated at 632 nm. ^1H NMR spectra were measured by a Bruker Fourier 300 NMR spectrometer.

5.2 Fabrication of anodized aluminum oxide (AAO) templates

High purity aluminum chips (Goodfellow, Al 99.999%) were placed in an anodization cell (the picture of set-up is shown in Figure 8) and electropolished in a vigorously stirred mixture of ethanol and perchloric acid (v/v 3:1) with an applied voltage of 20 V for 5 min at 5°C. Subsequently, the cells were washed with deionized water and isopropanol. For the fabrication of the AAO templates, a well-established two-step anodization process was applied. In the first step, the electropolished aluminum was anodized in an aqueous solution of oxalic acid (0.3M) at 40 V, 5°C or phosphoric acid (1.0 wt%) at 195 V, ~0.5°C for 24 h. After the first anodization, the aluminum oxide layer was removed in aqueous solution of chromic acid (1.8 wt%) and phosphoric acid (6.0 wt%) at 45°C for 24 h. For the second anodization, the process was performed in aqueous solution of oxalic acid (0.3M) at 40 V, 5°C or phosphoric acid (1.0 wt%) at 195 V, ~0.5°C for a certain of time depending on a desired length of pores.

5.3 Fabrication of hierarchically branched AAO templates

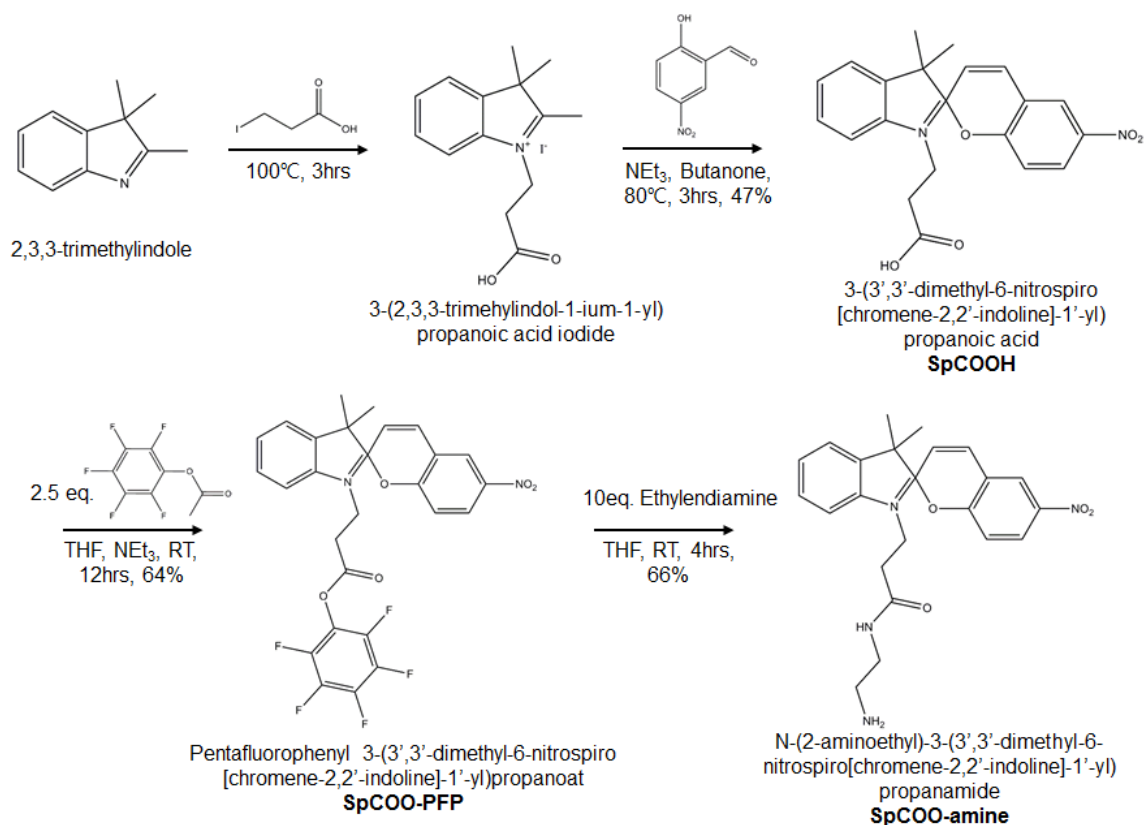
High purity aluminum chips (Goodfellow, Al 99.999%) were placed in an anodization cell and electropolished in a vigorously stirred mixture of ethanol and perchloric acid (v/v 3:1) with an applied voltage of 20 V for 5 min at 5 °C. Subsequently, the cells were washed with deionized water and isopropanol. For the fabrication of the hierarchically branched AAO templates, an asymmetric two-step anodization was applied. In the first step, the electropolished aluminum was anodized in an aqueous solution of phosphoric acid (1.0 wt%) at 175 V for 3 h, and sequentially the voltage was increased to 195 V and applied for 21 h. After the first anodization, the aluminum oxide layer was removed in aqueous solution of chromic acid (1.8 wt%) and phosphoric acid (6.0 wt%) at 45 °C for 48 h. For a fabrication of branched shape of AAO, the second anodization was initially performed in aqueous solution of phosphoric acid (1.0 wt%) at 195 V for 12 min and the barrier layer was subsequently thinned out by consecutive reduction of the applied voltage down to 80 V (-0.02 V/s). After exchanging the electrolyte against oxalic acid (0.3M), the reduction of the applied voltage was continued to 0 V (exponential decay of the applied voltage). Further thinning process of the barrier layer of the template was conducted in phosphoric acid (10 wt%) for 1 h at r.t. A subsequent anodization resulted in the formation of branched pores, which were further processed in oxalic acid (0.3M) at 40 V for 3 to 7 min. Pore widening was performed in aqueous phosphoric acid (10 wt%) at r.t. for 15 min. In order to fabricate a raspberry shape of AAO, the second anodization step was performed at 40V for 3 to 7 min in 0.3M oxalic acid solution at 1~8 °C. Pore widening was performed in aqueous phosphoric acid (5 wt%) solution at r.t.

5.4 Synthesis of PFPA

35.0 g (190 mmol) pentafluorophenol and 27.7 mL (199 mmol) trimethylamine were dissolved in 700 mL diethyl ether in a three neck flask, which was cooled with an ice bath. After 10 min stirring, 18 mL (223 mmol) acryloyl chloride was added drop-wise to the solution and cooling was continued for 30 min. The solution was stirred for additional 3 h at r.t. Next, the solution was separated from the precipitated salt via filtration, and diethyl ether was removed via rotary evaporation. PFPA was then purified via column chromatography with petroleum ether as eluent. Finally, the gathered PFPA fractions were evaporated to remove petroleum ether and 17.9 mL (109 mmol) of a colorless liquid were obtained, which represents a 57 % yield.¹⁸³

$^1\text{H-NMR}$ (300 MHz, Chloroform- d , 25 °C): δ [ppm] = 6.72 (d, J = 17.2, 1H, a), 6.37 (dd, J = 17.2, 10.5 Hz, 1H, a), 6.18 (d, J = 10.5, 1H, b). Further signals: 3.86 (t), 3.17 (t), 1.57 (s, water). $^{19}\text{F-NMR}$ (Chloroform- d): δ [ppm] = -153.79, -156.90, -162.43.¹²¹ FT-IR (ATR): $\tilde{\nu}$ [cm^{-1}] = 1771 (middle, $-\text{C}=\text{O}$ reactive ester band), 1635 (m, ethylenic $-\text{C}=\text{C}-$ valence), 1515 (strong, $-\text{C}=\text{C}-$ aromatic band), 1405 (m, $-\text{CH}_3$ and $-\text{CH}_2-$ deformation), 1218 (m, $-\text{COC}-$ valence), 1112 (s, $-\text{CO}-$ valence), 1070 (m, $-\text{COC}-$ valence), 991 (s, $=\text{CH}-$ deformation).

5.5 Synthesis of spiropyran-amine



5.5.1 Synthesis of 3-(2,3,3-trimethylindol-1-ium-1-yl)propanoic acid iodide

9.3 g (46 mmol) 3-iodopropionic acid were added to 7.8 mL (49 mmol) 2,3,3-trimethylindolenine in a 500 mL round bottom flask. After three freeze-pump-thaw cycles, the solution was heated at 100 °C while being stirred under reflux for 3 h. A red solid was obtained, which was dissolved in 100 mL water and stirred overnight at r.t. Then, the solution was washed three times with 50 mL chloroform. The organic phase was red and the water phase, which contained the product, yellow. Evaporation of water led to 15.7 g (43.8 mmol) of 3-(2,3,3-trimethylindol-1-ium-1-yl)propanoic acid iodide (95 % yield).¹⁸⁴

¹H-NMR (300 MHz, DMSO-d₆, 25 °C): δ [ppm] = 8.03–7.94 (m, 1H, aromatic proton), 7.88–7.80 (m, 1H, aromatic proton), 7.68–7.57 (m, 2H, aromatic protons), 4.65 (t, J = 7.0 Hz, 2H, NCH₂), 2.98 (t, J = 7.0 Hz, 2H, CH₂COO), 2.86 (s, 3H, NCH₃), 1.53 (s, 6H, 2 CH₃). Further signals: 3.60 (m).

5.5.2 Synthesis of 3-(3',3'-dimethyl-6-nitrospiro(chromene-2,2'-indoline)-1'-yl)propanoic acid (SpCOOH)

3-(2,3,3-Trimethylindol-1-ium-1-yl) propanoic acid iodide, 7.32 g (43.8 mmol) 2-hydroxy-5-nitrobenzaldehyde and 4.34 mL (43.8 mmol) piperidine were dissolved in 200 mL 2-butanone and the red solution was refluxed for 3 h (100 °C). Afterwards, the flask was stored at 4 °C overnight. The product precipitated as a yellow powder, which was filtered and washed with methanol to give 6.82 g (17.9 mmol) SpCOOH (41 % yield).¹⁸⁴

¹H-NMR (300 MHz, DMSO-d₆, 25 °C): δ [ppm] = 12.22 (s, 1H), 8.21 (d, J = 2.8 Hz, 1H), 8.00 (dd, J = 9.0, 2.8 Hz, 1H), 7.21 (d, J = 10.4 Hz, 1H), 7.12 (t, J = 6.8 Hz, 2H), 6.86 (d, J = 9.0 Hz, 1H), 6.80 (t, 1H), 6.66 (d, J = 7.6 Hz, 1H), 5.99 (d, J = 10.4 Hz, 1H), 3.57–3.37 (m, 2H), 2.65–2.53 (m, 1H), 2.48–2.37 (m, 1H), 1.18 (s, 3H), 1.07 (s, 3H). Further signals: 3.33 (s, H₂O), 2.06 (s, CH₃CO, butanone), 0.91 (t, CH₂CH₃, butanone).

5.5.3 Synthesis of Pentafluorophenyl 3-(3',3'-dimethyl-6-nitrospiro (chromene-2,2'-indoline)-1'-yl)propanoate (SpCOO-PFP)

6.80 g (17.9 mmol) SpCOOH were dissolved with 6.23 mL (4.52 g, 44.7 mmol) trimethylamine in 80 mL dry THF in a three neck flask. Under nitrogen atmosphere, 7.67 mL (12.52 g, 44.7 mmol) of pentafluorophenyl trifluoroacetate in 30 mL THF were added drop-wise at r.t. The solution was stirred overnight under reflux. Additionally, 100 mL of dichloromethane were added and the solution was transferred into a separation funnel. The organic phase was washed three times with 50 mL of DI water and dried over sodium sulfate. After removing dichloromethane, the crude product was recrystallized from 160 mL of a petroleum ether-toluene-mixture (3:1 v/v) resulting in 8.87 g (16.2 mmol) of a yellow colored crystal (91 % yield).⁹⁹

¹H-NMR (300 MHz, DMSO-d₆, 25 °C): δ [ppm] = 8.21 (d, J = 2.8 Hz, 1H), 8.00 (dd, J = 9.0, 2.8 Hz, 1H), 7.23 (d, J = 10.4 Hz, 1H), 7.19–7.10 (m, 2H), 6.88 (d, J = 9.1 Hz, 1H), 6.80 (dd,

7.8, 7.8 Hz, 2H), 6.00 (d, $J = 10.4$ Hz, 1H), 3.74–3.43 (m, 2H), 3.27–2.95 (m, 2H), 1.20 (s, 3H), 1.09 (s, 3H).

5.5.4 Synthesis of N-(2-aminoethyl)-3-(3',3'-dimethyl-6-nitro-spiro(chromene-2,2'-indoline)-1'-yl)propanamide (SpCOO-NH)

A three neck flask was filled with 10.8 mL (9.74 g, 162 mmol) ethylenediamine, which were diluted in 60 mL THF. Then, 8.86 g (16.2 mmol) SpCOO-PFP were dissolved in 80 mL THF and slowly added with a dropping funnel to the ethylenediamine solution. The reaction solution was stirred overnight at r.t. The precipitated solid was filtrated, dissolved in 200 mL dichloromethane and washed 3 times with 30 mL DI water. After separation, the remaining water in the organic phase was dried over sodium sulfate and the solvent was removed via rotary evaporation. 6.34 g (15 mmol) of a bronze-colored crystal were obtained. This represents a 93 % yield.⁹⁹

¹H-NMR (300 MHz, DMSO-d₆, 25 °C): δ [ppm] = 8.51 (s, 1H), 8.38 (s, 1H), 8.11 (s, 1H), 8.21 (d, $J = 2.9$ Hz, 1H), 7.99 (dd, $J = 8.9, 2.7$ Hz, 1H, t), 7.18 (d, $J = 6.4$ Hz, 1H, u), 7.15–7.08 (m, 2H, b), 6.85 (d, $J = 8.9$ Hz, 1H, f), 6.82–6.72 (m, 2H, a, e), 6.67 (t, 1H, p), 5.97 (d, $J = 10.4$ Hz, 1H, o), 4.37 (d, $J = 9.7$ Hz, 1H, k), 3.92 (t, 1H, i), 3.85 (t, 1H, i), 3.74 (t, 1H, l), 3.45 (t, 1H, l), 3.14–2.99 (m, 2H, m), 2.67–2.54 (m, 2H, j), 1.24 (s, 6H, g, h), 1.17 (s, 2H, n), 1.06 (s, 2H). Further peaks: 5.75 (s, dichloromethane), 4.22 (m), 3.60 (m, tetrahydrofuran), 2.50 (p, DMSO-d₆), 2.46–2.20 (m), 1.76 (m, THF). FT-IR (ATR): $\tilde{\nu}$ [cm⁻¹] = 3300 (m, –NH– amide valence), 3060 (m-w, aromatic =C–H– valence), 2960 (w, –CH₂– valence), 1645 (m, ethylenic –C=C– valence), 1606 (m, –NH– deformation), 1547 (m, –NH– deformation), 1486 (s, aromatic valence), 1324 (s, aromatic –NO₂ valence), 1260 (s, aromatic –COC– valence), 742 (s, =CH– deformation).

5.6 Preparation of self-assembled monolayer (SAM)

The substrates, such as PET film and glass, was exposure by oxygen plasma for 30 min to oxidase the surface. Directly after the plasma, the substrates were immersed in a 0.1wt% vinyltriethoxysilane solution in THF, and heated at 40 °C for 48 h. After then, the substrates were removed from the solution and sufficiently washed with THF.

5.7 Fabrication of PPFPA nanopillars

A solution of PPFPA with 1,6-hexanediol diacrylate (10 wt%) and diphenyl (2,4,6-trimethylbenzoyl) phosphine oxide (TPO) (5 wt%) was drop cast onto an AAO template and vacuum was applied for 5 min at r.t. to assist infiltration into the pores. Afterwards, a PET film, which was modified with vinyltrimethoxysilane and hence exposing the vinyl group on the surface to enhance adhesion, was covered on top of AAO as a supporting substrate and was irradiated with UV light (365 nm) for 30 min to polymerize the PPFPA. The sacrificial AAO was removed in subsequent steps. First, aluminum was removed by a $\text{CuCl}_2 \cdot \text{HCl}$ (0.02M) solution with an ice bath, and then aluminum oxide was removed by 10 wt% phosphoric acid solution at 45 °C for 1 h. Subsequently, the sample was washed with sufficient deionized water. Before the water evaporated, the sample was frozen by dipping it into the liquid nitrogen and was placed in a freeze-drying station for several days.

5.8 Surface modification of PPFPA nanopillars

Spiropyran-amine (5 wt%) was dissolved in methanol and stirred for several days until a homogeneous solution was obtained. The free-standing nanopillars were immersed in the solution for 18 h under ambient conditions, and then washed with de-ionized water and methanol. The freeze-drying technique was applied to prevent the collapse of the nanopillars. For the photo-isomerization of spiropyran, the sample was irradiated with UV light (254 nm) for 20 min.

5.9 Fabrication of PNVCL nanostructured thin films

To prepare a solution, *N*-vinylcaprolactam (NVCL) (679 mg), 1,6-hexanediol diacrylate (115 mg), and diphenyl (2,4,6-trimethylbenzoyl) phosphine oxide (TPO) (34.6 mg) were dissolved in 1 g methanol, and the mixture was stirred at r.t. for 3-5 h under dark. After then, the NVCL solution (30 μl) was drop-casted onto a prepared AAO template, and the solution was spin-coated at 2000 rpm for 15 sec. Afterwards, UV light (365 nm) was irradiated onto the surface for 1 h to polymerize NVCL. Aluminum of AAO template was removed by $\text{CuCl}_2 \cdot \text{HCl}$ (0.02 mol) solution at 45°C and washed by excess DI water. Al etched samples were then placed in 10 wt% H_3PO_4 solution at 45°C for 1 h 30 min. To keep the temperature consistently, the water bath was used.

5.10 Adsorption and release of dye and drug

The nanostructured PNVCL thin film was placed in Rhodamine B solution (1.75×10^{-3} g/L) or Aspirin (acetylsalicylic acid) solution (0.25×10^{-3} g/L) in water and stirred constantly at r.t.. The amount of adsorption of dye or drug was monitored by UV-vis spectroscopy for 24 h. The dye adsorbed nanostructured PNVCL thin film was washed with DI water gently and put into pure DI water and heated at 36°C or 50°C. The release of dye was recorded by UV-vis spectroscopy up to certain time.

5.11 Fabrication of TPT molds

Trimethylolpropane propoxylate (2 PO/OH) triacrylate (TPT) was mixed with 2-hydroxy-2-methyl-propophenone (photo-initiator) in a volume ratio 95 to 5. After vigorous stirring, 20 μ l TPT solution was drop-casted onto the AAO template, and the vacuum was applied on the template for 5min. 20 to 30 μ l TPT solution was more drop-casted, and a glass having SAM was covered on top of template. For the polymerization of TPT, UV light (365 nm) was irradiated for 1 h. After one day, the sacrificial AAO template was removed by phosphoric acid.

5.12 Fabrication of physically bonded block-like nanorods

A 20 wt% styrene solution with 1,6-hexanediol diacrylate (2 wt%) and diphenyl (2,4,6-trimethylbenzoyl) phosphine oxide (TPO) (0.2 wt%) in ethanol was drop cast onto an AAO template and spin-coated at 2000 rpm for 15 sec. After then, the styrene was polymerized by UV light (365 nm) for 30 min, and the half of fabricating PS nanorods was subsequently etched by oxygen plasma. A 40 wt% NIPAM solution with 1,6-hexanediol diacrylate (4 wt%) and diphenyl (2,4,6-trimethylbenzoyl) phosphine oxide (TPO) (0.4 wt%) in methanol was then drop cast onto the PS nanorods and spin-coated at 9000 rpm for 15 sec. UV light (365 nm) was irradiated for 30 min to polymerize the NIPAM.

5.13 Fabrication of chemically bonded block-like nanorods

5.13.1 Chemically bonded nanorods by using APTES

A 20 wt% styrene solution with 1,6-hexanediol diacrylate (2 wt%) and diphenyl (2,4,6-trimethylbenzoyl) phosphine oxide (TPO) (0.2 wt%) in ethanol was drop cast onto an AAO template and spin-coated at 2000 rpm for 15 sec. After then, the styrene was polymerized by

UV light (365 nm) for 30 min, and the half of fabricating PS nanorods was subsequently etched by oxygen plasma. After then, the template containing the PS nanorods was directly immersed in a 0.4 % APTES solution in DI water for 15 min at r.t. A 40 wt% NIPAM solution with PFPA (20 wt%), 1,6-hexanediol diacrylate (4 wt%), and diphenyl (2,4,6-trimethylbenzoyl) phosphine oxide (TPO) (0.4 wt%) in methanol was then drop cast onto the modified PS nanorods and the template was pressed by a non-structured PDMS pad. Subsequently, UV light (365 nm) was irradiated for 30 min to polymerize the monomers.

5.13.2 Chemically bonded nanorods by using EDA (1)

A 20 wt% styrene solution with PFPA (10 wt%), 1,6-hexanediol diacrylate (2 wt%), and diphenyl (2,4,6-trimethylbenzoyl) phosphine oxide (TPO) (0.2 wt%) in ethanol was drop cast onto an AAO template and spin-coated at 2000 rpm for 15 sec. After then, the styrene was polymerized by UV light (365 nm) for 30 min, and the half of fabricating PS nanorods was subsequently etched by oxygen plasma. After then, the template containing the PS nanorods was directly immersed in a 50 wt% EDA solution in methanol for 30 min and in a 40 wt% NIPAM solution with PFPA (20 wt%), 1,6-hexanediol diacrylate (4 wt%), and diphenyl (2,4,6-trimethylbenzoyl) phosphine oxide (TPO) (0.4 wt%) in methanol for 30min at r.t.. Afterwards, the template was spin-coated at 5000 rpm for 15 sec to remove excess NIPAM solution. Subsequently, UV light (365 nm) was irradiated for 30 min to polymerize the monomers.

5.13.3 Chemically bonded nanorods by using EDA (2)

A 20 wt% styrene solution with PFPA (1 wt%), 1,6-hexanediol diacrylate (2 wt%), and diphenyl (2,4,6-trimethylbenzoyl) phosphine oxide (TPO) (0.2 wt%) in ethanol was drop cast onto an AAO template and spin-coated at 2000 rpm for 15 sec. After then, the styrene was polymerized by UV light (365 nm) for 30 min, and the half of fabricating PS nanorods was subsequently etched by oxygen plasma. After then, the template containing the PS nanorods was directly immersed in a 20 wt% EDA solution in methanol for 1 h at r.t. A PFPA solution with 1,6-hexanediol diacrylate (10 wt%), and diphenyl (2,4,6-trimethylbenzoyl) phosphine oxide (TPO) (5 wt%) was then drop cast onto the modified PS nanorods, and the template was squeezed between two glasses with clip. Vacuum was applied for 2h at r.t., and then, UV light (365 nm) was irradiated for 30 min to polymerize the PFPA.

5.14 Fabrication of PPFPA nanowires

A solution of PFPA with 1,6-hexanediol diacrylate (10 wt%) and diphenyl (2,4,6-trimethylbenzoyl) phosphine oxide (TPO) (5 wt%) was drop cast onto an AAO template, and the template was squeezed between two glasses with a clip. Afterwards, vacuum was applied for 2 h at r.t. to assist the infiltration of the PFPA solution. After then, UV light (365 nm) was irradiated for 30 min to polymerize the PFPA. The residual PPFPA layer on top of AAO templates was removed by oxygen plasma.

5.15 Removal of barrier layer via RIE

Aluminum was removed by a $\text{CuCl}_2 \cdot \text{HCl}$ (0.02M) solution with an ice bath, and then the barrier layer of AAO template was removed by CF_4 reactive ion etching. The reactive ion etching was conducted at 0.16 mbar with 180W for 15 – 180 min.

5.16 Removal of barrier layer via wet-etching

After aluminum was removed as described above, the barrier layer was removed by 5 wt% or 10 wt% phosphoric acid solution at 30°C for up to 50 min and 71 min, respectively.

5.17 Tip modification of PPFPA nanowires

NBD-amine (0.01 wt%) was dissolved in methanol and stirred for several hours until a homogeneous solution was obtained. The AAO template containing PPFPA nanowires with one open end was immersed in the solution for 1 h under ambient conditions, and then washed with methanol and de-ionized water. After the removal of barrier layer, the other end of nanowires was modified with cresyl violet fluorescence dye. 0.01 wt% cresyl violet was dissolved in methanol and stirred for several hours until a homogeneous solution was obtained. The one side of AAO template which was modified with NBD-amine was covered by PET film and tapes and the AAO template with the other open end was immersed in the cresyl violet solution for 1 h. After sufficient washing, aluminum oxide which supports the nanowires was removed by 10wt% phosphoric acid solution at 45°C for 1 h. To remove the excess dyes, dialysis was conducted overnight.

5.18 List of chemicals

Chemicals	Hazard symbol	H-Phrases	P-Phrases
1,6-hexanediol diacrylate	 GHS07	H315, H317, H319	P280-P305 + P351 + P338
2-hydroxy-2-methyl-propophenone	 GHS07 GHS09	H302, H400, H410, H412	P264, P270, P273, P301+P312, P330, P391, P501
2-Hydroxy-5-nitrobenzaldehyde	 GHS07	H302, H315, H319	P305 + P351 + P338
2,3,3-trimethylindolenine	 GHS07	H315, H319, H335	P280-P305 + P351 + P338-P337 + P313
3-iodopropionic acid	 GHS05	H314	P280-P305 + P351 + P338-P310
Acetylsalicylic acid	 GHS07	H302, H315, H319, H335	P261-P305 + P351 + P338

Experimental section

<p>Acryloyl chloride</p>	  <p>GHS02 GHS06</p>   <p>GHS05 GHS09</p>	<p>H225, H290 H330, H314 H302+H312 H400</p>	<p>P210, P280, P273,P301+P330+ P331, P302+P352, P304+P340, P305+P351+P338, P309+P310</p>
<p>Aminopropyltriethoxysilane</p>	  <p>GHS05 GHS07</p>	<p>H302, H314, H317</p>	<p>P280-P305 + P351 + P338-P310</p>
<p>Chromic acid</p>	  <p>GHS05 GHS09</p>   <p>GHS07 GHS03</p>   <p>GHS08 GHS06</p>	<p>H271, H301+H311, H314, H317, H330, H334, H340, H350, H361, H372, H400, H410</p>	<p>P:201, 202, 210, 220, 221, 260, 264, 270, 271, 272, 273, 280, 283, 284, 301+330+331, 303+361+353, 304+340, 305+351+338, 306+360, 308+313, 310, 333+313, 342+311, 363, 370+378, 371+380+375, 391, 403+233, 405, 501</p>
<p>Cresyl Violet perchlorate</p>	 <p>GHS07</p>	<p>H315, H319, H335</p>	<p>P261-P305 + P351 + P338</p>

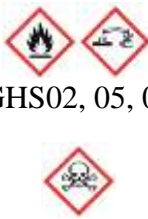
Experimental section

Diphenyl (2,4,6-trimethylbenzoyl) phosphine oxide	 GHS07, 09 GHS08	H317, H361, H411	P280
Ethylenediamine	 GHS05, 07 GHS08, 02	H226, H302+H312, H314, H317, H334	P:210, 233, 240, 241, 242, 243, 260, 264, 270, 272, 280, 284, 301+330+331, 303+361+353, 304+340, 305+351+338, 310, 363, 403+235, 405, 501
<i>N</i> -isopropylacrylamide	 GHS07	H302, H319	P264, P270, P280, P330, P301+312, P337+313, P305+351+338
<i>N</i> -vinylcaprolactam	 GHS07, 08	H302 + H312, H317, H319, H372	P260-P280-P301 + P312 + P330-P305 + P351 + P338
Oxalic acid	 GHS05 GHS07	H302, H312, H318	P280, P264, P305+351+310, P301+312, P302+352, P501
Pentafluorophenol	 GHS07	H302+312+ 332, H315, H319, H335	P280
Pentafluorophenyl acrylate	 GHS07	H315, H319, H335	P280, P302+352, P304+340, P305+351+338, P312, P321

Experimental section

Pentafluorophenyl trifluoroacetate	  GHS02, 07	H226, H315, H319, H335	P261-P305 + P351 + P338
Perchloric acid	  GHS05, 07   GHS08, 02	H271, H290, H302, H314, H373	P210-P280-P303 + P361 + P353-P304 + P340 + P310- P305 + P351 + P338-P371 + P380 + P375
Phosphoric acid	 GHS05	H290, H314	P280-P303 + P361 + P353-P304 + P340 + P310-P305 + P351 + P338
Piperidine	  GHS02, 05  GHS06	H225, H302, H311 + H331, H314	P210-P280-P304 + P340 + P310-P305 + P351 + P338- P370 + P378-P403 + P235
Rhodamine B	  GHS05, 07	H302, H318, H412	P273-P280-P305 + P351 + P338
Styrene	  GHS02, 07  GHS08	H226, H315, H319, H332, H361d, H372	P201-P210-P261- P280-P304 + P340 + P312-P308 + P313

Experimental section

<p>Triethylamine</p>	 <p>GHS02, 05, 06</p>	<p>H225, H302, H311 + H331, H314, H335</p>	<p>P210-P261-P280- P303 + P361 + P353-P305 + P351 + P338-P370 + P378</p>
<p>Trimethylolpropane propoxylate (2 PO/OH) triacrylate</p>	 <p>GHS07</p>	<p>H315, H319, H335</p>	<p>P261-P305 + P351 + P338</p>
<p>Vinyltrimethoxysilane</p>	 <p>GHS02, 07</p>	<p>H225, H332</p>	<p>P210</p>

6. References

- (1) Biswas, A.; Bayer, I. S.; Biris, A. S.; Wang, T.; Dervishi, E.; Faupel, F. *Advances in Colloid and Interface Science*. **2012**, *170*, 2–27.
- (2) Barth, J. V.; Costantini, G.; Kern, K. *Nature*. **2005**, *437* (7059), 671–679.
- (3) Menard, E.; Meitl, M. A.; Sun, Y.; Park, J. U.; Shir, D. J. L.; Nam, Y. S.; Jeon, S.; Rogers, J. A. *Chem. Rev.* **2007**, *107* (4), 1117–1160.
- (4) Pokroy, B.; Epstein, A. K.; Persson-Gulda, M. C. M.; Aizenberg, J. *Adv. Mater.* **2009**, *21* (4), 463–469.
- (5) Qin, D.; Xia, Y.; Whitesides, G. M. *Nat. Protoc.* **2010**, *5* (3), 491–502.
- (6) Roca-Cusachs, P.; Rico, F.; Martínez, E.; Toset, J.; Farré, R.; Navajas, D. *Langmuir*. **2005**, *21* (12), 5542–5548.
- (7) Lockwood, D. J.; Wehrspohn, R. B.; Masuda, H. *Ordered Porous Nanostructures Appl.* **2005**, *Nanostruct*, 37–55.
- (8) Md Jani, A. M.; Losic, D.; Voelcker, N. H. *Prog. Mater. Sci.* **2013**, *58* (5), 636–704.
- (9) Lee, J. I.; Cho, S. H.; Park, S. M.; Kim, J. K.; Kim, J. K.; Yu, J. W.; Kim, Y. C.; Russell, T. P. *Nano Lett.* **2008**, *8* (8), 2315–2320.
- (10) Starbird, R.; García-González, C. A.; Smirnova, I.; Krautschneider, W. H.; Bauhofer, W. *Mater. Sci. Eng. C*. **2014**, *37* (1), 177–183.
- (11) Masuda, H.; Fukuda, K.; Chaikin, P. M.; Register, R. A.; Adamson, D. H.; Masuda, H.; Fukuda, K.; Gupta, R.; McClelland, J. J.; Jabbour, Z. J.; Celotta, R. J.; Lercel, M. J.; Wendel, M.; Kuhn, S.; Lorenz, H.; Kotthaus, J. P.; Holland, M.; McCord, M. A.; Awschalom, D. D.; Whitesides, G. M.; Mathias, J. P.; Seto, C. T.; Hofstadter, D.; Thouless, D. J.; Kohmoto, M.; Nightingale, M. P.; Nijs, M. den; Weiss, D.; Kang, W.; Stormer, H. L.; Pfeiffer, L. N.; Baldwin, K. W.; West, K. W.; Volkmuth, W. D.; Austin, R. H.; Volkmuth, W. D.; Duke, T.; Wu, M. C.; Austin, R. H.; Szabo, A.; Chou, S. Y.; Wei, M. S.; Krauss, P. R.; Fischer, P. B.; Morkved, T. L.; Morkved, T. L.; Wiltzius, P.; Jaeger, H. M.; Grier, D. G.; Witten, T. A.; Mansky, P.; Harrison, C. K.;

References

- Chaikin, P. M.; Register, R. A.; Yao, N.; Bates, F. S.; Fredrickson, G. H. *Science*. **1995**, *268* (5216), 1466–1468.
- (12) Shingubara, S.; Morimoto, K.; Sakaue, H.; Takahagi, T. *Electrochem. Solid-State Lett.* **2004**, *7* (3), E15.
- (13) Byun, J.; Lee, J. I.; Kwon, S.; Jeon, G.; Kim, J. K. *Adv. Mater.* **2010**, *22* (18), 2028–2032.
- (14) Buff, H. *Justus Liebigs Ann. Chem.* **1857**, *102* (3), 265–284.
- (15) Diggle, J. W.; Downie, T. C.; Goulding, C. W. *Chem. Rev.* **1969**, *69* (3), 365–405.
- (16) Keller, F.; Hunter, M. S.; Robinson, D. L. *J. Electrochem. Soc.* **1953**, *100* (9), 411.
- (17) Despić, A. R. *J. Electroanal. Chem. Interfacial Electrochem.* **1985**, *191* (2), 417–423.
- (18) Thompson, G. . E. *Thin Solid Films.* **1997**, *297* (1–2), 192–201.
- (19) Furneaux, R.C., Rigby, W.R., Davidson, a. P. *Nature*. **1989**, *337*, 147.
- (20) Thompson; Wood. *Nature*. **1981**, *290*, 230–232.
- (21) Masuda, H.; Satoh, M. *Japanese J. Appl. Physics, Part 2 Lett.* **1996**, *35* (1 B).
- (22) Lee, W.; Park, S.-J. *Chem. Rev.* **2014**, *114* (15), 7487–7556.
- (23) Wade, T. L.; Wegrowe, J.-E. *Eur. Phys. J. Appl. Phys.* **2005**, *29*, 3–22.
- (24) Mijangos, C.; Hernández, R.; Martín, J. *Progress in Polymer Science.* **2016**, *54 - 55*, 148–182.
- (25) Sapp, B. S. a; Lakshmi, B. B. *Adv. Mater.* **1999**, *11* (5), 402–404.
- (26) Steinhart, M.; Wendorff, J. H.; Wehrspohn, R. B. *ChemPhysChem.* **2003**, *4*, 1171–1176.
- (27) Steinhart, M.; Wehrspohn, R. B.; Gösele, U.; Wendorff, J. H. *Angewandte Chemie - International Edition.* **2004**, *43*, 1334–1344.
- (28) Wang, Y.; Gösele, U.; Steinhart, M. *Chem. Mater.* **2008**, *20* (2), 379–381.

References

- (29) Darling, S. B.; Yufa, N. A.; Cisse, A. L.; Bader, S. D.; Sibener, S. J. *Adv. Mater.* **2005**, *17* (20), 2446–2450.
- (30) Klein, J. D.; Li, R. D. H.; Palmer, D.; Sailor, M. J.; Brumlik, C. J.; Martin, C. R. *Chem. Mater.* **1993**, *5* (36), 902–904.
- (31) Penner, R. M. *J. Electrochem. Soc.* **1986**, *133* (8), 2206.
- (32) Kriha, O.; Zhao, L.; Pippel, E.; Gösele, U.; Wehrspohn, R. B.; Wendorff, J. H.; Steinhart, M.; Greiner, A. *Adv. Funct. Mater.* **2007**, *17* (8), 1327–1332.
- (33) Schlitt, S.; Greiner, A.; Wendorff, J. H. *Macromolecules.* **2008**, *41* (9), 3228–3234.
- (34) Zhang, R.; Zeng, X.; Prehm, M.; Liu, F.; Grimm, S.; Geuss, M.; Steinhart, M.; Tschierske, C.; Ungar, G. *ACS Nano.* **2014**, *8* (5), 4500–4509.
- (35) Xue, L.; Kovalev, A.; Dening, K.; Eichler-Volf, A.; Eickmeier, H.; Haase, M.; Enke, D.; Steinhart, M.; Gorb, S. N. *Nano Lett.* **2013**, *13* (11), 5541–5548.
- (36) Zhang, M.; Dobriyal, P.; Chen, J. T.; Russell, T. P.; Olmo, J.; Merry, A. *Nano Lett.* **2006**, *6* (5), 1075–1079.
- (37) Chen, D.; Zhao, W.; Russell, T. P. *ACS Nano.* **2012**, *6* (2), 1479–1485.
- (38) Liang, Y.; Zhen, C.; Zou, D.; Xu, D. *J. Am. Chem. Soc.* **2004**, *126* (50), 16338–16339.
- (39) Lakshmi, B. B.; Patrissi, C. J.; Martin, C. R. *Chem. Mater.* **1997**, *9* (11), 2544–2550.
- (40) Steinhart, M.; Wendorff, J. H.; Greiner, A.; Wehrspohn, R. B.; Nielsch, K.; Schilling, J.; Choi, J.; Gösele, U. *Science.* **2002**, *296* (5575), 1997.
- (41) Fox, H. W.; Hare, E. F.; Zisman, W. a. *J. Phys. Chem.* **1955**, *59* (10), 1097–1106.
- (42) Alvarez, S. D.; Li, C. P.; Chiang, C. E.; Schuller, I. K.; Sailor, M. J. *ACS Nano.* **2009**, *3* (10), 3301–3307.
- (43) Lakshmi, B. B.; Martin, C. R. *Nature.* **1997**, *388* (6644), 758–760.
- (44) Kohli, P.; Harrell, C. C.; Cao, Z.; Gasparac, R.; Tan, W.; Martin, C. R. *Science.* **2004**, *305* (5686), 984–986.

References

- (45) Martín, J.; Maiz, J.; Sacristan, J.; Mijangos, C. *Polymer*. **2012**, *53* (6), 1149–1166.
- (46) Sanz, B.; Ballard, N.; Asua, J. M.; Mijangos, C. *Macromolecules*. **2017**, *50* (3), 811–821.
- (47) Giussi, J. M.; Blaszczyk-Lezak, I.; Cortizo, M. S.; Mijangos, C. *Polym. (United Kingdom)* **2013**, *54* (26), 6886–6893.
- (48) Begum, F.; Zhao, H.; Simon, S. L. *Polym. (United Kingdom)* **2012**, *53* (15), 3238–3244.
- (49) Berezhkovskii, A. M.; Pustovoit, M. A.; Bezrukov, S. M. *J. Chem. Phys.* **2003**, *119* (7), 3943–3951.
- (50) Hernandez, H. F.; Tauer, K. *Ind. Eng. Chem. Res.* **2008**, *47* (24), 9795–9811.
- (51) Cui, Y.; Tao, C.; Tian, Y.; He, Q.; Li, J. *Langmuir*. **2006**, *22* (19), 8205–8208.
- (52) Cui, Y.; Tao, C.; Zheng, S.; He, Q.; Ai, S.; Li, J. *Macromol. Rapid Commun.* **2005**, *26* (19), 1552–1556.
- (53) Hui, C. Y.; Jagota, A.; Lin, Y. Y.; Kramer, E. J. *Langmuir*. **2002**, *18* (4), 1394–1407.
- (54) Chandra, D.; Taylor, J. A.; Yang, S. *Soft Matter*. **2008**, *4* (5), 979.
- (55) Campo, a Del; Greiner, C. *J. Micromechanics Microengineering*. **2007**, *17* (6), R81–R95.
- (56) Chen, G.; Soper, S. A.; McCarley, R. L. *Langmuir*. **2007**, *23* (23), 11777–11781.
- (57) Chandra, D.; Yang, S. *Langmuir*. **2009**, *25* (18), 10430–10434.
- (58) Kondo, T.; Juodkazis, S.; Misawa, H. *Applied Physics A: Materials Science and Processing*. **2005**, *81*, 1583–1586.
- (59) Tanaka, T.; Morigami, M.; Oizumi, H.; Ogawa, T. *Jpn. J. Appl. Phys.* **1993**, *32*, 5813–5814.
- (60) Jochum, F. D.; Theato, P. *Chem. Soc. Rev.* **2013**, *42* (17), 7468–7483.

References

- (61) Cabane, E.; Zhang, X.; Langowska, K.; Palivan, C. G.; Meier, W. *Biointerphases*. **2012**, *7*, 1–27.
- (62) Qiu, Y.; Park, K. *Advanced Drug Delivery Reviews*. **2012**, *64*, 49–60.
- (63) Bajpai, A. K.; Shukla, S. K.; Bhanu, S.; Kankane, S. *Progress in Polymer Science (Oxford)*. **2008**, *33*, 1088–1118.
- (64) Zhao, Y. *Macromolecules*. **2012**, *9*, 3647–3657.
- (65) Nath, N.; Chilkoti, A. *Adv. Mater.* **2002**, *14* (17).
- (66) Ward, M. A.; Georgiou, T. K. *Polymers*. **2011**, *3* (3), 1215–1242.
- (67) Moerkerke, R.; Koningsveld, R.; Berghmans, H.; Dusek, K.; Solc, K. *Macromolecules*. **1995**, *28* (4), 1103–1107.
- (68) Moerkerke, R.; Meeussen, F.; Koningsveld, R.; Berghmans, H.; Mondelaers, W.; Schacht, E.; Dusek, K.; Solc, K. *Macromolecules*. **1998**, *31* (7), 2223–2229.
- (69) Dimitrov, I.; Trzebicka, B.; Müller, A. H. E.; Dworak, A.; Tsvetanov, C. B. *Progress in Polymer Science (Oxford)*. **2007**, *32*, 1275–1343.
- (70) Schild, H. G. *Progress in Polymer Science*. **1992**, *17*, 163–249.
- (71) Lin, Shaojian.; Schattling, Philipp.; Theato, P. *Sci. Adv. Mater.* **2015**, *7* (5), 948–955.
- (72) Cao, P.-F.; Mangadlao, J. D.; Advincula, R. C. *Polym. Rev.* **2015**, *55* (4), 706–733.
- (73) Gil, E. S.; Hudson, S. M. *Progress in Polymer Science (Oxford)*. **2004**, *29*, 1173–1222.
- (74) Li, P. F.; Wang, W.; Xie, R.; Yang, M.; Ju, X. J.; Chu, L. Y. *Polym. Int.* **2009**, *58* (2), 202–208.
- (75) Cheng, H.; Shen, L.; Wu, C. *Macromolecules*. **2006**, *39* (6), 2325–2329.
- (76) Ramos, J.; Imaz, A.; Forcada, J. *Polym. Chem.* **2012**, *3*, 852–856.
- (77) Meeussen, F. *Polymer*. **2000**, *41* (24), 8597–8602.
- (78) Rao, K.; Rao, K.; Ha, C.-S. *Gels*. **2016**, *2* (1), 6.

References

- (79) Beija, M.; Marty, J.-D.; Destarac, M. *Chem. Commun.* **2011**, 47 (10), 2826–2828.
- (80) Meeussen, F.; Bauwens, Y.; Moerkerke, R.; Nies, E.; Berghmans, H. *Polymer*. **2000**, 41 (10), 3737–3743.
- (81) Diab, C.; Akiyama, Y.; Kataoka, K.; Winnik, F. M. *Macromolecules*. **2004**, 37 (7), 2556–2562.
- (82) Lowe, A. B.; McCormick, C. L. *Chem. Rev.* **2002**, 102 (11), 4177–4189.
- (83) Alvarez-Lorenzo, C.; Bromberg, L.; Concheiro, A. *Photochemistry and Photobiology*. **2009**, 85, 848–860.
- (84) Rapoport, N. *Progress in Polymer Science (Oxford)*. **2007**, 32, 962–990.
- (85) Lim, H. S.; Han, J. T.; Kwak, D.; Jin, M.; Cho, K. *J. Am. Chem. Soc.* **2006**, 128 (45), 14458–14459.
- (86) Wang, G.; Tong, X.; Zhao, Y. *Macromolecules*. **2004**, 37 (24), 8911–8917.
- (87) Chen, Z.; He, Y.; Wang, Y.; Wang, X. *Macromol. Rapid Commun.* **2011**, 32 (13), 977–982.
- (88) Jacquemin, P.-L.; Robeyns, K.; Devillers, M.; Garcia, Y. *Chem. Commun.* **2013**, 50 (6), 649–651.
- (89) Özçoban, C.; Halbritter, T.; Steinwand, S.; Herzig, L. M.; Kohl-Landgraf, J.; Askari, N.; Groher, F.; Fürtig, B.; Richter, C.; Schwalbe, H.; Suess, B.; Wachtveitl, J.; Heckel, A. *Org. Lett.* **2015**, 17 (6), 1517–1520.
- (90) Yager, K. G.; Barrett, C. J. *J. Photochem. Photobiol. A Chem.* **2006**, 182 (3), 250–261.
- (91) Kumar, G. S.; Neckers, D. C. *Chem. Rev.* **1989**, 89 (8), 1915–1925.
- (92) Natansohn, A.; Rochon, P. *Chem. Rev.* **2002**, 102 (11), 4139–4175.
- (93) Yu, Y.; Nakano, M.; Ikeda, T. *Nature*. **2003**, 425 (6954), 145–145.
- (94) Akiyama, H.; Kanazawa, S.; Okuyama, Y.; Yoshida, M.; Kihara, H.; Nagai, H.; Norikane, Y.; Azumi, R. *ACS Appl. Mater. Interfaces*. **2014**, 6 (10), 7933–7941.

References

- (95) Cao, P. F.; Su, Z.; De Leon, A.; Advincula, R. C. *ACS Macro Lett.* **2015**, *4* (1), 58–62.
- (96) Samanta, S.; Locklin, J. *Langmuir.* **2008**, *24* (17), 9558–9565.
- (97) Saragi, T. P. I.; Spehr, T.; Siebert, A.; Fuhrmann-Lieker, T.; Salbeck, J. *Chem. Rev.* **2007**, *107*, 1011–1065.
- (98) Hirshberg, Y. *J. Am. Chem. Soc.* **1956**, *78* (10), 2304–2312.
- (99) Kessler, D.; Jochum, F. D.; Choi, J.; Char, K.; Theato, P. *ACS Appl. Mater. Interfaces.* **2011**, *3* (2), 124–128.
- (100) Rosario, R.; Gust, D.; Hayes, M.; Jahnke, F.; Springer, J.; Garcia, A. A. *Langmuir.* **2002**, *18* (21), 8062–8069.
- (101) Vlassiouk, I.; Park, C. Do; Vail, S. A.; Gust, D.; Smirnov, S. *Nano Lett.* **2006**, *6* (5), 1013–1017.
- (102) Lee, H. Il; Wu, W.; Oh, J. K.; Mueller, L.; Sherwood, G.; Peteanu, L.; Kowalewski, T.; Matyjaszewski, K. *Angew. Chemie - Int. Ed.* **2007**, *46* (14), 2453–2457.
- (103) Crano, J. C.; Guglielmetti, R. J. (2002). *Organic Photochromic and Thermochromic Compounds*. New York: Kluwer Academic Publishers.
- (104) Theato, P. *J. Polym. Sci. Part A Polym. Chem.* **2008**, *46* (20), 6677–6687.
- (105) Gauthier, M.; Gibson, M.; Klok, H.-A. *Angew. Chemie Int. Ed.* **2009**, *48* (1), 48–58.
- (106) Cunningham, W. a. *J. Chem. Educ.* **1935**, *12* (3), 120–124.
- (107) Friedrich, C.; Part, S. *J. Chem. Educ.* **1929**, *6* (4), 677–685.
- (108) Theato, P.; Klok, H. A. (2013). *Functional Polymers by Post-Polymerization Modification: Concepts, Guidelines, and Applications*. Weinheim: Wiley-VCH Verlag GmbH & Co. KGaA.
- (109) Wang, J. S.; Matyjaszewski, K. *J. Am. Chem. Soc.* **1995**, *117* (6), 5614–5615.
- (110) Chiefari, J.; Chong, Y. K. B.; Ercole, F.; Krstina, J.; Jeffery, J.; Le, T. P. T.; Mayadunne, R. T. A.; Meijs, G. F.; Moad, C. L.; Moad, G.; Rizzardo, E.; Thang, S. H.; South, C. *Macromolecules.* **1998**, *31* (16), 5559–5562.

References

- (111) Hawker, C. J.; Bosman, A. W.; Harth, E. *Chem. Rev.* **2001**, *101* (12), 3661–3688.
- (112) Wong, L.; Sevimli, S.; Zareie, H. M.; Davis, T. P.; Bulmus, V. *Macromolecules.* **2010**, *43* (12), 5365–5375.
- (113) Mansfeld, U.; Pietsch, C.; Hoogenboom, R.; Becer, C. R.; Schubert, U. S. *Polym. Chem.* **2010**, 1560–1598.
- (114) Barner-Kowollik, C.; Du Prez, F. E.; Espeel, P.; Hawker, C. J.; Junkers, T.; Schlaad, H.; Van Camp, W. *Angew. Chemie - Int. Ed.* **2011**, *50* (1), 60–62.
- (115) Yang, S. K.; Weck, M. *Soft Matter.* **2009**, *5* (3), 582–585.
- (116) Xu, J.; Prifti, F.; Song, J. *Macromolecules.* **2011**, *44* (8), 2660–2667.
- (117) Hawker, C. J. *J. Am. Chem. Soc.* **1994**, *116* (24), 11185–11186.
- (118) Matyjaszewski, K.; Xia, J. *Chem. Rev.* **2001**, *101* (9), 2921–2990.
- (119) Batz, H. G.; Franzmann, G.; Ringsdorf, H. *Angew. Chemie Int. Ed. English.* **1972**, *11* (12), 1103–1104.
- (120) Ferruti, P.; Bettelli, A.; Feré, A. *Polymer.* **1972**, *13* (10), 462–464.
- (121) Kessler, D.; Theato, P. *Langmuir.* **2009**, *25* (24), 14200–14206.
- (122) Eberhardt, M.; Théato, P. *Macromol. Rapid Commun.* **2005**, *26* (18), 1488–1493.
- (123) Cline, G.; Hanna, S. *J. Am. Chem. Soc.* **1987**, No. 8, 3087–3091.
- (124) Theato, P.; Kim, J. U.; Lee, J. C. *Macromolecules.* **2004**, *37* (15), 5475–5478.
- (125) Barz, M.; Tarantola, M.; Fischer, K.; Schmidt, M.; Luxenhofer, R.; Janshoff, A.; Theato, P.; Zentel, R. *Biomacromolecules.* **2008**, *9* (11), 3114–3118.
- (126) Favier, A.; D’Agosto, F.; Charreyre, M. T.; Pichot, C. *Polymer.* **2004**, *45* (23), 7821–7830.
- (127) Gitsas, A.; Yameen, B.; Lazzara, T. D.; Steinhart, M.; Duran, H.; Knoll, W. *Nano Lett.* **2010**, *10* (6), 2173–2177.

References

- (128) Steinhart, M.; Jia, Z.; Schaper, A. K.; Wehrspohn, R. B.; Gösele, U.; Wendorff, J. H. *Adv. Mater.* **2003**, *15* (9), 706–709.
- (129) Dersch, R.; Steinhart, M.; Boudriot, U.; Greiner, A.; Wendorff, J. H. *Polym. Adv. Technol.* **2005**, *16* (2–3), 276–282.
- (130) Greiner, A.; Wendorff, J. H.; Yarin, A. L.; Zussman, E. *Applied Microbiology and Biotechnology.* **2006**, *71*, 387–393.
- (131) Hulteen, J. C.; Martin, C. R. *J. Mater. Chem.* **1997**, *7* (7), 1075–1087.
- (132) Huczko, A. *Appl. Phys. A Mater. Sci. Process.* **2000**, *70* (4), 365–376.
- (133) Cepak, V. M.; Martin, C. R. *Chem. Mater.* **1999**, *11* (5), 1363–1367.
- (134) Al-Kaysi, R. O.; Ghaddar, T. H.; Guirado, G. J. *Nanomater.* **2009**, *2009*.
- (135) Haberkorn, N.; Nilles, K.; Schattling, P.; Theato, P. *Polym. Chem.* **2011**, *2* (3), 645.
- (136) Roth, P. J.; Theato, P. *Chem. Mater.* **2008**, *20* (4), 1614–1621.
- (137) Roth, P. J.; Theato, P. *Macromol. Chem. Phys.* **2012**, *213* (23), 2550–2556.
- (138) Nasreen, S. A. A. N.; Sundarrajan, S.; Nizar, S. A. S.; Balamurugan, R.; Ramakrishna, S. *Membranes.* **2013**, *3*, 266–284.
- (139) Thielke, M. W.; Bruckner, E. P.; Wong, D. L.; Theato, P. *Polym. (United Kingdom)* **2014**, *55* (22), 5596–5599.
- (140) Jo, H.; Haberkorn, N.; Pan, J.-A.; Vakili, M.; Nielsch, K.; Theato, P. *Langmuir.* **2016**, *32* (25), 6437–6444.
- (141) Lee, Y.; Park, S. H.; Kim, K. B.; Lee, J. K. *Adv. Mater.* **2007**, *19* (17), 2330–2335.
- (142) Lee, W.; Jin, M. K.; Yoo, W. C.; Lee, J. K. *Langmuir.* **2004**, *20* (18), 7665–7669.
- (143) Lee, Y.; Ju, K. Y.; Lee, J. K. *Langmuir.* **2010**, *26* (17), 14103–14110.
- (144) Jeong, H. E.; Kwak, R.; Khademhosseini, A.; Suh, K. Y. *Nanoscale.* **2009**, *1* (3), 331–338.
- (145) Cho, W. K.; Choi, I. S. *Adv. Funct. Mater.* **2008**, *18* (7), 1089–1096.

References

- (146) Kustandi, T. S.; Samper, V. D.; Ng, W. S.; Chong, A. S.; Gao, H. *J. Micromechanics Microengineering*. **2007**, *17* (10), N75–N81.
- (147) Lu, G.; Hong, W.; Tong, L.; Bai, H.; Wei, Y.; Shi, G. *ACS Nano*. **2008**, *2* (11), 2342–2348.
- (148) Del Campo, A.; Arzt, E. *Macromolecular Bioscience*. **2007**, *7*, 118–127.
- (149) Xue, L.; Kovalev, A.; Thöle, F.; Rengarajan, G. T.; Steinhart, M.; Gorb, S. N. *Langmuir*. **2012**, *28* (29), 10781–10788.
- (150) Xia, F.; Feng, L.; Wang, S.; Sun, T.; Song, W.; Jiang, W.; Jiang, L. *Adv. Mater.* **2006**, *18* (4), 432–436.
- (151) Fu, Q.; Rao, G. V. R.; Basame, S. B.; Keller, D. J.; Artyushkova, K.; Fulghum, J. E.; López, G. P. *J. Am. Chem. Soc.* **2004**, *126* (29), 8904–8905.
- (152) Bracco, G.; Holst, B. *Springer Ser. Surf. Sci.* **2013**, *51* (1).
- (153) Wenzel, R. N. *J. Phys. Colloid Chem.* **1949**, *53* (9), 1466–1467.
- (154) Hammarson, M.; Nilsson, J. R.; Li, S.; Lincoln, P.; Andréasson, J. *Chem. - A Eur. J.* **2014**, *20* (48), 15855–15862.
- (155) Hammarson, M.; Andersson, J.; Li, S.; Lincoln, P.; Andréasson, J. *Chem. Commun.* **2010**, *46* (38), 7130.
- (156) Hammarson, M.; Nilsson, J. R.; Li, S.; Beke-Somfai, T.; Andréasson, J. *J. Phys. Chem. B*. **2013**, *117* (43), 13561–13571.
- (157) Ercole, F.; Davis, T. P.; Evans, R. a. *Polym. Chem.* **2010**, *1* (1), 37.
- (158) Xin, B.; Hao, J. *Chem. Soc. Rev.* **2010**, *39* (2), 769–782.
- (159) Hoffman, A. S. *Advanced Drug Delivery Reviews*. **2013**, *65*, 10–16.
- (160) Ramos, J.; Imaz, A.; Callejas-Fernández, J.; Barbosa-Barros, L.; Estelrich, J.; Quesada-Pérez, M.; Forcada, J. *Soft Matter*. **2011**, *7* (11), 5067–5082.
- (161) Motornov, M.; Roiter, Y.; Tokarev, I.; Minko, S. *Progress in Polymer Science (Oxford)*. **2010**, *35*, 174–211.

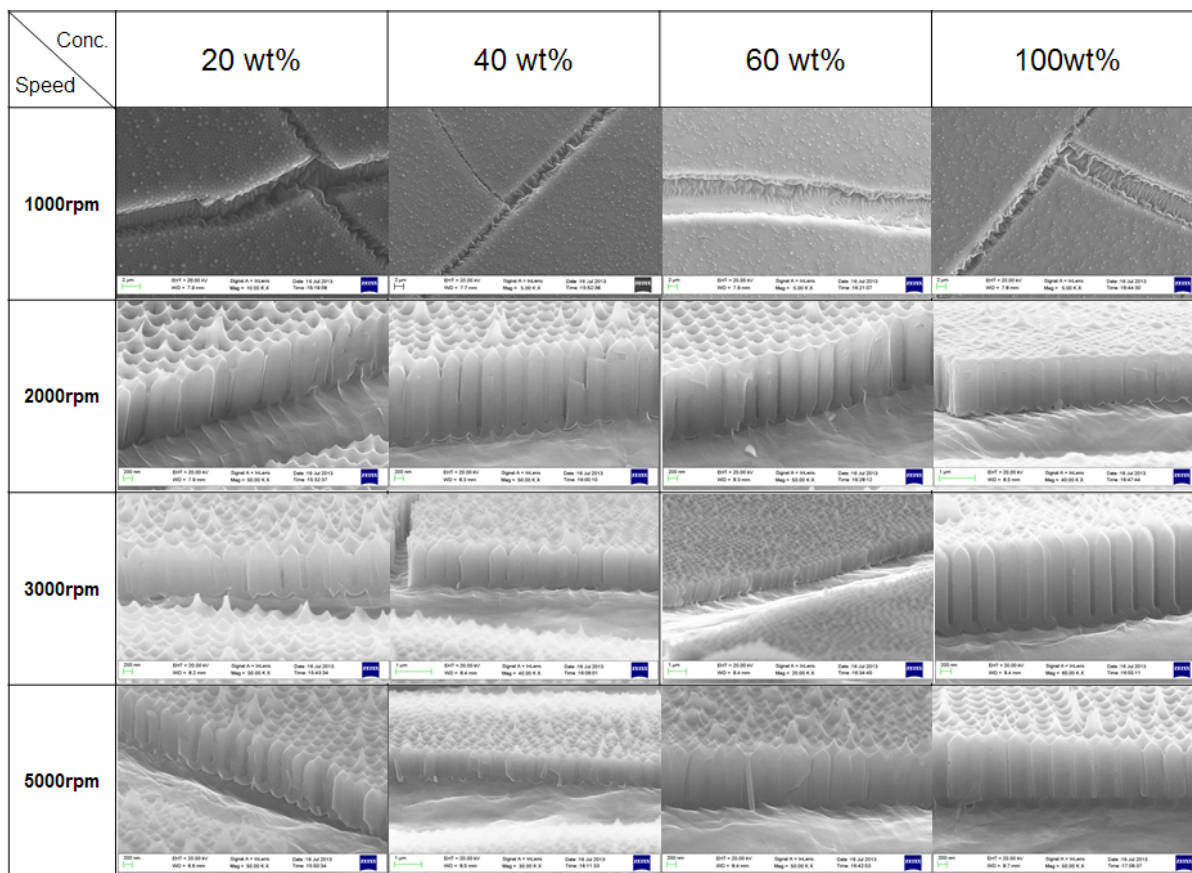
References

- (162) Saunders, B. R.; Laajam, N.; Daly, E.; Teow, S.; Hu, X.; Stepto, R. *Advances in Colloid and Interface Science*. **2009**, *147 - 148*, 251–262.
- (163) Langer, R.; Peppas, N. A. In *AIChE Journal*. **2003**, *49*, 2990–3006.
- (164) Aguilar, M. R.; San Román, J. *Smart Polym. their Appl.* **2014**, 1–11.
- (165) Schild, H. G.; Tirrell, D. A. *J. Phys. Chem.* **1990**, *94* (17), 4352–4356.
- (166) Vihola, H.; Laukkanen, A.; Valtola, L.; Tenhu, H.; Hirvonen, J. *Biomaterials*. **2005**, *26* (16), 3055–3064.
- (167) Imaz, A.; Forcada, J. *J. Polym. Sci. Part A Polym. Chem.* **2010**, *48* (5), 1173–1181.
- (168) Liang, X.; Liu, F.; Kozlovskaya, V.; Palchak, Z.; Kharlampieva, E. *ACS Macro Lett.* **2015**, *4* (3), 308–311.
- (169) Akimoto, J.; Nakayama, M.; Okano, T. *Journal of Controlled Release*. **2014**, *193*, 2–8.
- (170) Liu, F.; Kozlovskaya, V.; Medipelli, S.; Xue, B.; Ahmad, F.; Saeed, M.; Cropek, D.; Kharlampieva, E. *Chem. Mater.* **2015**, *27* (23), 7945–7956.
- (171) O’Neil, M. J. (2013). *The Merck Index - An Encyclopedia of Chemicals, Drugs, and Biologicals*. Merck & Co.
- (172) Petzetakis, N.; Dove, A. P.; O’Reilly, R. K. *Chem. Sci.* **2011**, *2* (5), 955–960.
- (173) Chécot, F.; Lecommandoux, S.; Gnanou, Y.; Klok, H. A. *Angew. Chemie - Int. Ed.* **2002**, *41* (8), 1339–1343.
- (174) Meng, F.; Zhong, Z.; Feijen, J. *Biomacromolecules*. **2009**, *10* (2), 197–209.
- (175) Hansen, C. M. (2013). *Hansen Solubility Parameters A User’s Handbook*. Boca Raton, FL: CRC Press.
- (176) Hansen, C. M. *Progress in Organic Coatings*. **2004**, *51*, 77–84.
- (177) Hansen, C. M. *Progress in Organic Coatings*. **2004**, *51*, 55–66.
- (178) García, M. T.; Gracia, I.; Duque, G.; Lucas, A. De; Rodríguez, J. F. **2009**, *29*, 1814–1818.

References

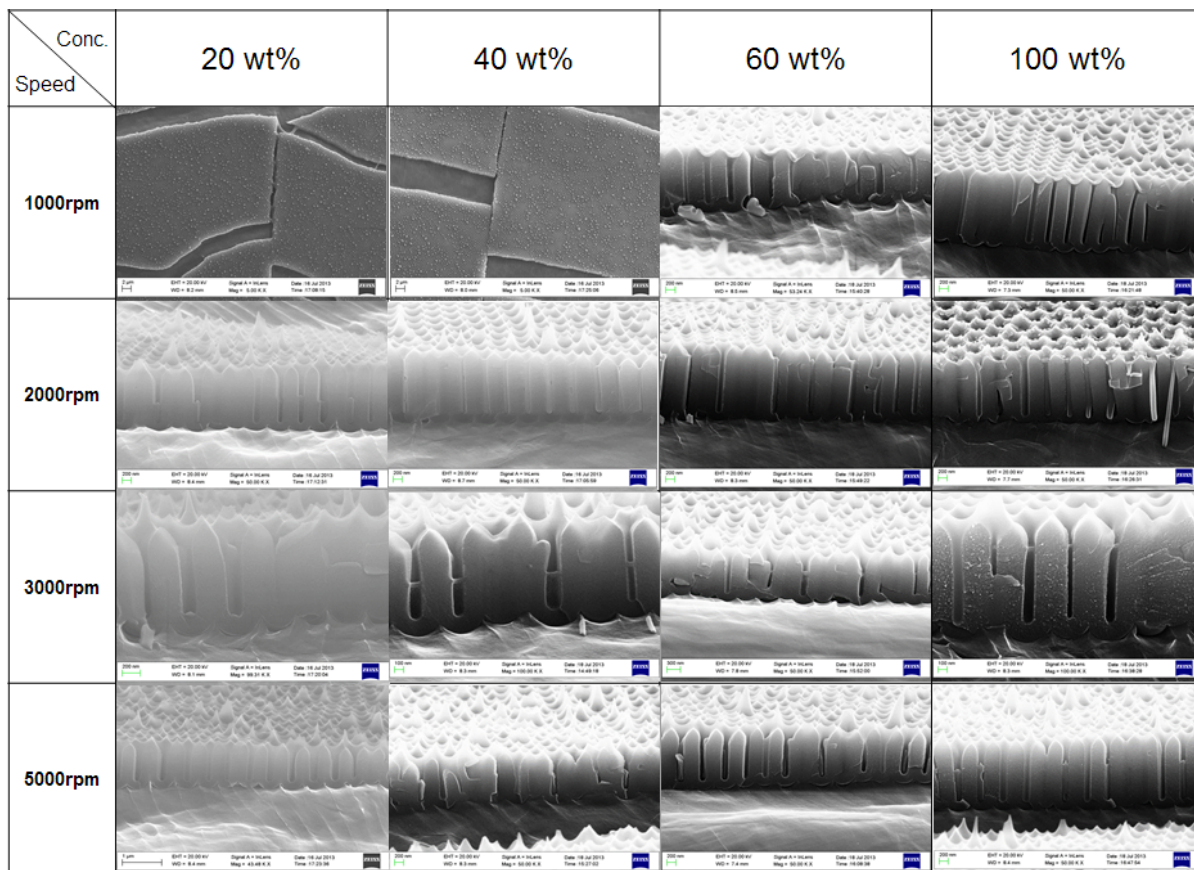
- (179) Brandrup, J.; Immergut, E. H.; Grulke, E. A. (2013). *Polymer Handbook*, 4th ed.; John Wiley and Sons.
- (180) Barton, A. F. M. (1990). *CRC Handbook of Polymer-Liquid Interaction Parameters and Solubility Parameters*. CRC Press.
- (181) Miller, R. G.; Bowles, C. Q.; Chappelow, C. C.; Eick, J. D. In *Journal of Biomedical Materials Research*. **1998**, *41*, 237–243.
- (182) Zaraska, L.; Sulka, G. D.; Jaskula, M. *J. Solid State Electrochem.* **2011**, *15* (11–12), 2427–2436.
- (183) Choi, J.; Schattling, P.; Jochum, F. D.; Pyun, J.; Char, K.; Theato, P. *J. Polym. Sci. Part A Polymer Chem.* **2012**, *50* (19), 4010–4018.
- (184) Fissi, A.; Pieroni, O.; Ruggeri, G.; Ciardelli, F. *Macromolecules*. **1995**, *28* (1), 302–309.

7. Appendix

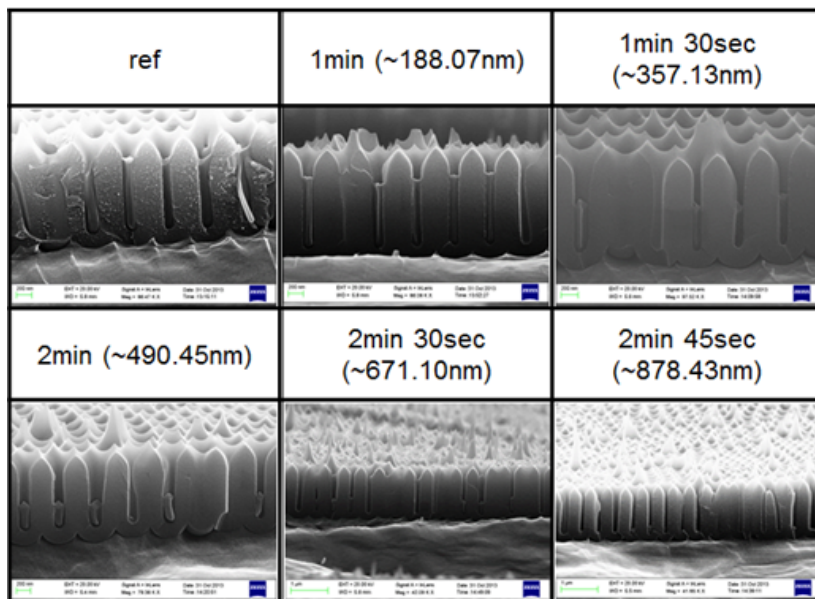


Appendix A. SEM images of the PS nanorods as a function of the concentration of styrene solution in ethanol and the speed of spin-coating.

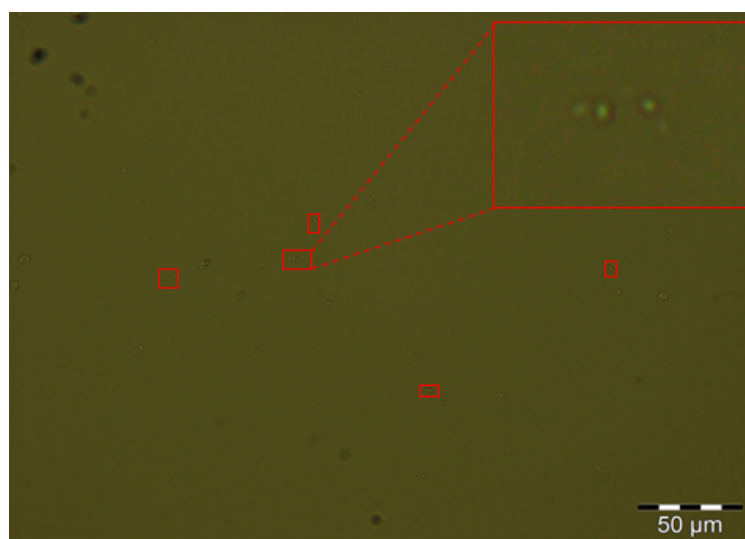
Appendix



Appendix B. SEM images of the half PS nanorods after oxygen plasma treatment (2 min, 990 W, 0.6 mbar) as a function of the concentration of styrene solution in ethanol and the speed of spin-coating.



Appendix C. SEM images of the PS nanorods after oxygen plasma treatment for a certain amount of time (the lengths next to the time show the thickness of the removed part of PS nanorods).



Appendix D. Fluorescence optical microscopy image of the functionalized PPFPA nanowires.

Acknowledgement

First of all, I'd like to thank to Prof. Patrick Theato that he gives me a chance to study in Germany. It was a new journey which made my life fully different. Still I remember the day we met first time in Seoul. Having a chance to getting know you and getting an Evonik scholarship were truly an amazing opportunity for me.

I must thank to Prof. Kornelius Nielsch as well. I thank him that he allows me to research at his working group. It is not too much to say that I spent half of Ph.D. period in his laboratory. I appreciate his support for the fabrication of AAO templates. Furthermore, I could get the precious and meaningful supports from many of group members in Nielsch's group. First, I thank to Dr. Changdeuck Bae for his sincere support and numerous discussions. His great support helped me to settle down and start new life in Germany, and the active discussion upon various scientific topics always inspired and motivated me. Dr. Josep M. Montero and Dr. Javier Garcia from Spain gave me truly great help and also their knowledge on AAO. I could learn much things from them which were not able to know somewhere else. In addition, I thank to Mr. Lewis Olaniyi Akinsinde and Dr. Hosun Shin for their great help.

Special thanks to Prof. Martin Trebbin for a kind reviewing of the thesis and also thanks to Mrs. Christina Khenkhar for her great effort on the numerous English correction of my works. Without her wonderful works, I couldn't publish the readable journals and thesis.

In addition, I want to thank to Prof. Jürgen Rühle's group in IMTEK, Freiburg. Even though, it wasn't a long-term staying in his group, it was a great time to research there with great people. Especially, I'd like to thank to Dr. Thomas Brandstetter and Mr. Holger Frey for their great support in the laboratory.

The research could not be conducted without the helps from the others. Especially, I thank to Mohamad, Jia-Ahn, and Sören for their great help. It was a great pleasure to work with them. Their diligence and brilliance motivated me a lot. I wish all the best for their successful carrier in the future. Special thanks to Aina Reich at the department of physical chemistry, university of Hamburg for the fluorescence microscopy measurement, and thanks to Thomas Halbritter at University of Frankfurt for the active discussions and measurement on spiropyran. Furthermore, I thank to Mrs. Renate Walter, Mr. Stefan Bleck, and Mr. Michael Gröger for their support in the various measurements.

Evonik foundation gave me not only the financial support but also the opportunity to meet various great people. I thank to my mentor, Dr. Gerd Löhden, for his great support and sincere mentoring.

I also thank to all the members in our group. Phillipp and Inna personally helped me a lot in the beginning of study. I truly appreciate their help and time. I thank to a cool crew, Alex, Michael, Tim, and Linsey. I support their next step in another places and country. I thank to my office members, Shaojian, Heba, Anindita, Jiaojiao, Lirong, and Natalie as well. Especially, thanks to Shaojian and Heba for their cheerful comments and unlimited encouragement. I thank to my only one AAO team member, Xia, for her great support. I also thank to the people who already changed their locations. I thank to Denis and Hui for their warm and great smile, and I also thank to Ryohei for his support. Furthermore, I thank to our visiting students, Emma, Willaiporn, Daniel, Bam, and Robert.

I sincerely thank my family and friends in Korea. Especially, I'd like to thank my parents and brother. Without their love and support, I couldn't go through this journey far from my home country. Not only from family, but also from my friends, I got a lot of support and encouragement. I thank to my true friends, Sesil, Hyun, and Siyun for their endless support. Saying thank you is not enough to repay their sincere and thoughtful support. I thank to another half of my family, as well. It was a miracle that I got a family in Germany. I truly appreciate their warm support. Thanks to all of you. Last but most importantly, I thank to my husband, Fokko Rendel, from the heart. I wouldn't be able to finish the study without his tremendous supports for everything.

Once again, thanks to everyone who share the time and experience together with me.

Eidesstattliche Versicherung

Declaration on oath

Hiermit versichere ich an Eides statt, die vorliegende Dissertation selbst verfasst und keine anderen als die angegebenen Hilfsmittel benutzt zu haben. Die eingereichte schriftliche Fassung entspricht der auf dem elektronischen Speichermedium. Ich versichere, dass diese Dissertation nicht in einem früheren Promotionsverfahren eingereicht wurde.

I hereby declare on oath, that I have written the present dissertation by my own and have not used other than the acknowledged resources and aids. The submitted written version corresponds to the version on the electronic storage medium. I hereby declare that I have not previously applied or pursued for a doctorate (Ph.D. studies).

Hamburg, den *city and date*

Unterschrift *signature*